LCSEA GHG Accounting Framework — Table of Contents

Section 4 **Page**

LCSEA GHG Accounting Framework

This Annex describes the Life-Cycle Stressor-Effects Assessment (LCSEA) Greenhouse Gas (GHG) Accounting Framework. The Annex contains four sections:

- Section 1 describes general parameters of the LCSEA GHG Accounting Framework and enumerates the steps involved in applying this general framework to global and regional climate GHG accounting.
- Section 2 describes the global LCSEA GHG accounting protocols that conform to this Framework.
- Section 3 describes the Arctic and Antarctic LCSEA GHG accounting protocols that conform to this Framework.
- Section 4 lists specific category indicators, associated algorithms and characterization factor equations used to calculate loadings for "key GHGs" — i.e., greenhouse gases and other climate-impacting particulates and aerosols.[1,2]

1.0. General Parameters

The LCSEA GHG Accounting Framework is intended for use by climate registries, policy makers, business managers, life-cycle assessment (LCA) practitioners and other stakeholders interested in evaluating the emissions of key GHGs associated with organizations, operations, and projects. The framework is built upon a detailed life-cycle impact assessment methodology that is ISO-14044 conformant, in which specific GHGs are quantitatively linked to current and projected climate anomalies and exceedances of thresholds.[3] It is specifically designed as a tool to integrate up-to-date research, data and knowledge pertaining to climate change and to bridge the disciplines of climate science and life-cycle assessment.

The framework builds upon earlier GHG accounting systems based on protocols developed by the Intergovernmental Panel on Climate Change (IPCC). IPCC-based accounting protocols rely on carbon dioxide equivalencies established through the Global Warming Potential (GWP) Index. This index represents the radiative efficiencies of specific GHG emissions relative to carbon dioxide on a per tonne equivalency basis ("tonne CO_2e"). The GWP Index is based on the relative radiative forcing of specific GHGs compared to an equivalent amount of carbon dioxide, factoring in the differences in atmospheric lifetimes. [4,5]

---

[1] A loading refers to the amount of emissions released into an environment that deposits into or resides in areas that exceed identified thresholds. The loading incorporates relative potency, fate and transport of the emission(s), as well as the spatial and temporal characteristics of the identified endpoints.

[2] The acronym "GHG" is used throughout this document as shorthand to refer to both gases and non-gaseous substances that contribute to positive or negative radiative forcing linked to climate change, except where otherwise noted.

[3] LCSEA is a life-cycle assessment (LCA) framework conformant to the ISO-14044 standard for LCA, including that standard's rigorous life-cycle impact assessment (LCIA) requirements for making comparative assertions. The LCSEA framework quantitatively and comprehensively tracks the individual biological, physical and chemical "stressors" generated by a particular industrial system to various midpoint and endpoint effects (i.e., "nodes") along the stressor-effects network.

[4] According to the IPCC (1990, 1992, 1994) and the Second Assessment Report (IPCC, 1996): "The radiative forcing of the surface-troposphere system due to the perturbation in or the introduction of an agent (say, a change in greenhouse gas concentrations) is the change in net (down minus up) irradiance (solar plus long-wave; in Wm-2) at the tropopause after allowing

The IPCC GWP Index serves as the basis for warming potency equivalencies used within this LCSEA framework. These equivalencies are applied to convert the initial emissions — the first "node" in the stressor-effects network — into GHG loadings tonnes CO_2e (see Table B1-1). However, the GWP Index alone is not sufficient in itself to calculate GHG loadings; additional characterization is required to represent the cause-effect linkages to known and projected global and regional exceedances of thresholds that result in critical climate anomalies. This additional characterization is described in detail in this Annex.

1.1. General Accounting Framework Description

The LCSEA GHG Accounting Framework establishes GHG accounting protocols for specific climate stressor-effects networks in a manner that conforms to ISO-14044 — addressing distinct environmental (in this case, climate) impact mechanisms and modeling their corresponding stressor-effects networks. To date, sufficient data are available with respect to global, Arctic and Antarctic climate impact mechanisms to warrant the development of separate GHG accounting protocols for each.

Key elements of the framework, summarized as follows, are described in detail in the remainder of this Annex:

- For global calculations, GHGs are classified as "key GHGs" if they contribute (or are projected to contribute) to global and/or regional radiative forcing, either positively or negatively, by at least ± 0.1 W/m^2. For regional calculations, GHGs are classified as key GHGs if they meet the ± 0.1 W/m^2 current or projected radiative forcing threshold, and if their contribution to radiative forcing in turn will cause the GMT or RMT to change by at least ± 0.1°C over the relevant time horizon.
- Relevant time horizons are assigned to the global and regional GHG accounting protocols, based upon timeframes of the observed or projected exceedances of linked thermal and structural thresholds.
- The assignment of GWP values involves two additional considerations beyond standard IPCC protocols: 1) the lower limit for GWP values must be consistent with the GHG's atmospheric lifetime, including both pulse and continuous emission sources, and 2) the GWP time horizon must be consistent with the time horizon assigned to the global and regional GHG accounting protocols.
- GWPs, Regional Warming Potentials (RWPs), and supporting equations are established for the short-lived GHGs — tropospheric ozone (TO) and black carbon (BC).
- Global Cooling Potentials (GCPs), Regional Cooling Potentials (RCP) and supporting equations are established for halocarbons (i.e., CFCs, HCFCs, and halons) and tropospheric sulfate aerosols (TSA).

---

for stratospheric temperatures to readjust to radiative equilibrium, but with surface and tropospheric temperatures and state held fixed at the unperturbed values."

[5] The IPCC GWP Index covers the gases addressed in the Kyoto Protocol: carbon dioxide (CO_2), methane (CH_4), nitrous oxide (N_20), hydrofluorocarbons (HFCs), perfluorocarbons (PFCs) and sulfur hexafluoride (SF_6), with calculations over 20-year, 100-year and 500-year time horizons.

- Characterization factors beyond the GWP Index are established to account for regional and global effects.
- "Pulse warming potentials" (PWPs) are established to account for large biogenic pulses that radically change the relative concentrations of key GHGs in the atmosphere over time.
- Equations and accumulated GWP ("GWP*") values are established to account for accumulated GHG loadings from major continuous sources.
- Protocols are provided to establish baselines for use in making comparisons (e.g., to consider different energy source options before they are installed and operated). These protocols take into account the various investment periods that provide strategic and security-level assessments for such new source options.

1.2. Establishing Specific LCSEA GHG Accounting Protocols

The following process is followed in the establishment of global or regional GHG accounting protocols:

Step 1. Establishment of the global and significant regional climate stressor-effect networks.

Step 2. Classification and characterization of the stressor-effects network, whereby current and projected changes (i.e., anomalies and intensifications) are quantified at each stressor-effects node.

Step 3. Assignment of time horizons to specific stressor-effects networks that correspond with observed or projected exceedances of thresholds.

Step 4. Classification of key GHGs based on their contribution to global and regional radiative forcing.

Step 5. Characterization of key GHGs within specific global and regional climate stressor-effects networks.

Step 6. Establishment of environmentally relevant global and regional GHG category indicators, along with appropriate characterization (i.e., equivalency) factors (e.g., global and regional warming potentials, global and regional cooling potentials, environmental characterization factors).

Step 7. Establishment of the equations to calculate loadings for key GHGs.

Life-cycle assessment is iterative by nature. As such, all seven steps are necessary, but will not necessarily unfold in a strictly linear fashion. Whether they are applied globally or regionally, these steps provide the basis by which all key GHGs contributing to observed and projected effects can be fully and accurately accounted.

Step 1: Establishment of Global and Significant Regional Climate Stressor-Effect Networks

A climate-related "stressor-effect network" is the cause-effects chain that links key GHGs to climate impact midpoints and endpoints on a global or regional scale. The global climate stressor-effects network and the global GHG accounting protocols are based on the IPCC global accounting framework (see section 2). Regional accounting protocols are provided to account for regional radiative forcing anomalies that form distinct "hot spots" or "cooling zones," such as those found in the Arctic and Antarctica.

- **Evidence of the Arctic Climate Stressor-Effects Network**

The rapid rise in the Arctic regional mean temperature (RMT) relative to overall GMT, coupled with the rapid loss of the perennial Arctic ice sheet, points to a hot spot within the Arctic region. This regional temperature anomaly is being driven by regional radiative forcing vectors from a specific subset of GHGs.

Figure B1-1 shows the upper latitude RMT to be increasing at three times the rate of the lower latitude RMT, with reported +2.9°C anomalies in Arctic sub-regions.[6] Even without considering the likely potential for increased biogenic methane releases in the Arctic, these anomalies exceed threshold values, warranting separate focus on the Arctic climate stressor-effect network and the establishment of Arctic GHG accounting protocols.

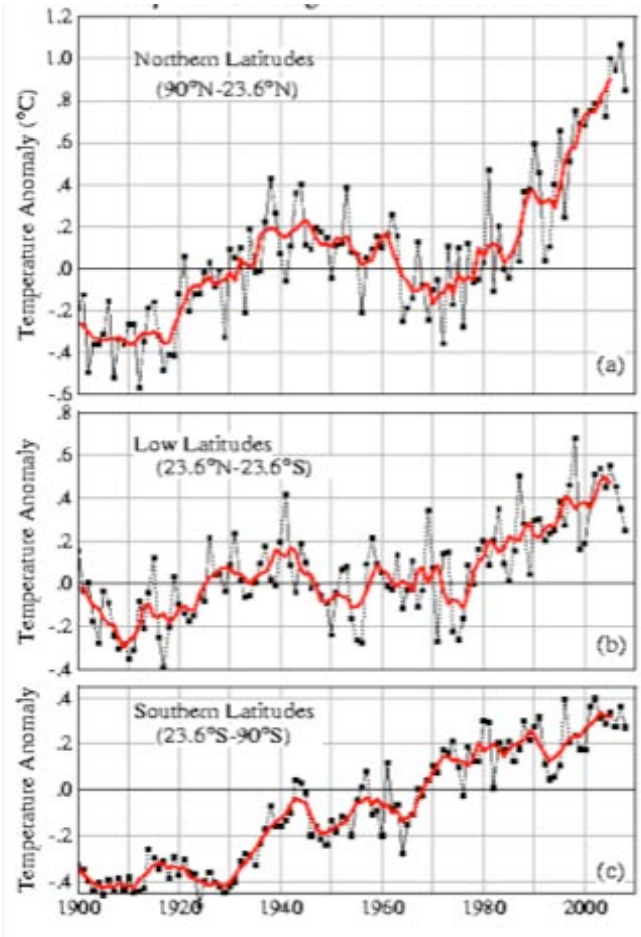

Figure B1-1. Surface Mean Temperature Changes for Three Latitude Bands
Source: NASA (http:data.giss.nasa.gov/modelforce/)

[6] Drew Shindell and Greg Faluvegi. "Climate Response to Regional Radiative Forcing During the 20th Century," *Nature Geoscience*, Vol. 2, April 2009.

The potential for a near-term exceedance of a "tipping point" threshold beyond which irreversible, catastrophic changes could occur is another consideration in the establishment of the Arctic GHG accounting protocols. The possibility of an imminent threshold exceedance is associated with a feedback loop in which the current level of warming is predicted to lead to the release of huge biogenic stores of methane and methane hydrates from northern tundra and shallow seabed sediments.[7] The potential consequence of such releases would be a 2-to-5-fold increase in Arctic methane concentrations compared with current levels by 2025 (see further discussion, Section 3).

• **Evidence of the Antarctic Climate Stressor-Effect Network**

Tropospheric ozone (TO) plumes from South Africa and South America are significantly contributing to the radiative forcing anomaly of up to 4.0 W/m^2 recorded in oceans surrounding Antarctica in 2009. According Steig *et al.,* the principal cause for the breakup of ocean ice in the region is warmer ocean water currents.[8] Figure B1-2 provides an image of the changes in oceanic temperatures near Antarctica since 1957.

Figure B1-2. Oceanic Temperature Changes Surrounding Antarctica (Steig *et al.*, 2009)[9]

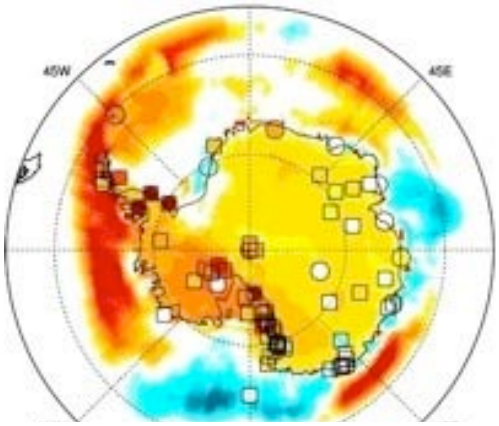

As sea ice melts along the coastline of Antarctica, the melting of land-based ice will accelerate. Therefore, Antarctic GHG accounting protocols should model the major regional radiative forcing vectors within the context of the Antarctic climate and land-based ice stability.

In addition to those GHGs causing warming in Antarctica, several classes of halocarbons — including chlorofluorocarbons (CFCs), hydrochlorofluorocarbons (HCFCs), halons and other subclasses – are having a net cooling effect and are thereby contributing to an Antarctic "cooling zone" (Figure B1-3).[10] In other words, while these GHGs are causing a dangerous breach in the protective properties of stratospheric ozone over Antarctica,

[7] For example, see British Broadcasting Corporation, "Methane seeps from Arctic sea bed." August 18, 2009. http://news.bbc.co.uk/2/hi/science/nature/8205864.stm

[8] Eric J. Steig, David P. Schneider, Scott D. Rutherford, Michael E. Mann, Josefino C. Comiso and Drew T. Shindell. "Warming of the Antarctic Ice-Sheet Surface Since 1957," *Nature.* Vol. 457, January 22, 2009.

[9] *Ibid.*

[10] NASA, http://www.nasa.gov/vision/earth/lookingatearth/ozone_record.html

they are simultaneously cooling the region (by -4.0 to -6.0 W/m^2 in regional radiative forcing in 2009, as calculated from based on real time data from the MOZART-4 model) by destroying stratospheric and tropospheric ozone.[11] The MOZART-4 data show a combined loss of stratospheric and tropospheric ozone in the range of 100-120 Dobson Units (DUs) as compared to historic levels within the Antarctic vortex in 2009, based on the IPCC conversion factor of 0.04 W/m^2 per DU. This chemically-induced Antarctic cooling zone is expected to maintain its current intensity for another 20 years, followed by a gradual warming, until the zone disappears altogether by around 2050. At that time, ozone levels will return to normal, and the Antarctic RF will regain +4.0 to 6.0 W/m^2, effectively tripling the heat of the Antarctica atmosphere. This increase of RF will push the Antarctic RMT anomaly over +1.2°C, up from the current RMT anomalies observed in Western Antarctica of +0.6°C.[12]

Figure B1-3. The Antarctic Cooling Zone Corresponds with the Ozone Hole[1]
Source: NASA Satellite Image

The ozone hole of 2006 is the most severe ozone hole (least amount of ozone) observed to date. NASA's Aura satellite observed a low value of 85 Dobson Units (DU) on Oct. 8 2006 in a region over the East Antarctic ice sheet. Dobson Units are a measure of ozone amounts above a fixed point in the atmosphere. This severe ozone hole resulted from very high ozone depleting substance levels and record cold conditions in the Antarctic stratosphere.

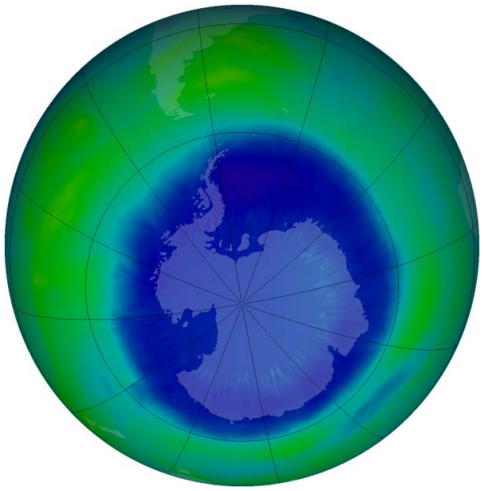

Section 3 describes the Arctic and Antarctic climate stressor-effects networks in greater detail, and provides Arctic GHG accounting protocols.

Step 2: Classification and Characterization of Stressor-Effects Networks

Each distinct midpoint node along a specific biophysical impact pathway within a stressor-effects network is classified in terms of the strength of its linkages to significant global and regional climate endpoints (Table B1-1). Once classified, each node is characterized in terms of the magnitude of effects observed or projected, and whether identified exceedances of thresholds have been observed or projected.

[11] The MOZART Model (Model for Ozone and Related Chemical Tracers) is a global 3-D chemical transport model driven by offline meteorological fields, developed by National Center for Atmospheric Research (NCAR), the Max-Planck-Institute for Meteorology, and the National Oceanic and Atmospheric Administration's Geophysical Fluid Dynamics Laboratory (NOAA/GFDL). MOZART-3 includes tropospheric and stratospheric chemistry and MOZART-4 is particularly suited for tropospheric and air quality studies. http://www.acd.ucar.edu/gctm/

[12] Steig *et al.* (2009)

Table B1-1. Classification of the General Climate Change Stressor-Effects Network by Node

Node	Description of the Node	Exceedance of Threshold	Linkage between Nodes
Node 1 (Stressor)	All GHG emissions	*Not applicable*	• No linkage to midpoints or endpoints • Strong linkage to Node 1 emission sources
Node 2 (Midpoint)	Loadings of short-lived, mid-lived and long-lived GHGs	*Not applicable*	• Strong linkage to Node 4 radiative forcing anomalies • Strong linkage to Node 1 emission sources
Node 3 (Midpoint)	Accumulation of long-lived (i.e., "legacy") GHG loadings	*Not applicable*	• Strong linkage to Node 4 anomalies • Strong linkage to Node 1 emission sources
Node 4 (Midpoint)	Global and regional radiative forcing anomalies associated with each key GHG (W/m^2)	*Not applicable*	• Strong linkage to Node 2 and 3 loadings • Strong linkage to Node 5 anomalies • Strong linkage to Node 1 emission sources
Node 5 (Midpoint)	Anomalies in Global Mean Temperature (GMT) and Regional Mean Temperature (RMT)	GMT/RMT ≥1.5°C	• Strong linkage to Node 4 anomalies • Weak linkage to Node 1 emission sources
Node 6 (Midpoint)	Structural changes or ecosystem damage	*Irreversible structural changes*	• Strong linkage to Node 4 and 5 anomalies, changes and damage • No linkage to Node 1 emission sources
Node 7 (Midpoint)	Climate change	Irreversible climate change	• Strong linkage to Node 4 and 5 anomalies, changes and damage • No linkage to Node 1 emission sources
Node 8 (Endpoints)	Catastrophic structural changes or ecosystem damage	Multiple irreversible catastrophic impacts	• Strong linkage to Node 7 changes • No linkage to Node 1 emission sources

- **Classification: Determining Linkages between Significant Climate Anomalies**
  Node 1 represents the annual inventory of GHG emissions by major sources, as monitored and compiled by the United Nations Framework Convention on Climate Change (UNFCCC).

  The midpoint nodes (nodes 2-7) represent a well-established and distinct biophysical pathway, reflecting direct thermodynamic linkages between increases in key GHG loadings and resultant changes in atmospheric radiative absorption. Corresponding changes in radiative forcing are measured in positive or negative watts per square meter (W/m^2) on both global and regional bases. For example, the net radiative forcing at node 4 (radiative forcing anomalies associated with individual key GHGs) drives changes in the "global mean temperature" (GMT) as well as "regional mean temperatures" (RMTs) at node 5. The current and projected increases in GMT and RMTs are subsequently linked to significant node 6 climate and habitat changes, including but not limited to the rapid melt of the perennial Arctic ice sheet, increases in severe weather events over Southern China, and desertification of parts of Africa.

- **Characterization: Determining the Magnitudes and Exceedances of Thresholds Associated with Climate Anomalies**
  Once each node is classified, observed or projected impact intensification and resultant anomalies are measured with respect to global or specific regional GHG accounting protocols. Each node is justified based on its linked climate nodes. For example, the observed intensification in radiative forcing (node 4) should account for observed increases in GMT or RMT anomalies (node 5). Similarly, total annual key GHG loadings should be consistent with radiative forcing values. Sensitivity analysis is used to test the modeled assumptions and data quality for individual nodes.

  The characterization of each midpoint:
    - addresses relevant spatial and temporal conditions;
    - compares climate anomalies to recognized historic baselines; and
    - assesses the reversibility of impacts.

  In order to characterize nodes 1 and 2 of regional stressor-effects networks, major sources of key GHGs are identified and mapped, and corresponding regional loading levels are established. (As an example, regional tropospheric ozone and black carbon plumes that contribute to annual Arctic warming should be characterized and mapped.)

  Characterization of nodes 3, 4, 5 and 6 is based upon data from established government and intergovernmental models and databases (e.g., NASA, IPCC). Characterization of nodes 7 and 8 uses recognized field ecology protocols.

Step 3: Assignment of Time Horizons to Global and Regional Stressor-Effects Networks Based on Exceedances of Thresholds

While the IPCC GHG accounting protocols include time horizons for 20-year, 100-year and 500-year timeframes, the IPCC provides no guidance to connect these time horizons to observed or projected exceedances of threshold of key climate anomalies, as described above. In practice, the 100-year time horizon has been widely used without regard to oncoming exceedances of threshold in both GMT and RMT as well as large structural changes at the poles. A number of climate researchers have suggested that the 100-year time horizon is no longer sufficient to address these near-term changes. For example, Dr. Ed J. Dlugokencky of the National Oceanic and Atmospheric Administration (NOAA) has described the importance of considering use of the 20-year time horizon (see excerpt below).

Significance of the 20-year Time Horizon
Dr. Ed J. Dlugokencky, NOAA[13], March 2008

"The selection of a time horizon of a radiative forcing index is largely a 'user' choice (i.e., a policy decision) . . . if the policy emphasis is to help guard against the possible occurrence of potentially abrupt, non-linear climate responses in the relatively near future, then a choice of a 20-year time horizon would yield an index that is relevant to making such decisions regarding appropriate greenhouse gas abatement strategies."

- **Current and Projected Exceedances of Thresholds**
  The framework assigns specific time horizons to global and regional GHG accounting protocols based on evidence of exceedances of threshold of the key climate anomalies. Unprecedented intensification of climate anomalies and exceedances of thresholds recorded in recent years indicate the need to assign annual and 20-year time horizons in lieu of the 100-year time horizon. For example, the 2009 annual mean global radiative forcing (RF) anomaly is +3.07 W/m^2, with a GMT anomaly of +0.4°C. By comparison, the Arctic RMT anomaly, now reported by Shindell to be +2.9°C, far exceeds +1.5°C (see Table B1-1, Node 5). Extensive structural changes to habitats, ice sheets and oceanic temperatures already observed represent exceedances of structural thresholds. As will be shown in Section 2, the GMT anomaly threshold of +1.5°C will be reached by around 2030.

  Global and specific regional accounting protocols developed under this general framework apply a fixed baseline year of 2010 and a fixed time interval of assessment from that baseline, based upon evidence of current or projected exceedances of temperature, structural or climate thresholds.

  1) Global GHG Accounting Protocols: Annual and 20-Year Time Horizons
  A consensus on the GMT anomaly threshold beyond which irreversible structural and ecosystem damage will occur has yet to be reached. However, a consensus has emerged around the need to set such a threshold limit. Although scientists participating in the 2007 IPCC conference in Bali proposed a not-to-exceed GMT anomaly goal of +2°C, the Alliance of Small Island States (AOSIS) supports an even stricter threshold of +1.5°C.[14] There is a growing likelihood that, at the current rate of intensification, the +1.5°C GMT anomaly threshold will be reached within the 20-year time horizon by 2030.[15] This projected threshold exceedance lends support to the adoption of a fixed baseline year set at 2010 and a time horizon not to exceed a 20-year time interval ending in 2030, rather than relying upon the 100-year time horizon. Section 2 of this Annex provides the

[13] Dr. Ed Dlugokencky, National Oceanic and Atmospheric Administration, 2008, cited in "Beyond Kyoto: Why Climate Policy Needs to Adopt the 20-year Impact of Methane," available at http://www.ecocycle.org/ZeroWaste/climate/index.cfm/
[14] 2007 Bali Climate Declaration by Scientists, http://www.ccrc.unsw.edu.au/news/2007/Bali.html; AOSIS Press Conference at United Nations headquarters, July 10 2009, http://www.un.org/News/briefings/docs/2009/090710_AOSIS.doc.htm
[15] *Ibid.*

characterization data used to support an annual and 20-year time horizon for the global GHG accounting protocols.

2) **Arctic GHG Accounting Protocols: Annual Time Horizon**
The perennial Arctic ice sheet acts as the major heat sink for the region and provides significant radiative reflectivity (albedo). It has kept the Arctic climate relatively stable for 65 million years.[16] In 2008, NASA satellite data showed that the ice had shrunk from coverage of 50-60 percent of the Arctic to less than 30 percent.[17] As discussed in Section 3 below, this perennial ice sheet may melt entirely as soon as 2013, and likely no later than 2040.[18] Thus, the stability of the Arctic climate and the perennial ice sheet could be determined during the next decade (2010-2020). The annual time horizon is used to approximate the seasonal nature of radiative forcing anomalies in the Arctic.

3) **Antarctic GHG Accounting Protocols: 20-Year Time Horizon**
Western Antarctica is now undergoing significant warming and southern ocean temperatures are rising significantly resulting in significant loss of sea ice. This is projected to speed up the movement of land-based ice towards ice-free ocean areas. However, the Antarctic Ozone Hole is projected to be stable at least until 2030. Therefore no exceedance of threshold (e.g., RMT or major land-based ice collapses) is projected until then. Thus a 20-year time horizon is justified for Antarctica.

Step 4: Classification of Key GHGs Based on Minimum Contribution to Radiative Forcing

Contribution analysis is used to classify "key GHGs." Only those GHGs that contribute a minimum global radiative forcing of ±0.1 W/m^2 (about 3%) to the total global annual radiative forcing of +3.07 W/m^2 are classified as key GHGs (see further discussion in Section 2). For example, nitrous oxide (N_2O) contributes +0.16 W/m^2 to global forcing and is classified as a key GHG.

The key GHGs contributing to positive or negative global and regional radiative forcing are listed in Table B1-2. These GHGs account for more than 95 percent of total regional and global GHG loadings (either anthropogenic and biogenic). These GHGs are discussed at greater length in the remaining sections of this Annex.

[16]According to NASA, "Perennial sea ice is the long-lived, year-round layer of ice that remains even when the surrounding short-lived seasonal sea ice melts away in summer to its minimum extent."
http://www.nasa.gov/topics/earth/features/seaice_conditions_feature.html

[17] NASA, http://www.nasa.gov/vision/earth/environment/arcticice_decline.html

[18]Based on NASA satellite findings, scientists such as Dr. Wieslaw Maslowski of the Naval Postgraduate School in Monterey, California and Dr. Julienne Stroeve of the U.S. National Snow and Ice Data Center warned that the Arctic could be ice-free as early as the summer of 2013." (http://news.nationalgeographic.com/news/2007/12/071214-warming-arctic.html; also, BBC News Website — Wednesday 18 June 2008, "Arctic Sea Ice Melt 'Even Faster'", Richard Black.)

Table B1-2. Atmospheric Lifetime and Radiative Forcing of Key GHGs

GHG	Atmospheric Lifetime	Current Global Radiative Forcing W/m^2	Regional Radiative Forcing and RMT Contribution	
			Radiative Forcing	RMT
GHGs contributing to Increased Radiative Forcing				
Carbon dioxide (CO_2)	150 years*	+1.66 W/m^2	Arctic: +0.27 W/m^2	< +0.1°C
Nitrous Oxide (N_2O)	114 years	+0.16 W/m^2	Arctic: +0.02 W/m^2	< +0.1°C
Hydrofluorocarbons (HFCs)	Variable depending on gas: 1-60 years (most)	+0.02 W/m^2 (current) +0.34 W/m^2 (2030 projection)	Arctic: +0.05 W/m^2	< +0.1°C
CFCs	Variable depending on specific gas: one to thousands of years	+0.33 W/m^2	Arctic: +0.05 W/m^2	< +0.1°C
Methane (CH_4)	8.5 – 20 years (tropics / polar)	+0.48 W/m^2	Arctic: +0.57 W/m^2	+0.3 to 0.4°C
Tropospheric Ozone (TO)	22 days	+0.37 W/m^2	Arctic and southern oceans near Antarctica: ≤ +4 W/m^2	+0.5°C
Black Carbon (BC)	4-30 days	+0.9 W/m^2	Insufficient data	+1.0 to 1.5°C
GHGs contributing to Negative Radiative Forcing				
Tropospheric Sulfate Aerosols	4-8 days	-0.9 W/m^2	Known Arctic Coolant: ≤ -3.0 W/m^2	> -1.2°C
Halocarbons - CFCs - HCFCs - Halons - Methyl Bromide	Variable depending on specific gas: one to thousands of years	Negligible	Known Antarctic Coolants: -4.0 to -6.0 Wm^2	> -1°C (Antarctica)
Sea Salt Aerosols and Mineral Dust (Direct) *Increase in scattering and albedo*	Variable: on the order of days	-0.5 W/m^2	Potential Arctic Coolant: - 3.0 to -7.0 W/m^2	*To be determined*
Sea Salt Aerosols and Mineral Dust (Indirect) *Increase in cloud albedo*	Variable: on the order of days	-0.7 W/m^2 (IPCC)	Potential Indirect Cooling From Arctic Aerosols -14.0 W/m^2	*To be determined*

HFCs and CFCs are listed as key GHGs because their current or projected contribution to global radiative forcing meets the minimum +0.1 W/m^2 (Figure B1-4).[19] The HCFCs, halons, perfluorocarbons (PFCs) and sulfur hexafluoride (SF_6) are not included among the key GHGs, despite their long atmospheric lifetimes and high GWPs, since they are projected to contribute less that +0.1 W/m^2 from the present through 2050.[20] Many older halocarbons are listed as "key GHG coolants" based on their negative radiative forcing potential on a regional basis because they meet the -0.1 W/m^2 minimum.

[19] Guus J. M. Velders, David W. Fahey, John S. Daniel, Mack McFarland, and Stephen O. Andersen. "The Large Contribution of Projected HFC Emissions to Future Climate Forcing." Proceedings of the National Academy of Sciences of the United States, Vol. 106, No. 27, July 7, 2009, pp. 10949 –10954. www.pnas.org/content/early/2009/06/19/0902817106.abstract

[20] David G. Victor and Gordon McDonald. "A Model for Estimating Future Emissions of Sulfur Hexafloride and Perfluorocarbons," *Climate Change.* Vol. 42, No. 4, August 1999.

Sea salt is also listed as a coolant in the table, based on simulation modeling and testing.[21] At minus 10 W/m^2 without any apparent trade-offs, it would currently appear to be the optimal dispersion coolant.

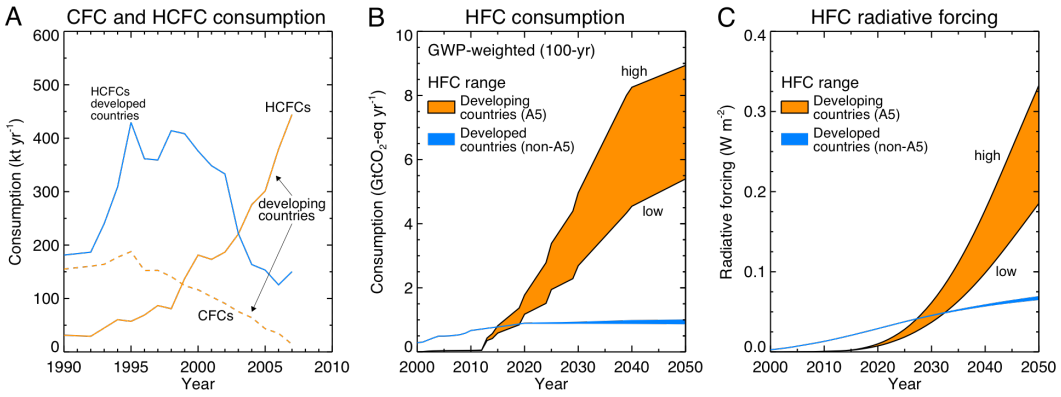

Fig. 1. CFC and HCFC consumption (*A*), HFC consumption (*B*), and HFC RF (*C*) for 2000–2050 in developing (A5) and developed (non-A5) countries. The CFC and HCFC mass consumption values in *A* are derived from reported data (1). The shaded regions for GWP-weighted consumption in *B* and RF in *C* are bounded by high and low limits as defined by the upper and lower ranges of the baseline scenarios in both developed and developing countries. The consumption values expressed in equivalent $GtCO_2$ per year in *B* are sums over the consumption of individual HFC compounds each multiplied by their respective GWP (100-year time horizon) (3).

Figure B1-4. Projected HFC RF Increases through 2050[22]

Step 5: Characterization of Key GHGs within Specific Stressor-Effects Networks

- **Temporal Characterization**

Key GHGs are assigned environmentally relevant time horizons, based on their atmospheric lifetimes (Table B1-3). For example, a 100-year time horizon for shorter-lived GHGs (such as tropospheric ozone, aerosols and black carbon) is inappropriate, as their atmospheric lifetimes limit their actual forcing to very short time periods. The short-term heating or cooling effects of GHGs that last only days or months should not be amortized for 99+ years after they have left the atmosphere. For these GHGs, GWP indexing based upon 100 years skews the analysis, resulting in significantly understated GWP values that fail to sufficiently predict currently measured impacts.

The atmospheric lifetime of carbon dioxide listed in the table is an approximation. Many resources list it simply as 100 years or more. Other scientists note that vestiges of a pulse release could last for thousands of years.[23]

[21] Takemura Toshihiko, Nakajima Teruyuki, Higurashi Akiko, Ohta Sachio, and Sugimoto Nobu. "Aerosol distributions and radiative forcing over the Asian Pacific region simulated by Spectral Radiation-Transport Model for Aerosol Species (SPRINTARS): Characterization of Asian aerosols and their radiative impacts on climate," *Journal of Geophysical Research.* Vol. 108, 2003, pp. ACE27.1-ACE27.10 (27 ref.).

[22] *Ibid.*

[23] Mason Inman. "Carbon is Forever." *Nature Reports: Climate Change.* Published online: 20 November 2008 http://www.nature.com/climate/2008/0812/full/climate.2008.122.html

Table B1-3. Temporal and Spatial Characterization of GHGs

Key GHG*	Source of Major Release	Atmos. lifetime	Fate and Transport Temporal Characteristics	Assigned Time Horizons
Carbon Dioxide (CO_2)	Incremental increases	~150 years	The accumulated CO_2 loading is expected to gradually increase over the next 20 years, while projections over the next 50 to 100 years are highly uncertain.	20-year and 100-year time horizons.
Methane (CH_4)	*Biogenic methane:*			
	Released from anaerobic digestion of tundra	12.5 years	Methane released is measured in annual pulses that are occurring or projected to occur over the next 20 years.	Annual time horizon, due to annual regional pulses affecting selected regions.
	Methane hydrate release ("methane pulse")	12.5 years	Methane hydrate released is measured in decadal pulses that are projected to occur over the next 20 years.	20-year time horizon.
	Anthropogenic Methane:			
	Agriculture-based sources (e.g., live-stock, rice production)	12.5 years	Industrial methane releases will increase significantly over the next 20 years (2010-2030).	Annual and 20-year time horizon.
	Off-gas from coal, oil and gas industries	12.5 years	Industrial methane releases will increase significantly over the next 20 years (2010-2030).	Annual and 20-year time horizon.
Tropos-pheric Ozone (TO)	Plumes and seasonal isopleths**	Weeks	Formation from NO_X, SO_X and VOCs in sunlight occurs seasonally. TO is detected and tracked by satellite in concentrated regional plumes over periods of weeks.	Annual time horizon fits best, but a 20-year time horizon is also appropriate for contin-uous emission sources.
Black Carbon (BC)	Plumes and seasonal concentration increases	Weeks or days	BC plumes are produced from forest fires over days and weeks.	Annual time horizon for specific events.
		Weeks or days	BC emissions are produced as emissions from cooking fires and diesel engines on a daily basis.	20-year time horizon for continuous emission sources.
		Weeks or days	Deposition of black carbon onto snow and ice sheets results in the loss of albedo on a seasonal basis each year.	Annual time horizon.
Nitrous Oxide (N_2O)	Concentration increases over decades and centuries	114 years	Accumulated N_2O loading will build over the next century.	20- and 100-year time horizons.
Tropo-spheric Sulfate Aerosols (TSA)	Continuous daily point source emissions	Weeks or days	Aerosols form steady-state isopleths of cooling over regions on a seasonal and daily basis.	Fate and transport is characterized with the annual time horizon. 20-year time horizon for continuous emission sources.

* Halocarbons and sea salt will be added to this table at a future date.
** Tropospheric ozone isopleth data are not currently available. For this practice, European Environmental Agency AOT-40 data (accumulated ozone concentrations over threshold during the ozone season) are used. http://dataservice.eea.europa.eu/

According to Archer *et al.*, (2009):

> *"Common measures of the atmospheric lifetime of CO_2, including the e-folding time scale, disregard the long tail. Its neglect in the calculation of global warming potentials leads many to underestimate the longevity of anthropogenic global warming. Here, we review the past literature on the atmospheric lifetime of fossil fuel CO_2 and its impact on climate, and we present initial results from a model intercomparison project on this topic. The models agree that 20–35% of the CO_2 remains in the atmosphere after equilibration with the ocean (2–20 centuries). Neutralization by CaCO3 draws the airborne fraction down further on timescales of 3 to 7 kyr."* [24]

The framework reverses the commonly used order and priority of establishing time horizons by modeling shorter time horizons first and then longer time horizons.[25] This approach is consistent with standardized life-cycle impact assessment (ISO-14044), starting at the point at which modeling certainty is greatest. As illustrated by the various GHG models referred to by IPCC (Figure B2-1 in Section 2 of this Annex), the certainty of modeled results for GHG is highest for projections within shorter time horizons; predictive accuracy decreases as time horizons increase.

Step 6: Establishment of LCSEA Category Indicators and Characterization Factors

The key GHGs are converted into LCA "category indicators," as defined by ISO-14044, in order to calculate current and projected loadings. Under the framework, the "legacy" loadings of longer-lived GHGs that have accumulated over time in the atmosphere are calculated for the baseline year 2010 (see Section 4). From this baseline, the loading from current annual emissions can be calculated, leading to projections of increases in accumulated loadings over various time horizons, taking into consideration the potential incremental loading over the specified time horizon and the rate of atmospheric decay.

The equations used to calculate GHG loadings integrate GWPs, RWPs, GCPs, RCPs, and ECFs, described in Sections 2 and 3. The equations are described in Section 4. The following equivalency factors are included in the equations.

[24] David Archer, Michael Eby, Victor Brovkin, Andy Ridgwell, Long Cao, Uwe Mikolajewicz, Ken Caldeira, Katsumi Matsumoto, Guy Munhoven, Alvaro Montenegro, and Kathy Tokos. "Atmospheric Lifetime of Fossil Fuel Carbon Dioxide," *Annual Review of Earth and Planetary Sciences*, Vol. 37: 117-134, May 2009. First published online January 26, 2009.

[25] Climate frameworks based solely on GWP indexing actually become less accurate the shorter the time horizon. Thus, climate frameworks rely upon the 100-year time horizon even though it has little environmental impact relevance in the near term. Such frameworks lack the algorithm structure to complete the 20-year time horizon for short-lived key GHGs, as well as the capacity to establish annual time horizons.

- **Loading Potency Factor: GWP and RWP**
  Loading potency factors apply only to anthropogenic emissions.
  - Global warming potentials (GWPs) represent the relative radiative forcing potencies of key GHGs amortized over a specific time horizon, using carbon dioxide as the reference GHG and reported in tonnes CO_2e.
  - Regional warming potentials (RWPs) factor in additional sources of radiative forcing affecting a region that are not covered under global accounting protocols. They also use carbon dioxide as the reference GHG and are reported in tonnes CO_2e within a regional framework.

- **Cooling Potency Factor: GCP and RCP**
  Cooling potency factors apply only to anthropogenic emissions.
  - Global cooling potentials (GCPs) represent the relative radiative cooling potencies of key GHGs amortized over a specific time horizon, using carbon dioxide as the reference GHG and reported in minus tonnes CO_2e.
  - Regional cooling potentials (RCPs) are the relative radiative cooling potencies of specific GHGs relative to particular regions, using carbon dioxide as the reference GHG and reported in minus tonnes CO_2e.

- **Pulse Warming Potential (PWP)**
  Pulse warming potentials represent specific biogenic emission pulses that are projected to be orders of magnitude larger than the largest current anthropogenic global loadings by aggregated major source (e.g., from total transportation, from total electricity generation). For example, although the largest global anthropogenic loading currently comes from carbon dioxide (expected to add approximately 386 billion tonnes over the next 20 years), the projected Siberian methane pulse from melting permafrost could be approximately 5,000 billion tonnes CO_2e over the same time horizon.[26] The PWP factors the scale of global loadings by major source compared to the scale of a specific pulse.

- **Precursor Conversion Factor (PCF)**
  The precursor conversion factor (PCF) represents the ratio at which a specific emission precursor leads to the formation of a key GHG on a per tonne CO_2e basis. For example, NO_X interacts with ultraviolet radiation to convert oxygen into tropospheric ozone.

- **Environmental Characterization Factor (ECF)**
  The ECF represents the relative degree to which a specific key GHG affects climate anomalies (midpoint intensification) on a global or regional basis. Characterization factors are described and defined throughout the remainder of this Annex.

[26] N. Shakhova, I. Semiletov, A. Salyuk, D. Kosmach, "Anomalies of Methane in the Atmosphere Over the East Siberian Shelf: Is There Any Sign of Methane Leakage from Shallow Shelf Hydrates?" *Geophysical Research Abstracts,* Vol. 10, EGU2008-A-01526, 2008 SRef-ID: 1607-7962/gra/EGU2008-A-01526 EGU General Assembly 2008.

Step 7: Establishment of Equations to Calculate Key GHGs

Section 4 of this Annex presents the basic equations and specific equivalencies for the key GHGs. All loadings are reported in tonnes CO_2e. Any data sources using parts per million volume (ppmv) or parts per billion volume (ppbv) units of measurement estimates are converted into mass concentrations (e.g., ppbm) before indicator results are calculated.

1.3. Key GHGs Included in Global and Regional GHG Accounting Protocols

- **Global GHG Accounting Protocols**
  All of the key GHGs are included in the global GHG accounting protocols. Annual loadings are established for the short-lived GHGs, while accumulated loadings are established for methane, carbon dioxide and nitrous oxide during the period from 1850 to 2010. Figure B1-5 shows the amount of emissions (in billion tonnes CO_2e) that each of the key GHGs with positive radiative forcing contribute to the total global GHG loading. Section 2 of this Annex provides information regarding the metadata supporting the figure. Carbon dioxide currently constitutes approximately 35 percent of the total accumulated global GHG loading.

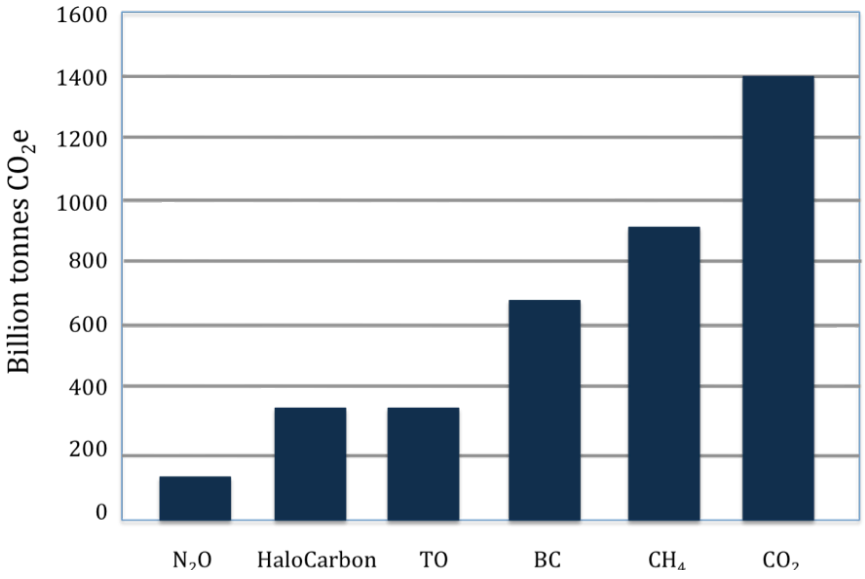

Figure B1-5.
2010 GHG Loadings

- **Arctic GHG Accounting Protocols**
  Black carbon, tropospheric ozone and methane are the predominant GHGs impacting the Arctic climate. Section 3 presents the detailed discussion of these key GHGs in the context of the Arctic GHG accounting protocols. Tropospheric sulfate aerosols are considered key GHG coolants for the region.

- **Antarctica GHG Accounting Protocols**
  Southern hemispheric sources of tropospheric ozone in South America and Southern Africa account for the strong TO anomalies modeled by Mozart 4 above the ocean water close to Antarctica. The halocarbons involved in the stratospheric ozone depletion over Antarctica are considered key Antarctic GHG coolants.

2.0. Global GHG Accounting Protocols

Within the LCSEA GHG Accounting Framework, global GHG accounting protocols have been developed to focus on global-scale key GHGs and their environmental and human health effects. The steps described in section 1.2 were used to establish these protocols. The following discussion identifies data sources and elaborates upon concepts discussed in Section 1 as they pertain to the global GHGs.

2.1. Global Stressor-Effects Network and Nodal Characterization

The global stressor-effects network represents the cause-effect linkages associated with key GHGs and their subsequent effects on a global scale. The global stressor-effects network is summarized in Column 1 of Table B2-1 below. The remaining columns of the table summarize the characterization conducted by node, based on currently published climate data and life-cycle environmental data.[1] Nodal characterization is provided for both the current (2010) timeframe, and for the projected 20-year timeframe ending in 2030. The 100-year time horizon for 2100 could not be characterized due to the uncertainties in projecting emissions that far into the future.

2.1.1. Node 1: Key GHG Emissions

For the 2010 emissions of carbon dioxide, methane, nitrous oxide, CFCs and HFCs, the major contributions from anthropogenic sources were established from emissions source data based on the United Nations Framework Convention on Climate Change (UNFCCC) National Inventory Submissions (annually updated).[2,3] The global sources for the short-lived key GHGs —tropospheric ozone, black carbon, and tropospheric sulfate aerosols — number in the millions. While an inventory of these GHGs has not been included in the UNFCCC protocols, they are often included in country-level environmental regulation and reporting requirements. Reliable regional air quality data therefore is often available. When available, these regional sources have been inventoried.

The data for Node 1 were derived from significant peer-reviewed journal articles, including: the 2007 IPCC Climate Change Synthesis Report and its supporting documents; the Earth Observing System (EOS); the Princeton University GDLP model; and the NASA Goddard Institute of Space Science (GISS) model. For short-lived GHGs, the nodal characterization data relies on the most recent research conducted by NASA/GISS. Shindell *et al.* (2008) described the importance of incorporating the short-lived GHG emissions into global climate calculations and projections.[4]

[1] Data quality assessment is an ongoing process and will continue during the draft phase of this practice. As a result, it is assumed that this table will be revised as new data become available.

[2] UNFCCC, National Inventory Submissions (by year), http://unfccc.int/national_reports/annex_i_ghg_inventories/national_inventories_submissions/items/4303.php.

[3] Sectoral contributions reported in the IPCC Climate Change 2007 Synthesis Report were not used here or elsewhere in this Annex, as those values are based on the 100-year time horizon.

[4] D.T. Shindell, H. Levy II, M.D. Schwarzkopf, L.W. Horowitz, J.F. Lamarque and G. Faluvegi, "Multimodel Projections of Climate Change From Short-Lived Emissions Due to Human Activities." *Journal of Geophysical Research*, Vol. 113, 2008.

Table B2-1. Global Climate Change Stressor-Effect Network — Characterization by Node

Node	Nodal Characterization: Current (as of 2010)		Nodal Characterization: Projected (as of 2030)	
Stressor Node 1: Annual Anthropogenic Emissions of Key GHGs by Type (Billion Tonnes)	*Key GHG* [a]	*Emission Level*	*Key GHG*	*Emission Level*
	CO_2	34.0	CO_2	To be determined
	CH_4	0.60	CH_4	To be determined
	N_2O	To be determined	N_2O	To be determined
	Halocarbons	To be determined	HFCs	To be determined
	TO	0.34	TO	To be determined
	BC	0.015-0.020	BC	To be determined
	TSA[b]	0.13 (SO_2e)	TSA	To be determined
Midpoint Node 2: Annual Anthropogenic Loadings of Key GHGs by Type (Billion Tonnes CO_2e)	*Key GHG*	*Annual Loading*	*Key GHG*	*Annual Loading*
	CO_2	34	CO_2	~ 50 to 76
	CH_4	37 to 45	CH_4	To be determined
	N_2O	3.5	N_2O	~ 7
	Halocarbons	To be determined	HFCs	To be determined
	TO	330	TO	~ 500
	BC	676	BC	~800
	TSA Coolant	To be determined	TSA	To be determined
Midpoint Node 3: Accumulated Loading Anomalies of Key GHGs (1850-2010) [c] (Billion Tonnes CO_2e)	*Key GHG*	*Accum. Ldg. Anomaly*	*Key GHG*	*Accum. Ldg. Anomaly*
	CO_2	1,400-1,558	CO_2	~1,400
	CH_4	916	CH_4	~1,500 to 3,000
	N_2O	134	N_2O	~ 400
	Halocarbons	320	HFCs	To be determined
	BC	--	BC	--
	TO	--	TO	--
	TSA	--	TSA	--
	Sum (∑)	2,881	*Sum (∑)*	~ 3,300 to 4,800
	Arctic Methane Pulse	Not measured	*Arctic Methane Pulse*	~ 5,850
	Pre-Industrial Baseline	~ 5,000	*Pre-Industrial Baseline*	~ 5,000
	Total	~ 7,881	*Total*	~ 14,150 to 15,650
Midpoint Node 4: Radiative Forcing Anomaly (W/m^2)	*Key GHGs*	*RF Anomaly*	*Key GHGs*	*RF Anomaly*
	CO_2	+1.66	CO_2	+2.0
	CH_4	+0.48	CH_4	+0.64 to 3.28 (or 7.4[d])
	N_2O	+0.16	N_2O	+0.3
	Halocarbons	+ 0.34	HFCs	< +0.4
	BC (direct & indirect)	+ 0.9	BC (direct & indirect)	+1.2 to 1.4
	TO	+0.37	TO	+0.6
	TSA (direct & indirect)	- 0.9	TSA (direct & indirect)	-1.4
	Total RF Anomaly	+3.0	*Total RF Anomaly*	+3.74 to ≥ +6.58
Midpoint Node 5: GMT Anomaly (°C) [e]	*GMT Anomaly*	0.4	*GMT Anomaly*	0.8 to 1.5 (or 4.4[d])
Nodes 6 - 8: Threshold Exceed-ances; Structural and Ecosystem changes	*Threshold Exceedances; Structural and ecosystem changes*	To be determined	*Threshold Exceedance Structural and ecosystem changes*	To be determined

a) As noted in Section 1 and discussed in greater detail below, several categories of emissions identified by IPCC as GHGs are not included here because they do not meet the "key GHG" radiative forcing threshold of ±0.1 W/m^2.
b) TSAs (tropospheric sulfate aerosols) provide a net cooling effect (i.e., negative radiative forcing), and thus can have indirect effects on tonnes CO_2e loading, both positive and negative, during cooling-degree days (CDD) and heating-degree days (HDD). Estimated values in the table include both direct and indirect effects on radiative forcing.
c) Only key GHGs with atmospheric lifetimes greater than one year have accumulating loadings; therefore, only carbon dioxide, methane, and nitrous oxide are included in Node 3.
d) Upper range includes the projected methane hydrate pulse. See Section 3, Arctic GHG Accounting Protocols.
e) The current and projected GMT anomalies are relative to the lower estimated GMT Threshold Anomaly of +1.5.

As stated above, the IPCC 100-year time horizon (from 2000 to 2100) could not be characterized due to the significant uncertainties in emissions projections that far into the future. For example, models highlighted in the IPCC 2007 Special Report on Emissions Scenarios (SRES) project that 2100 annual CO_2 loadings will range from a low of 30 to a high of 135 billion tonnes per year — a four-fold difference in projections.[5] Other sets of 100-year time horizon characterization data are equally uncertain (Figure B2-1). Note the broadly diverging trend lines in the figure as the time approaches one hundred years.

Projected increases in carbon monoxide, methane and NO_X are shown in Figure B2-2. Over the next twenty years, NO_X emissions are projected to double, while anthropogenic methane emissions are expected to increase by at least 70 percent.[6] Specific emissions are described further under the discussion of Node 2 in section 2.1.2.

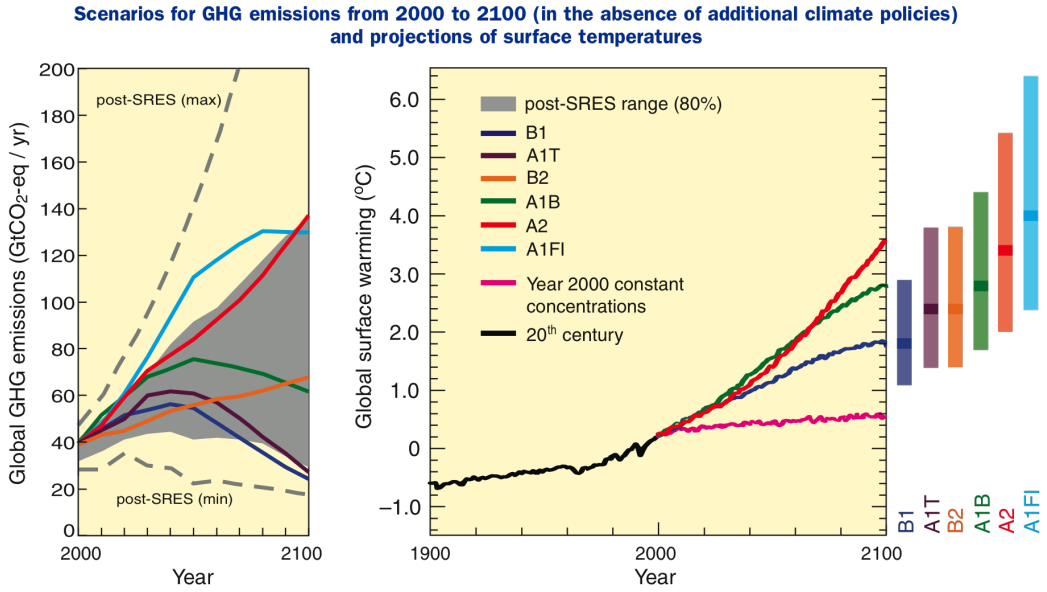

Figure SPM.5. ***Left Panel:*** *Global GHG emissions (in $GtCO_2$-eq) in the absence of climate policies: six illustrative SRES marker scenarios (coloured lines) and the 80th percentile range of recent scenarios published since SRES (post-SRES) (gray shaded area). Dashed lines show the full range of post-SRES scenarios. The emissions include CO_2, CH_4, N_2O and F-gases.* ***Right Panel:*** *Solid lines are multi-model global averages of surface warming for scenarios A2, A1B and B1, shown as continuations of the 20th-century simulations. These projections also take into account emissions of short-lived GHGs and aerosols. The pink line is not a scenario, but is for Atmosphere-Ocean General Circulation Model (AOGCM) simulations where atmospheric concentrations are held constant at year 2000 values. The bars at the right of the figure indicate the best estimate (solid line within each bar) and the* likely *range assessed for the six SRES marker scenarios at 2090-2099. All temperatures are relative to the period 1980-1999. {Figures 3.1 and 3.2}*

Figure B2-1. IPCC Synthesis 2007 Scenarios for GHG emissions from 2000 to 2100[7]

[5] Shorter-term projections also vary widely. The IPCC *Climate Change 2007 Synthesis Report, Fourth Assessment Report (AR4)* noted: "The IPCC Special Report on Emissions Scenarios (SRES, 2000) projects an increase of global GHG emissions by 25 to 90 percent (CO_2e) between 2000 and 2030." pp. 7.

[6] F. Dentener , D. Stevenson , J. Cofala , R. Mechler , M. Amann , P. Bergamaschi , F. Raes , and R. Derwent. "The Impact of Air Pollutant and Methane Emission Controls on Tropospheric Ozone and Radiative Forcing: CTM Calculations for the Period 1990–2030, *Atmospheric Chemistry and Physics*, Vol. 5, 2005, pp. 1731–1755.

[7] IPCC, *Climate Change 2007: Synthesis Report. Fourth Assessment Report (AR4). Summary for Policy Makers*, pp. 7.

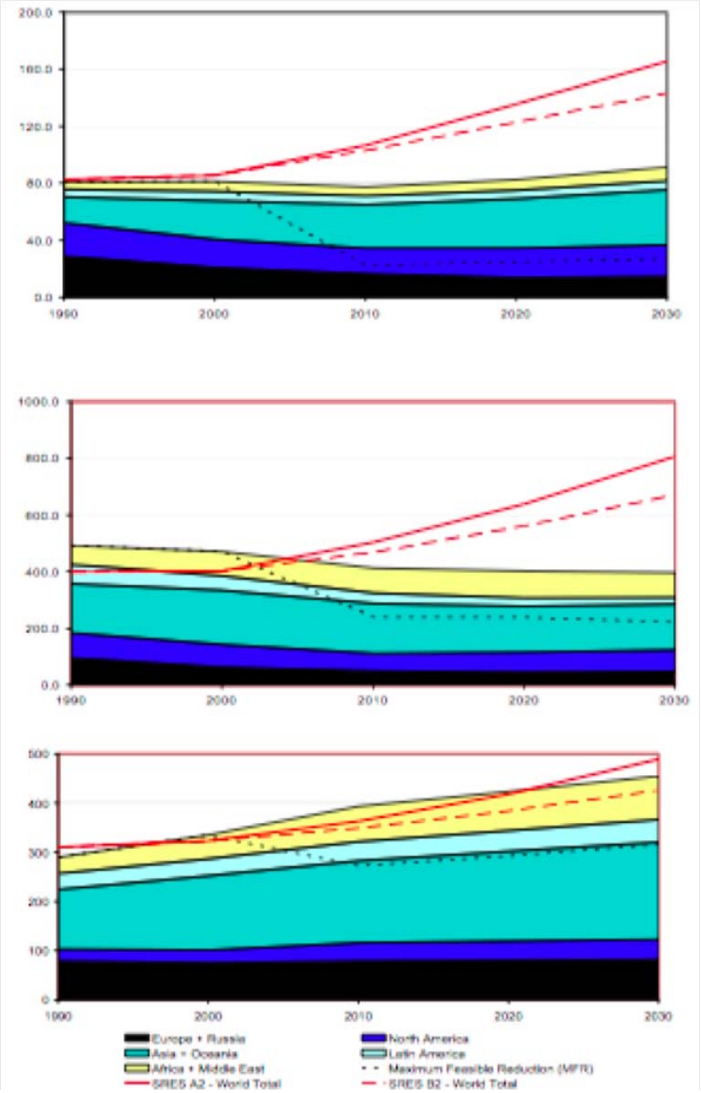

Figure B2-2. Projections of Anthropogenic NOx, CO and Methane Emissions through 2030.
Source: Excerpt of Figure 1 from Dentener et al., 2005: "Projected development of IIASA anthropogenic emission by SRES world regions upper NO_X (Tg NO2 yr^{-1}) middle CO (TG yr^{-1}) lower CH_4 (Tg yr^{-1}). Red lines indicate IPCC SRES scenarios; black dashed line MFR."

2.1.2. Node 2: Key GHG Loadings

In order to determine annual loadings for key GHGs, the global GHG accounting protocols apply an annual time-horizon GWP equation described in Section 4 of this Annex, which is extrapolated from the IPCC GWP Index. Table B2-2 provides the list of global category indicators, along with their respective GWP values over two time horizons — annual and 20-year — using the 100-year time horizon as a reference baseline and assuming the first 20-year time horizon interval starts in 2010 and ends in 2030.

Table B2-2. Global Category Indicators with Environmentally Relevant Global Warming Potentials for Annual, 20-year and 100-year Time Horizons[8]

Global Category Indicators	GWP — Annual	GWP — 20 Years	GWP — 100 Years
Carbon Dioxide Loading	1	1	1
Methane Loading	105	72	*
Nitrous Oxide Loading	286	289	310
Halocarbon Loadings and Cooling	See Section 2.1.2.1.		
Tropospheric Ozone Loading (non-plume specific)	970	66**	**
Black Carbon Loading (non-plume specific)	34,000	2,312**	**
Tropospheric Aerosol Sulfate Cooling	- 4,826	- 330**	**
Sea Salt Cooling (Anthropogenic)	TBD	TBD	TBD

** $GWP_{100\text{-}years}$ for methane has no environmental relevance, since methane converts to CO_2 within 8-20 years, and is thereafter present in the atmosphere as CO_2 for 80-92 years (GWP=1).*
*** Continuous daily emissions of short-lived GHGs from specific sources only have environmentally relevant GWPs over the operational lifetime of the sources.*
TBD is to be determined

- **Carbon Dioxide and Nitrous Oxide —** The IPCC 2007 Synthesis Report projected annual carbon dioxide emissions of approximately 34 billion tonnes for 2010. Since all of the key GHGs are benchmarked against carbon dioxide to calculate "loadings," 34 billion tonnes also serves as the loading value in Node 2. The IPCC report also provides data related to nitrous oxide emissions, which are then converted to loadings by the algorithms shown in section 4.

  2030 Projected Loading — The same report projected the 2030 carbon dioxide annual emissions to range from 50 to 76 billion tonnes. The increases in emissions of carbon dioxide and N_2O projected by IPCC were used for the nodal characterization summary data presented in Table B2-1 above.

- **Methane —** Total annual methane emissions from anthropogenic sources have been estimated at about 350-428 million tonnes on a global basis.[9] This rate of emissions translates into an annual loading of 37-45 billion tonnes CO_2e, if an annual time horizon GWP of 105 is applied, or 25-31 billion tonnes CO_2e, if the IPCC GWP for the 20-year time horizon of 72 is used.

  2030 Projected Loading — Projections for the 2030 methane loading are expected to increase by 55-60 percent over current levels, in line with the projected increase in background concentration from the current 1790 parts per billion (ppb) to 2500 – 2800 ppb (assuming that methane sinks remain largely unchanged).[10] These estimates remain highly uncertain, given that they do not include uncontrolled releases of biogenic emissions of methane from northern tundra decomposition or methane hydrates. If conditions in the Arctic result in the release of biogenic emissions from

[8] The 20 and 100-year GWPs for carbon dioxide, methane and nitrous oxide are values published by IPCC. The remaining GWPs in this table were calculated using the equations found in Section 4 of this Annex.
[9] IPCC, *Climate Change 2007: Synthesis Report* (AR4)
[10] Carlos Feu Alvim, Omar Campos Ferreira and José Israel Vargas. "Growth of Methane Concentration in the Atmosphere (Its Impact on the Implementation of Kyoto Protocol)" *Economy & Energy*, Year IX, No 55, April – May 2006.

these sources, they will far outweigh even the most aggressive estimates for anthropogenic methane emissions.

- **Halocarbon Loadings**

Halocarbons Cause both Positive and Negative Radiative Forcing

Halocarbons (CFCs, HCFCs, and halons) have complex atmospheric chemistry. When first released, they cause positive radiative forcing associated with high GWP values. Afterward, however, they decompose, releasing either chlorine or bromine free radicals that destroy both stratospheric and tropospheric ozone through a well understood chemical reactive pathway. One molecule of chlorine can destroy 100,000 molecules of ozone, while bromine can destroy up to one billion ozone molecules. This ozone destruction results in negative radiative forcing. By contrast, fluorine is incapable of forming free radicals, and thus causes only positive radiative forcing with no potential to cause negative forcing.

The IPCC has provided current data and projections of overall radiative forcing anomalies, both positive and negative, resulting from accumulated emissions of the various halocarbons subclasses from now through 2100 (Figure B2-3). These projections indicate that only CFCs currently meet the minimum RF threshold ($\pm 0.1 W/m^2$) to qualify as a key GHG, while HFCs will be projected to surpass this threshold by 2030.[11]

Figure B2-3. Radiative Forcings of GHGs

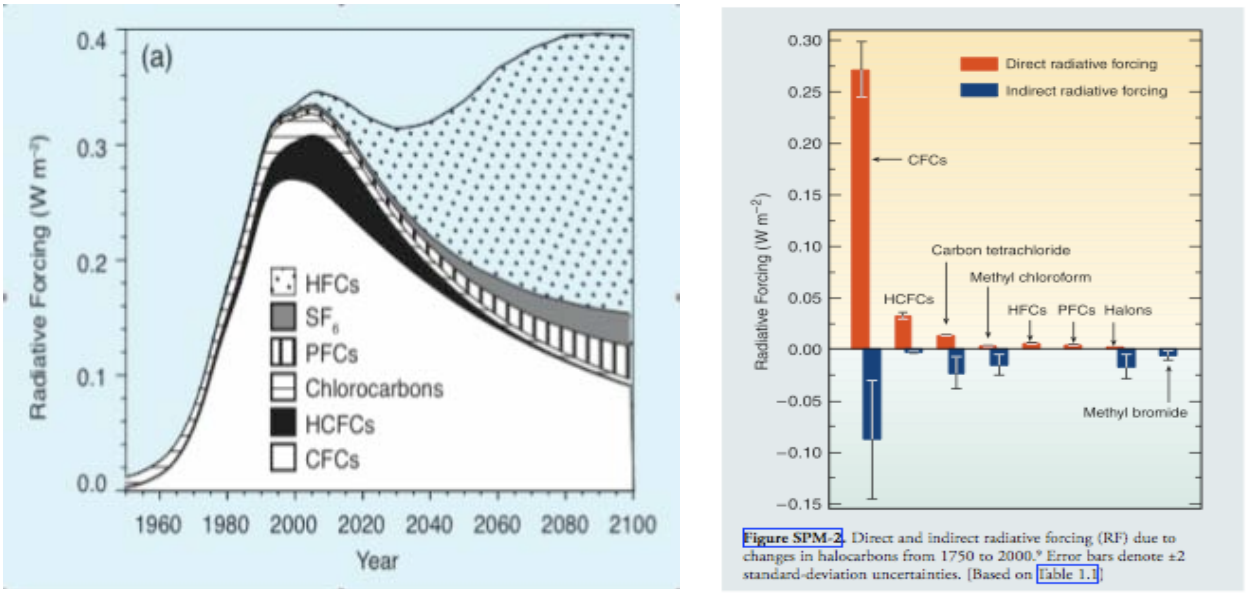

Sources: IPCC 2007 and 2008 [12,13]

Positive and Negative GWP values of the Halocarbons

[11] IPCC, *Special Report on Ozone and Climate*, 2007. Chapter 1. Page 123. Report accessible at: http://www.ipcc.ch/ipccreports/sroc.htm

[12] *Ibid.*

[13] IPCC/TEAP Special Report, *Safeguarding the Ozone Layer and the Global Climate System: Issues Related to Hydrofluorocarbons and Perfluorocarbons*, 2008.

The IPCC has recognized the both warming and cooling effects of halocarbons by assigning both positive and negative GWPs (referred to in this framework as radiative cooling potentials, or RCPs) to various subclasses of halocarbons (Table B2-3), along with assigning the halocarbons the standard positive GWP values.[14]

Table B2-3. Positive and Negative GWP Values for Halocarbons

Source: IPCC[15]

Table SPM-1. GWPs of halocarbons commonly reported under the Montreal Protocol and the UNFCCC and its Kyoto Protocol and assessed in this report relative to CO_2, for a 100-year time horizon, together with their lifetimes and GWPs used for reporting under the UNFCCC. Gases shown in blue (darker shading) are covered under the Montreal Protocol and gases shown in yellow (lighter shading) are covered under the UNFCCC. [Tables 2.6 and 2.7]

Gas	GWP for direct radiative forcing[a]	GWP for indirect radiative forcing (Emission in 2005[b])	Lifetime (years)	UNFCCC Reporting GWP[c]
CFCs				
CFC-12	10,720 ± 3750	–1920 ± 1630	100	n.a.[d]
CFC-114	9880 ± 3460	Not available	300	n.a.[d]
CFC-115	7250 ± 2540	Not available	1700	n.a.[d]
CFC-113	6030 ± 2110	–2250 ± 1890	85	n.a.[d]
CFC-11	4680 ± 1640	–3420 ± 2710	45	n.a.[d]
HCFCs				
HCFC-142b	2270 ± 800	–337 ± 237	17.9	n.a.[d]
HCFC-22	1780 ± 620	–269 ± 183	12	n.a.[d]
HCFC-141b	713 ± 250	–631 ± 424	9.3	n.a.[d]
HCFC-124	599 ± 210	–114 ± 76	5.8	n.a.[d]
HCFC-225cb	586 ± 205	–148 ± 98	5.8	n.a.[d]
HCFC-225ca	120 ± 42	–91 ± 60	1.9	n.a.[d]
HCFC-123	76 ± 27	–82 ± 55	1.3	n.a.[d]
HFCs				
HFC-23	14,310 ± 5000	~0	270	11,700
HFC-143a	4400 ± 1540	~0	52	3800
HFC-125	3450 ± 1210	~0	29	2800
HFC-227ea	3140 ± 1100	~0	34.2	2900
HFC-43-10mee	1610 ± 560	~0	15.9	1300
HFC-134a	1410 ± 490	~0	14	1300
HFC-245fa	1020 ± 360	~0	7.6	–[e]
HFC-365mfc	782 ± 270	~0	8.6	–[e]
HFC-32	670 ± 240	~0	4.9	650
HFC-152a	122 ± 43	~0	1.4	140
PFCs				
C_2F_6	12,010 ± 4200	~0	10,000	9200
C_6F_{14}	9140 ± 3200	~0	3200	7400
CF_4	5820 ± 2040	~0	50,000	6500
Halons				
Halon-1301	7030 ± 2460	–32,900 ± 27,100	65	n.a.[d]
Halon-1211	1860 ± 650	–28,200 ± 19,600	16	n.a.[d]
Halon-2402	1620 ± 570	–43,100 ± 30,800	20	n.a.[d]
Other Halocarbons				
Carbon tetrachloride (CCl_4)	1380 ± 480	–3330 ± 2460	26	n.a.[d]
Methyl chloroform (CH_3CCl_3)	144 ± 50	–610 ± 407	5.0	n.a.[d]
Methyl bromide (CH_3Br)	5 ± 2	–1610 ± 1070	0.7	n.a.[d]

[a] Uncertainties in GWPs for direct positive radiative forcing are taken to be ±35% (2 standard deviations) (IPCC, 2001).
[b] Uncertainties in GWPs for indirect negative radiative forcing consider estimated uncertainty in the time of recovery of the ozone layer as well as uncertainty in the negative radiative forcing due to ozone depletion.
[c] The UNFCCC reporting guidelines use GWP values from the IPCC Second Assessment Report (see FCCC/SBSTA/2004/8, http://unfccc.int/resource/docs/2004/sbsta/08.pdf).
[d] ODSs are not covered under the UNFCCC.
[e] The IPCC Second Assessment Report does not contain GWP values for HFC-245fa and HFC-365mfc. However, the UNFCCC reporting guidelines contain provisions relating to the reporting of emissions from all greenhouse gases for which IPCC-assessed GWP values exist.

However, the IPCC GWP values for HFCs are based upon the 100-year time horizon

[14] *Ibid.*
[15] IPCC, *Special Report on Ozone and Climate*, 2007.

and must be extrapolated into the annual and 20-year time horizons to meet LCSEA GHG Accounting Framework requirements.[16] As shown in Table B2-4, the GWP values for almost all HFCs increase by many-fold, reflecting their extreme potency during their atmospheric lifetimes and once again pointing out the inapplicability of the 100-year time horizon for establishing GWPs for the shorter-lived GHGs.

Table B2-4. GWP Values for HFCs for Various Time Horizons

		IPCC Reference		
Chemical	**Lifetime, yr**	**GWP-100**	**GWP-20**	**GWP-1**
HFC-23	270	12,240	**10,200**	**7,650**
HFC-245fa	7.6	1,020	**3,400**	**6,800**
HFC-236ea	10.7	1,350	**4,091**	**6,750**
HFC-32	5.6	650	**2,321**	**6,500**
HFC-134	10.6	1,000	**3,030**	**5,000**
HFC-134a	14.6	1,300	**3,714**	**4,815**
HFC-125	32.6	2,800	**5,091**	**4,667**
HFC-227ea	36.5	2,900	**4,833**	**4,462**
HFC-365mfc	8.6	782	**2,523**	**4,344**
HFC-43-10mee	17.1	1,300	**3,421**	**4,333**
HFC-143a	48.3	3,800	**5,067**	**4,318**
HFC-245ca	6.6	560	**1,867**	**4,000**
HFC-236fa	209	6,300	**5,250**	**3,938**
HFC-143	3.8	300	**1,071**	**3,750**
HFC-152a	1.5	140	**467**	**3,500**
HFC-41	3.7	150	**556**	**2,143**

The IPCC 2008 report cautions against using these published positive and negative GWP values in an additive manner, stating that the cooling effects of halocarbons occur through an entirely different chemical pathway in different locations than the warming effects. For example, while halocarbons cause positive radiative forcing on a global basis, their destructive effect on stratospheric ozone at the tropics and mid latitudes has become much less severe. Overall stratospheric ozone DU values are recovering due largely to the indirect effects of the warming of the troposphere from GHG emissions, that in turn has lowered the overall temperature of the stratosphere and reduced the thermal oxidation potential of ozone. Furthermore, the reduction in CFC and HCFC releases has allowed mid- and tropical latitude ozone layers to recover. Both chlorine and bromine halocarbon subclasses cause significant cooling within the Antarctic cooling zone (i.e., the Antarctic Ozone Hole), as well as less pronounced cooling in the Arctic Region, as described in section 3.

- **Tropospheric Ozone (TO) —** The annual tropospheric ozone burden (steady state concentration) has been described in the scientific literature, with climate models

[16] Guus Velders *et al.*, 2009.

providing emissions estimates of about 340 million tonnes (±40).[17] Using the annual GWP established within this global GHG accounting protocol (970), 340 million tonnes equates to an annual loading of about 330 billion tonnes CO_2e.

The source average of over 4,470 billion tonnes yields a steady-state concentration of 340 million tonnes, which represents the average annual burden of tropospheric ozone globally (Table B2-3). The difference between the source amounts and steady-state atmospheric concentrations is derived from the fact that much of the ozone generated has a much shorter atmospheric lifetime than the 22.5 day average reported for the steady-state concentration. Hence, 340 million tonnes represents the "effective" 22-day concentration of ozone in the troposphere over one year.

2030 Projected Loading — Tropospheric ozone 2030 loading projections were obtained from Unger *et al.* 2008 (Table B2-5).[18]

Table B2-5. Global Model Budgets of Tropospheric Ozone in Recent Literature

Source: Table 1 excerpted from Wu Et Al.: Global Budgets Of Tropospheric Ozone[19]

	Sources, Tg yr^{-1}		Sinks, Tg yr^{-1}			
Reference	Chem. Production[b]	Stratospheric Index	Chemical Loss[b]	Deposition	Burden, Tg	Lifetime[c] days
Lelieveld & Dentener [2000]	3310	570	3170	710	350	33
Bey et al. [2001][d]	4900	470	4300	1070	320	22
Sudo et al. [2002]	4895	593	4498	990	322	21
Horowitz et al. [2003]	5260	340	4750	860	360	23
Von Kuhlmann et al. [2003]	4560	540	4290	820	290	21
Shindell et al. [2003]	NR[e]	417	NR	1470	349	NR
Hauglustaine et al. [2004]	4416	523	3918	1090	296	22
Park et al. [2004]	NR	480	NR	1290	340	NR
Rotman et al. [2004]	NR	690	NR	830	NR	NR
Wong et al. [2004]	NR	600	NR	1100	376	NR
Stevenson et al. [2004]	4980	395	4420	950	273	19
Wild et al. [2004]	4090	520	3850	760	283	22
Stevenson et al. [2006][f]	5110 (±610)	550 ± 170	4670 ± 730	1000 ± 200	340 ± 40	22 ± 2

a From global model simulations published since the IPCC TAR compilation, describing the atmosphere of the last decade of the 20th century.

b Chemical production and loss rates are calculated for the odd oxygen family, usually defined as $O_x \equiv O_3 + O + NO_2 + 2NO_3 + 3N_2O_5 +$ peroxyacetylnitrates (PANs) + HNO_3 + HNO_4, to avoid accounting for rapid cycling of ozone with short-lived species that have little implication for its budget. Chemical production is mainly contributed by reactions of NO with peroxy radicals, while chemical loss is mainly contributed by the $O(^1D) + H_2O$ reaction and by the reactions of ozone with HO_2, OH, and alkenes. Several models in this table do not report production and loss separately (''NR'' entry in the table), reporting instead net production. However, net production is not a useful quantity for budget purposes because (1) it is a small residual between large production and loss, (2) it represents a balance between STE and dry deposition, both of which are usually parameterized to some degree as flux boundary conditions.

c Calculated as the ratio of the burden to the sum of chemical and deposition losses.

d A more recent version of GEOS-Chem by Martin et al. [2003b] gives identical rates and burdens.

e Not reported.

f Means and standard deviations from an intercomparison study of 21 global models constrained to use the same anthropogenic and biomass burning emissions for ozone precursors.

[17] S. Wu, S., L. Mickley, D. Jacob, J. Logan, R. Yantosca and D. Rind. "Why Are There Large Differences Between Models in Global Budgets of Tropospheric Ozone?" *Journal of Geophysical Research*, Vol. 112, 2007.

[18] N. Unger, D. Shindell, D. Koch and D. Streets. "Air Pollution Radiative Forcing from Specific Emissions Sectors at 2030." *Journal of Geophysics Research*,Vol. 113, 2008.

[19] Wu *et al.*, 2007.

- **Black Carbon (BC) —** The black carbon emission total is estimated at approximately 15-22 million tonnes for 2010, which converts to an annual loading of 676 billion tonnes, based on a GWP_{Annual} of 34,000 (Figure B2-4).

Figure B2-4. Total Global Emission of Black Carbon from Diesel (million tonnes CO_2e)[20]

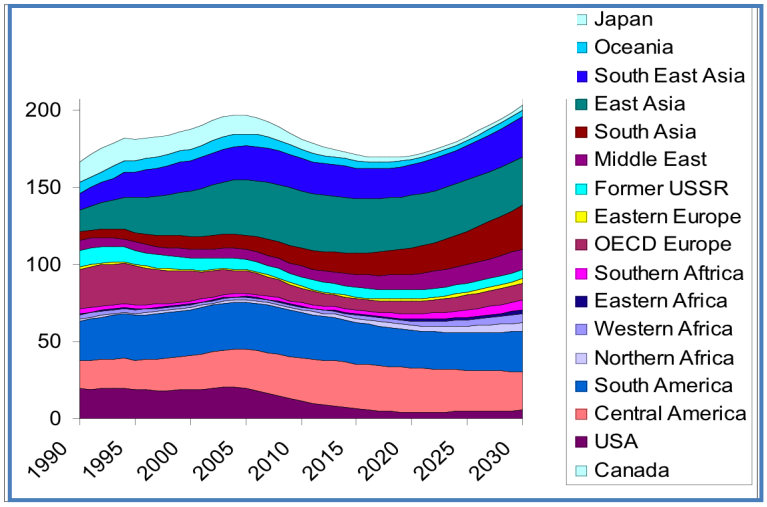

The major sources of black carbon are coal extraction and combustion, diesel combustion, cooking with fuel oils and dung, and wildfires.[21] While most black carbon has a very short atmospheric lifetime, ultra-fine black carbon has longer transport measured in weeks. Additionally, black carbon particulates deposited on ice sheets reduce the albedo of the ice and thereby contribute strongly to the loss of large ice sheets and glaciers.[22]

Aerial photographs provide striking evidence of the large quantities of black carbon produced by forest fires. This black carbon contributes to regional radiative forcing during the period of the burn. The amount of this loading that should be included in the global black carbon loading anomaly must be determined by estimating the current fire activity as compared to a baseline global fire activity level. In addition, because current fires are burning at hotter temperatures than in past years, they are producing much finer black carbon particulates that have greater transport potential. Thus, regional black carbon loadings, such as the Arctic black carbon loading, must factor in black carbon traveling great distances from forest fires. For example, black carbon loadings from boreal forest fires are considered a major threat to the perennial ice sheets of the Arctic and Greenland (see Section 3).

2030 Projected Loading — The black carbon loading is projected to increase by about 14 percent due to diesel emissions as compared to the 2010 loading (Figure B2-4).[23]

[20] Bond, Tami , Black carbon: Emission sources & prioritization *ICCT Black Carbon Workshop*, London, UK, January 5, 2009.
[21] *Ibid*
[22] Unger, N., and D. Shindell, D. Koch, and D Streets, "Air Pollution Radiative Forcing from Specific Emissions Sectors at 2030." Journal of Geophysics Research. Vol. 113, D02306. 2008.
[23] *Bond, Tami, January 5, 2009.*

- **Tropospheric Sulfate Aerosols**
  Annual global sulfur aerosol emissions from major sources are estimated at approximately 70 million tonnes. When converted to sulfur dioxide equivalents (SO_2e), this translates to 130 million tonnes of SO_2e emissions annually. The rate of conversion from SO_2e to sulfates is dependent on the time of year and the region, and has not yet been determined. The specific allocation of unwanted cooling versus "beneficial" cooling (by source) should also be determined by region and by season.

  2030 Projected Cooling — Projected emissions of tropospheric sulfate aerosols for 2030 have been estimated by GISS to increase by about 14 percent, while other estimates show a significant reduction in net annual TSA emissions.[24]

2.1.3. Node 3: Industrial Age Accumulated Loadings (1850-2010)

Node 3 involves establishing the "legacy" amounts of mid-lived (methane) and long-lived (CO_2 and N_2O) gases loaded into and accumulated in the atmosphere over the past 10,000 years, with the anomaly largely occurring between 1850-2010.

The IPCC 2007 Synthesis Report established the 10,000-year baseline and the current accumulated loadings for these gases as of 2005 (Figure B2-5). While the atmospheric concentrations of GHGs are often expressed in parts per million (ppm) or parts per billion (ppb), as in Figure B2-5, the global GHG accounting protocols require the calculation of loadings and accumulated loadings expressed in CO_2e to account for the levels of these key GHGs in the atmosphere.

The IPCC estimated the atmospheric concentration of carbon dioxide in 2005 to be about 375 ppm, as compared to the 150-year historic industrial baseline value of approximately 280-290 ppm.[25] This increase over baseline represents an anomaly of 85-95 ppm (avg. 90 ppm). When the 150-year anomalies from methane (+64 ppm CO_2e) and nitrous oxide (+4 ppm CO_2e) are included, the total anomaly from the background concentrations of these three GHGs is 158 ppm CO_2e compared to their collective historic industrial baseline value of 443 ppm CO_2e (from IPCC data, Figure B2-5), representing a 36 percent anomaly.

[24] Unger *et al.*, 2008.
[25] IPCC. *Climate Change 2007: Synthesis Report* (AR 4), 2007.

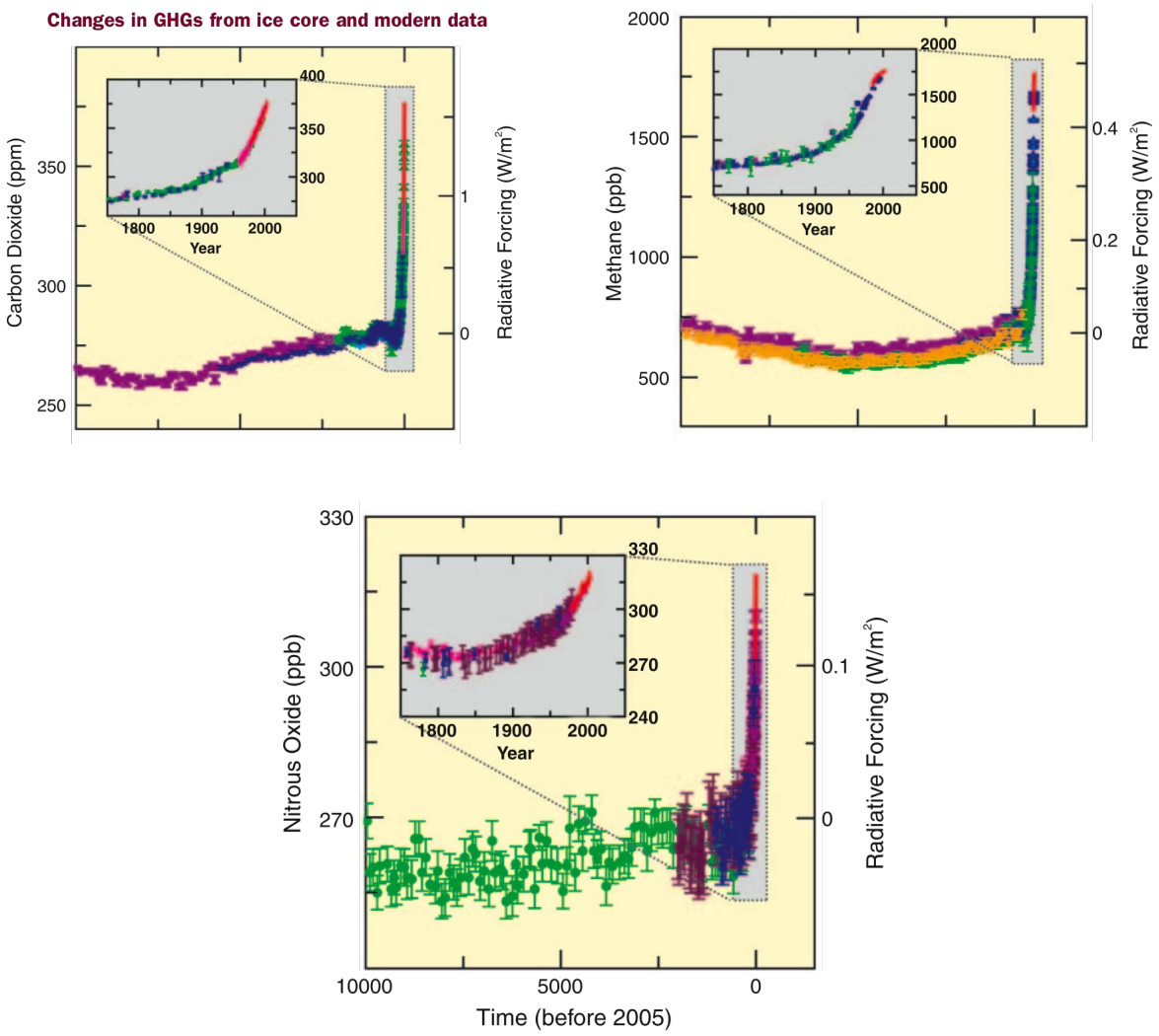

Figure B2-5. Current Accumulated Loadings of CO_2, CH_4 and N_2O over 10,000 Years in ppm
(Source: IPCC, 2007 Climate Change Synthesis Report, Fig. 2.3, transposed)

The total accumulated global loading of these three GHGs has been projected by the US Energy Information Administration at approximately 7,800 billion tonnes CO_2e for 2010 (Figure B2-5).

- **Accumulated Carbon Dioxide Estimates —** The current accumulated carbon dioxide loading anomaly falls between 1,400 and 1,558 billion tonnes CO_2, depending on methods of calculation used. The lower end of this range, 1,400 billion tonnes, was derived through the application of the LCSEA loading calculation methodology (section 4), while the upper end, 1,558 billion tonnes, is extrapolated directly from the IPCC data presented above.

- **Accumulated Methane Estimates —** The accumulated methane loading anomaly, as compared to the 150-year historic industrial baseline, is estimated at about 900 billion tonnes CO_2e, as extrapolated from IPCC data (Figure B2-4).

- **Accumulated Nitrous Oxide Estimates —** The accumulated nitrous oxide loading anomaly, as compared to the 150-year historic industrial baseline, is 134 tonnes CO_2e based on an extrapolation from IPCC data shown in Figure B2-5.

- **Accumulated CFC Estimates —** The accumulated loading of CFCs was estimated by extrapolating the known radiative forcing value of carbon dioxide compared to that of CFCs (+1.66 versus +0.34 W/m^2), yielding a total accumulated loading between 290 - 320 billion tonnes CO_2e, depending upon whether the lower or upper estimate of accumulated carbon dioxide loading is assumed.

Taken together, the total global accumulated loading anomaly for these four key GHGs is estimated at about 2,800 – 3,000 billion tonnes CO_2e compared to the total historic loading from all biogenic and anthropogenic sources of 7,800 billion tonnes CO_2e (see Figure B2-6).

Figure B2-6. Current and Projected Accumulated Well-Mixed Greenhouse Gas Loading (Node 3)
Source: Energy Information Administration, International Energy Outlook, 2003

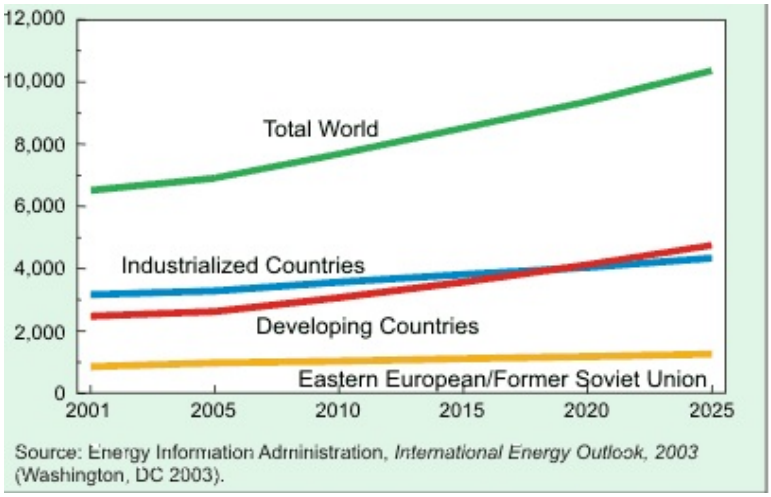

Figure B1-5 (section 1 above) highlights the summary data by combining both node 2 and node 3 data for each key GHG for 2010. As can be seen from that graph, the carbon dioxide loading contributes roughly 35 percent (in CO_2e) of the total loadings and loading anomalies from both the short-lived and longer-lived key GHGs.

2030 Projection of Accumulated CO_2 Loadings — The values for the projected carbon dioxide loadings are derived from IPCC-projected annual average increases. Projecting the methane loading is more problematic due to the potential for large, uncontrollable biogenic releases and the uncertainty surrounding the continuing capacity of existing sinks. The nitrous oxide loading is highly dependent upon agricultural practices, such as the use of fertilizers. Therefore, the 20-year projection for these two GHG emissions is highly uncertain, and should be updated over time with actual data.

Figure B2-7 shows that the projected accumulated carbon dioxide loading over the 20-year time horizon levels off. This leveling occurs even when applying an aggressive assumption of three percent compounded growth in annual emissions, which shows carbon dioxide growing from about 34 billion tonnes in 2010 to 60 billion tonnes by 2030 — the 95th percentile projection from the IPCC Special Report on Emissions Scenarios (SRES) modeling (Figure B2-1). The current annual carbon dioxide loading of 34 billion tonnes represents only two percent of the accumulated carbon dioxide loading at 1,400 billion tonnes.

Using IPCC decay equations, the accumulated 1,400 billion tonnes of legacy carbon dioxide will decay to just under 800 billion tonnes by 2030. In the meantime, the new accumulated loading from annual emissions between 2010 and 2030 will add approximately 598 billion tonnes by 2030, assuming three percent compounded annual growth based on a starting emission level of 34 billion tonnes CO_2e. Based on these assumptions, the new accumulated 2030 carbon dioxide loading will be just under 1,400 billion tonnes, slightly lower than the 2010 accumulated loading.

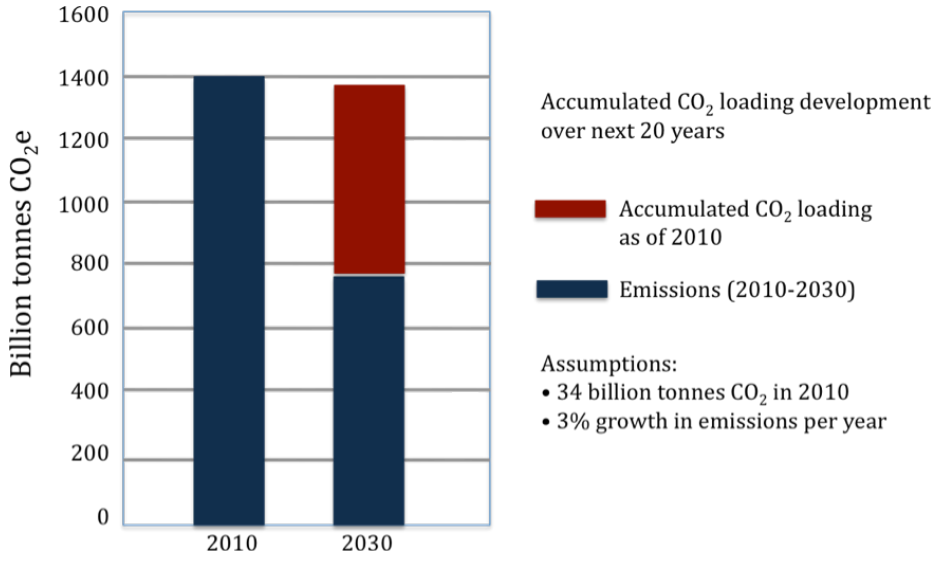

Figure B2-7. Integration of the legacy CO_2 and projected accumulated CO_2 loadings over the 20-year time horizon

Figure B2-7 suggests that carbon dioxide will not be a significant contributor to the GMT threshold by 2030.

Accumulated Carbon Dioxide Loadings beyond 2030

Using LCSEA methods, projections of the accumulated carbon dioxide loading beyond the 20-year time horizon are consistent with published IPCC projections, showing significant increases in accumulated loading by mid-century, provided that annual emission rates continue to increase in the 1-2 percent range. As illustrated in Figure B2-8, which shows the projected accumulated carbon dioxide loading in parts per million, the overall loading level does not rise above 2010 levels until about 2040, ten years beyond the projected 2030 GMT threshold. After 2040, carbon dioxide concentrations will rise significantly through the remainder of the century under a "business as usual" scenario, consistent with IPCC projections.

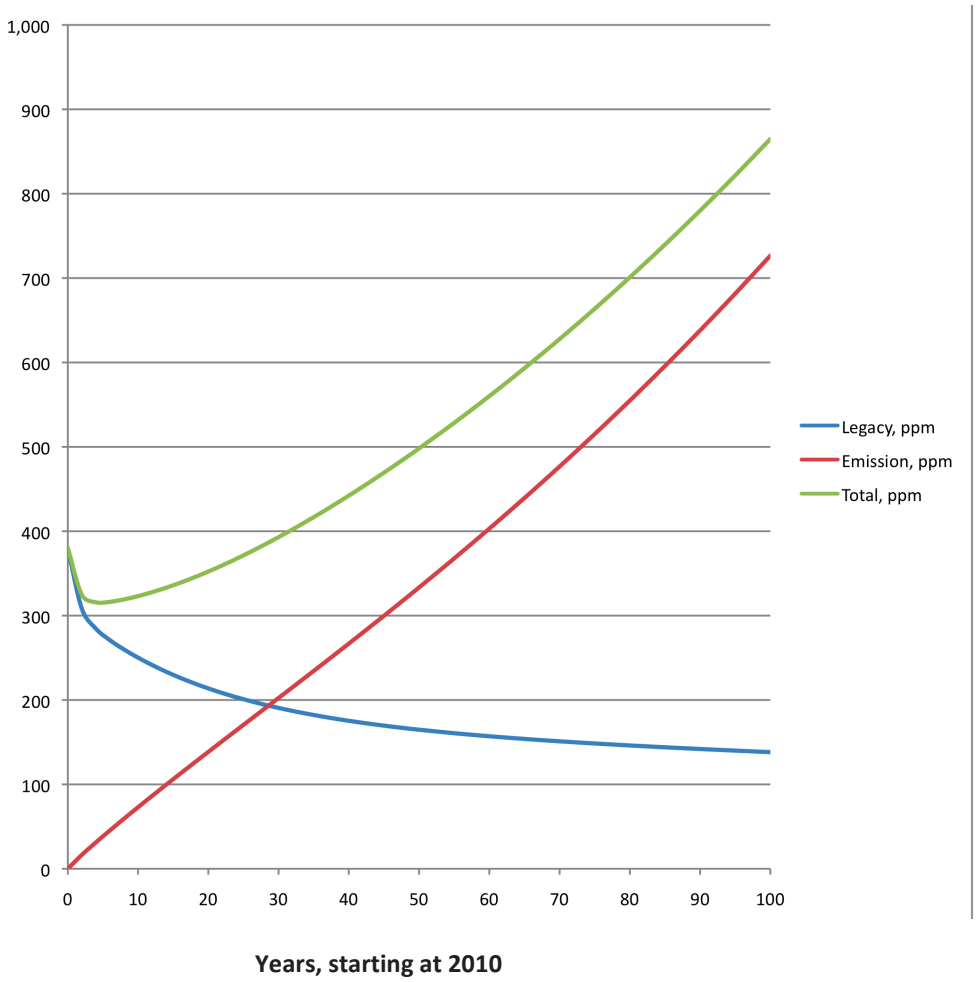

Figure B2-8. Long-term concentration of project carbon dioxide concentrations, as calculated by the LCSEA GHG Accounting Framework

2.1.4. Node 4: Global Radiative Forcing Anomalies of the Key GHGs

This node represents changes in global radiative forcing values since the start of the industrial age. These radiative forcing anomalies are consistent with those values presented in the IPCC 2007 Synthesis Report, adjusted by recent research and data on black carbon particulates and a growing consensus regarding the global radiative forcing of tropospheric ozone (e.g., Scripps, GISS).

Figure B4-9 shows the relative radiative forcing of various greenhouse gases and other drivers of climate change.

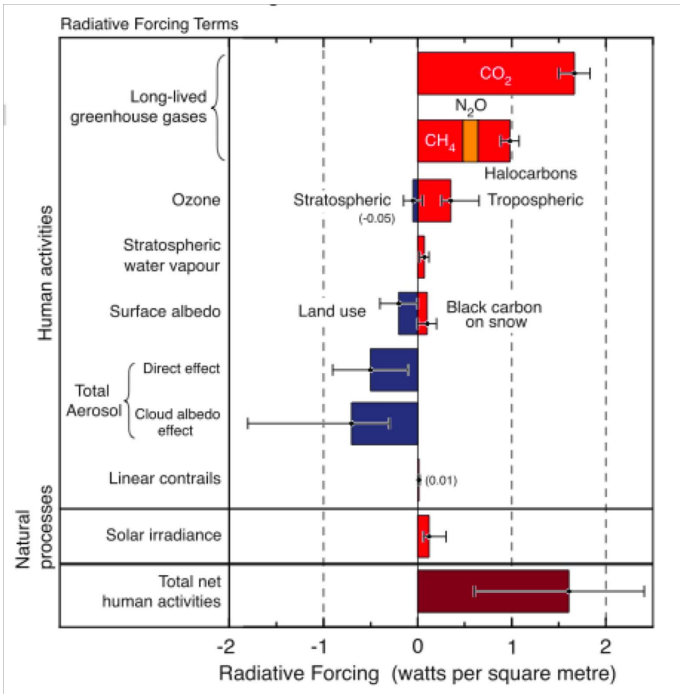

Figure B4-9. Radiative Forcing of Climate between 1750 and 2005
Source: IPCC 2007 Synthesis Report

2010 Radiative Forcing — 2007 NASA radiative forcing data (Figure B2-10) and the 2007 IPCC Synthesis Report provided the basic data for the characterization of the radiative forcing node for carbon dioxide, methane, nitrous oxide, halocarbons and tropospheric sulfate aerosols. With regard to black carbon, the Scripps Institute (2008) has studied its effects on global radiative forcing in the atmosphere, measuring an anomaly of approximately +0.9 W/m^2.[26] For tropospheric ozone, the most recent research has moved toward a consensus at the lower end of the IPCC estimates at around +0.43 W/m^2.[27] This level confirms that black carbon represents a significant global radiative forcing source and warrants inclusion as a key GHG.[28]

[26] Veerabhadran Ramanathan (Scripps Institution of Oceanography) and Greg Carmichael (University of Iowa). "Black Carbon Pollution Emerges as Major Player in Global Warming," *Nature*, March 23, 2008.
[27] M. Gauss *et al.* "Radiative Forcing Since Preindustrial Times Due to Ozone Change in The Troposphere and the Lower Stratosphere," *Atmospheric Chemistry and Physics*, Vol. 6, pp. 575–599, 2006.
[28] V. Ramanathan, 2008.

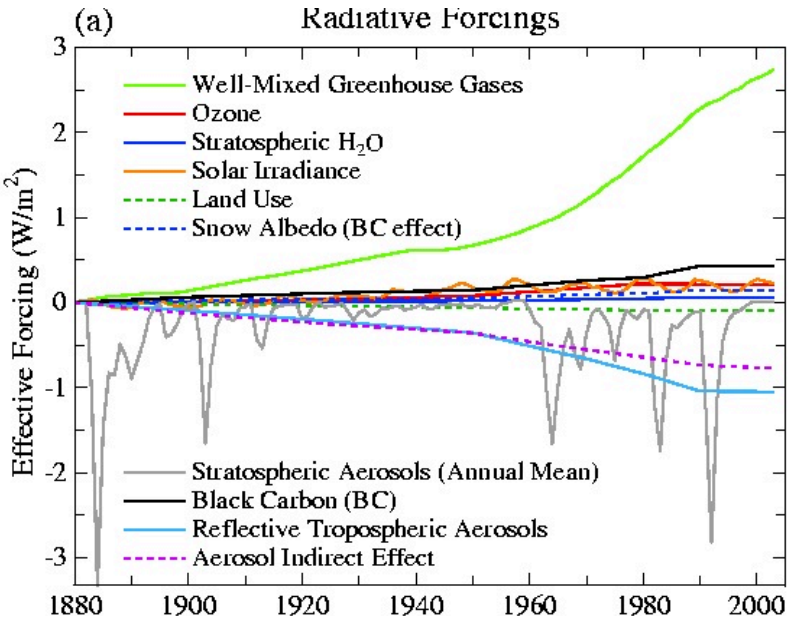

Figure B2-10. Radiative Forcing Anomaly from 1880 to 2005 from Various Sources (Node 4) ***(Source: NASA, based on calculations using 100 year time horizon protocols)***[29]

The isopleths presented in Figure B2-11 show the 2001 radiative forcing anomaly from anthropogenic sources of long-lived GHG emissions, with significant latitude-dependent variations. As can be seen, the 2001 radiative forcing anomaly from these long-lived GHG emissions ranged from a low value of +0.5 W/m^2 in the Antarctic to as much as +3.0 W/m^2 across wide bands in the northern and southern hemispheres.

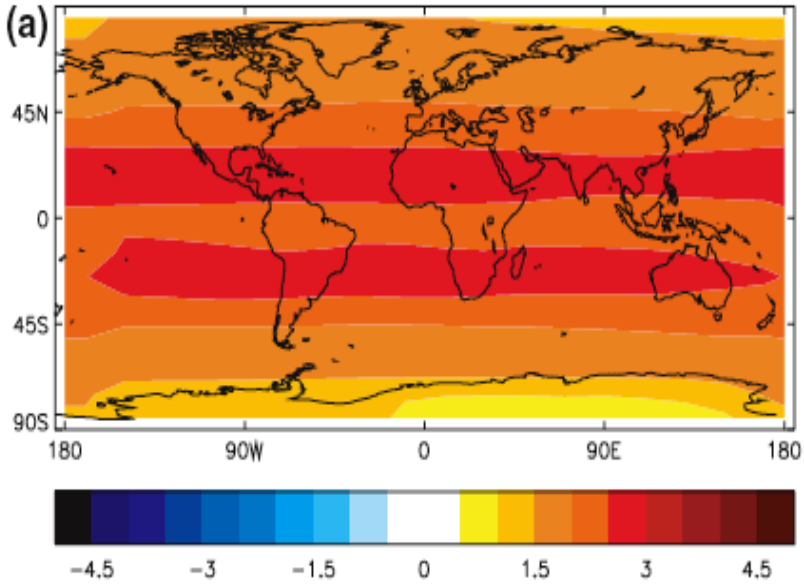

Figure B2-11. Isopleth mapping of Annual Average Radiative Forcing Anomaly from Anthropogenic Long-Lived GHGs— 2001 ***Source: IPCC (2001)***[30]

[29] NASA GISS Website: http://data.giss.nasa.gov/modelforce/
[30] IPCC Technical Report, *Radiative Forcing of Climate Change*, 2001.

More detailed estimates now show that the Arctic radiative forcing levels from the long-lived GHGs are less than +0.28 W/m^2 as opposed to the commonly assumed global average of 2.0 W/m^2.

2030 Projection of Radiative Forcing — The projected increases in radiative forcing shown in Table B2-6 were derived from values provided in Table B2-1 above. The contribution from carbon dioxide to total net increase in radiative forcing is projected to be no more than +0.4 W/m^2, which is a 10 to 23 percent contribution depending on the projections used.

Table B2-6. Net increase in radiative forcing between 2010 and 2030

Key GHG Emissions (Global)	*2010-2030 Radiative Forcing Increases, W/m^2*
CO_2	negligible to +0.4
CH_4	+0.6 to 3.0
CFCs, HFCs	+0.1 to +0.3
TO	+0.3 to +0.5
BC	+0.2 to +0.8
TSA	+0.1 to -0.6
Total	+1.7 to +4.2

2.1.5. Node 5: Global Mean Temperature Anomaly

This node accounts for both the current GMT anomaly and the projected anomaly through 2030. As can be seen in Figure B2-12, the present day GMT anomaly is greater than +0.4°C.

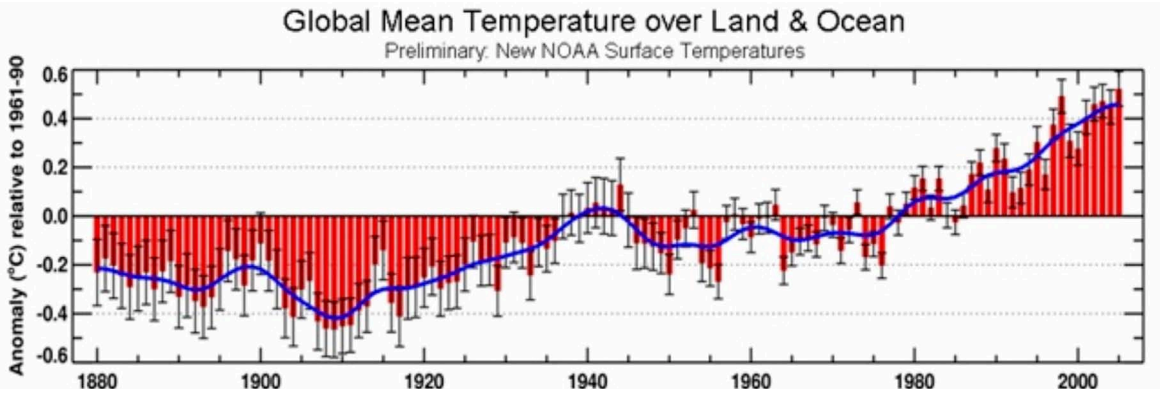

Figure B2-12. Average Surface Temperature Changes over Land and Ocean
Source: National Oceanic and Atmospheric Administration[31]

[31] IPCC. *Climate Change 2007: Synthesis Report* (AR 4), 2007.

Even though the GMT has risen only +0.4°C overall, the land-based mean temperatures have risen much higher, as seen in Figure B2-13. These higher temperature anomalies provide insight into the current anomaly observed worldwide over the major land masses.

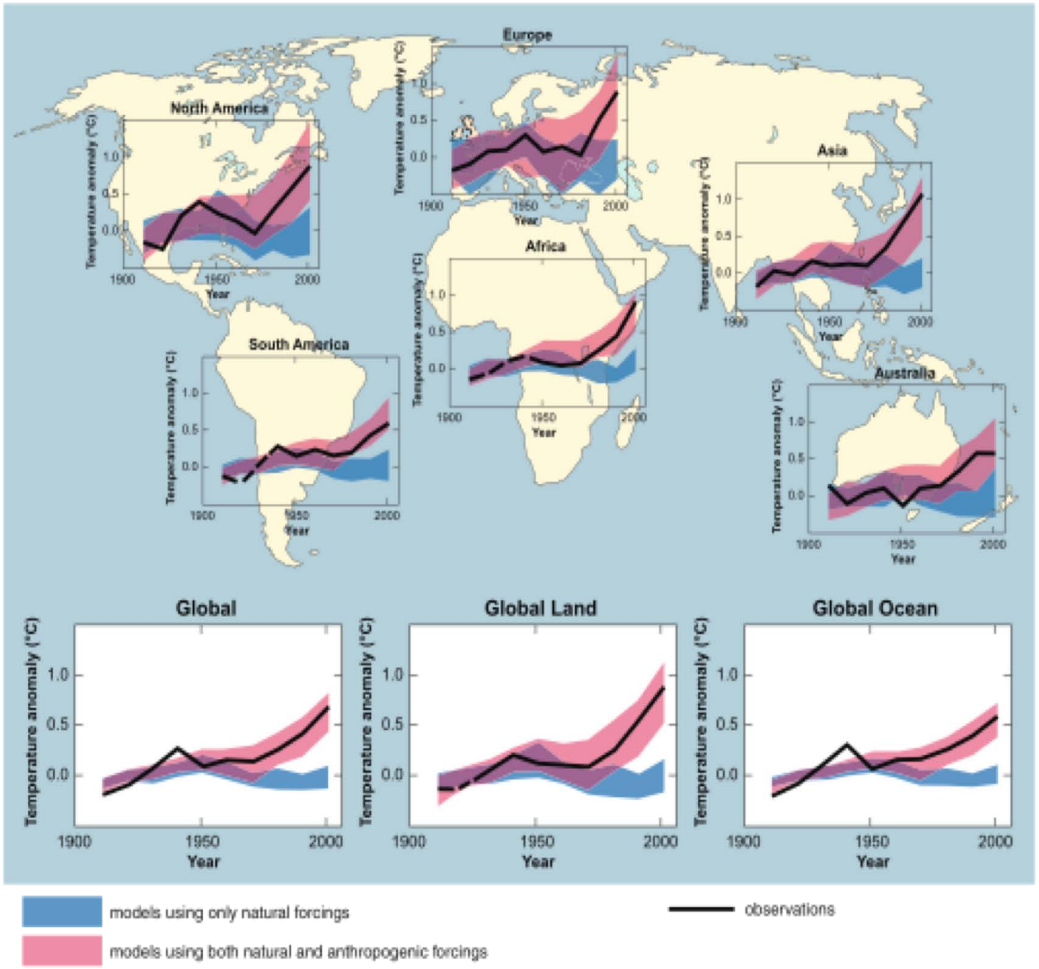

Comparison of observed continental and global scale changes in surface temperature with results simulated by climate models using either natural or both natural and anthropogenic forcings. Decadal averages of observations are shown for the period 1906-2005 (black line) plotted against the centre of the decade and relative to the corresponding average for 1901-1950. Lines are dashed where spatial coverage is less than 50 percent. Blue-shaded bands show the 5- to 95 percent range for 19 simulations from five climate models using only the natural forcings due to solar activity and volcanoes. Red shaded bands show the 5- to 95 percent range for 58 simulations from 14 climate models using both natural and anthropogenic forcings. (WGI Figure SPM.4).

Figure B2-13. Mean Temperature Changes over Land
Source: IPCC Climate Change, Synthesis Report (AR4) 2007

***Projections for the Global Mean Temperature Anomaly* —** The major climate models shown in Figure B2-14 project an additional GMT anomaly of +0.8 to +1.5°C by 2030, depending upon assumptions used. If the methane pulse is included, this anomaly could reach +4.4°C.

Figure B2-14.
GMT Anomaly Midpoint
***Source: IPCC*[32]**

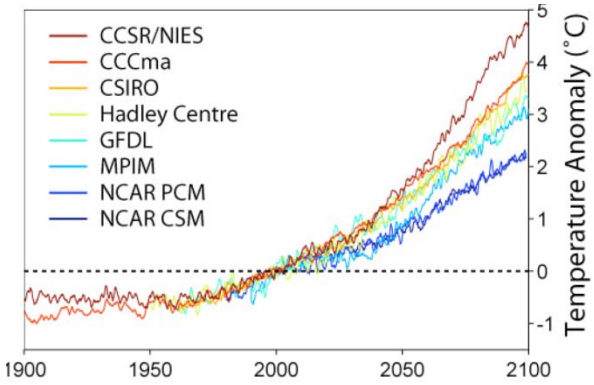

2.1.6. Nodes 6 - 8: Structural and Ecosystem Changes Stemming from Threshold Exceedances

Node 6 accounts for the degree to which the GMT anomaly exceeds a threshold beyond which structural and ecosystem changes are now occurring or are projected to occur, discounting the inherent fluctuation of the GMT. The current increase in the GMT of +0.4°C is not viewed within the global GHG accounting protocols as sufficient to be considered in exceedance of an irreversible global temperature threshold (node 7). However, the GMT anomaly is projected to reach the range of +0.8 to 1.5°C by 2030. (As discussed in Section 1 (step 3), while the Bali Draft Protocol considers +2.0°C to be the GMT anomaly threshold, a number of Small Island nations are calling for the GMT anomaly threshold to be recognized as +1.5°C, which is consistent with the upper end projections for the 20-year time horizon.

Structural and Ecosystem Changes (Nodes 6 and 8) — Nodes 6 and 8 are measured in terms of area loss by type of structural habitat affected and increased mortality of key species.

***Current Changes* —** There is ample and growing evidence of impacts on structural habitats and key species (e.g., the melting of the Arctic ice, loss of polar bear habitat). The IPCC has noted more than 25,800 examples of independent research showing habitat and/or species impacts consistent with global warming (2007 IPPC Synthesis Report, Figure 1.2).[33]

***2030 Projection* —** There remains considerable uncertainty about the type and extent of impacts to structural habitats and ecosystems resulting from the exceedance of global temperature thresholds.

[32] *Ibid.*
[33] *Ibid.*

2.1.7. Irreversible Exceedance of Thresholds (Node 7) — Node 7 represents the anomaly of accumulated key GHG loadings to levels frequently described as the "tipping point." The major thresholds expected to contribute to a global tipping point are described below:

- **Current Oceanic Warming —** The warming of the oceans, changes to weather patterns and other node 6 effects currently being tracked have not been definitively characterized. Nonetheless, it has been reported that these effects will take thousands of years to reverse.[34]

- **Irreversible CO_2 Loadings from Reduced Oceanic Absorption —** Oceans are now showing a dramatic slowdown in absorption of atmospheric carbon dioxide that will indirectly increase the accumulated loading anomaly projected for the next 20 years. Over the past thousand years, the percentage of annual carbon dioxide loading absorbed by the world's oceans has been about 17 percent. Reports from both the southern Atlantic Ocean and the Sea of Japan now show roughly a 50-percent reduction in oceanic absorption.[35] If this trend is confirmed globally, the world's oceans will be absorbing less than 10 percent of the annual carbon dioxide emissions when carbon dioxide reaches saturation levels in the ocean. If this decrease in carbon dioxide absorption rate is shown to be occurring in all major bodies of water, then the accumulated loading equation used to calculate Node 3 will also require adjustment. Such a reduction would add another four billion tonnes of carbon dioxide loading each year, and raise the accumulated carbon dioxide loading by over 130 billion tonnes by the year 2030.

- **Link of CO_2 Loadings to Economic Activity —** Carbon dioxide emissions are closely tied to economic activity where that activity is founded on fossil energy. Only a handful of countries rely on non-fossil energy resources. Because of their fundamental link to economic activity, these carbon dioxide emissions are unlikely to decrease, and in fact have been increasing in the near term. This fundamental driver of carbon dioxide emissions can explain the significant increases in the UNFCCC emissions inventory for countries.

  For example, the Canadian national GHG inventory data has shown an increase of 33 percent over the past 18 years even though Canada is a signatory to the Kyoto Treaty. This increase came largely from carbon dioxide emissions tied to a single province, Alberta, and the development of its oil sands industry, one of the most important pillars of the Canadian economy. It is also interesting to note that the total mitigation of the Kyoto Treaty countries through 2008 was reported to have resulted in a decrease of just 0.4 percent of the CO_2 loading. This decrease was later confirmed to be a result of the collapse of the eastern European and Russian economies.[36]

[34] http://www.cnn.com/2009/WORLD/europe/03/12/irreversible.climate/index.html

[35] S. Khatiwala, F. Primeau and T. Hall. "Reconstruction of the History of Anthropogenic CO_2 Concentrations in the Ocean, *Nature*, Vol. 462, pp. 346-349, November 19, 2009.

[36] UNFCCC, Annual Emission Report, 2006.

- **Irreversible Loss of Land-Based Ice Sheets in Greenland and Antarctica** — It has been projected that, once lost, restoration of these large land-based ice sheets will take thousands of years. The unit of measure is the loss of total land-based ice sheet, measured as percentage of ice volume.

2.2. Calculating GHG Loading and Cooling on a 20-Year Time Horizon

As discussed above, the projected GMT anomaly for 2030 ranges from +0.8°C to +1.5°C, or as high as +4.4°C if the biogenic methane pulse is included. Given a GMT anomaly threshold level of +1.5°C to +2°C, the time horizon that best fit this set of circumstances, given the current data, is the 20-year time horizon.

More than half of the major climate models now project that the GMT will increase by at least +1.5°C by 2030 (Figure B2-14 above). Given this high probability of exceedance of threshold, the global GHG accounting protocols use a 20-year time horizon ending in 2030. This time horizon allows for the calculation of GHG loadings from continuous sources in a manner that integrates the radiative forcing effects of short-lived and longer-lived GHG emissions under one framework.

In addition to considering the GHG loadings over the 20-year time horizon, calculating the GHG loading on an annual time horizon basis accounts for the radiative forcing effect of the short-term GHGs within the scale of their atmospheric lifetimes. This secondary level of calculations provides a more precise accounting of the immediate effects of short-term emissions, and is consistent with generally accepted LCA functional unit timeframes.

The 100-year time horizon GWP has no environmental relevance to this projected threshold exceedance. For example, methane's 20-year time horizon GWP (72) provides a full accounting of the radiative forcing of methane over its actual atmospheric lifetime of 8-20 years, yielding an annual methane loading for 2010 of 37-45 billion tonnes CO_2e. By contrast, if the published IPCC 100-year time horizon GWP for methane (25) is used, the annual loading estimate for methane is only 10-12 billion tonnes CO_2e. Comparing these results to the 2010 projected loading for carbon dioxide of 34 billion tonnes, the 20-year time horizon GWP shows methane levels to be 26 percent higher than carbon dioxide, while the IPCC 100-year GWP shows methane to be only one-third the carbon dioxide amount.

3.0. Arctic and Antarctic Regional GHG Accounting Protocols

The Arctic and Antarctic GHG accounting protocols are specific regional applications of the LCSEA GHG Accounting Framework, focused on emissions and effects impacting the polar regions. The following discussion identifies data sources and elaborates upon concepts discussed in sections 1 and 2 above as they pertain to the polar regions. At the time of this writing, only the Arctic protocols have been completed.

3.1. Establishing the Arctic Stressor-Effects Network

The Arctic GHG accounting protocols address regional climate anomalies within the Arctic Circle, which roughly defines the physical boundaries of the Arctic stressor-effects network (Figure B3-1). It is within this area — the region of perennial ice sheets and frozen tundras — that impacts and feedback loops from key GHGs are occurring at a rate distinct from that accounted for within the global accounting protocols, with regional and global implications.

Figure B3-1: The Arctic Region, as defined by the Arctic Circle

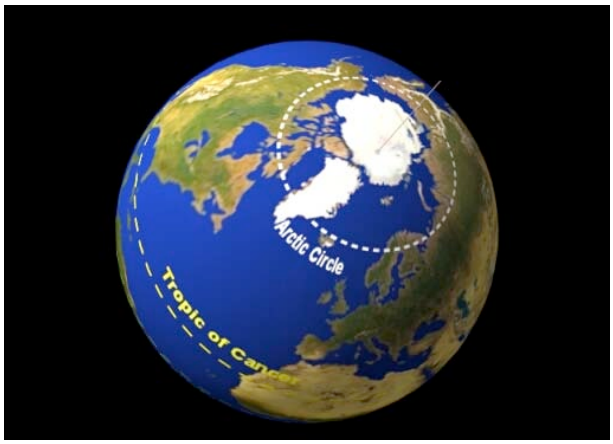

3.1.1. Arctic Stressors

Stressor contribution analysis is used to track and account for all major stressors that affect midpoint and endpoint nodes in the Arctic stressor-effects network, whether these stressors originate from within or outside of the Arctic region. The major global stressors, identified in section 2 above, as well as specific stressors that originate from within or nearby the region, are integrated into the Arctic stressor-effects network through this contribution analysis.

The major Arctic stressors are listed in Table B3-1. Significant global and regional sources contributing to these stressors should be identified before the Arctic accounting protocols are put to use. The percentage of a given global or regional stressor that contributes to climate impacts in the Arctic, whether that stressor originates inside or outside the region, is represented by the environmental characterization factor (ECF_{RC}), where a 100% contribution results in an ECF_{RC} of 1, and smaller percentage contributions result in a fraction.

Table B3-1. Allocating the Percent Contribution of Major Stressors to the Arctic Stressor-Effects Network

Major Global and Regional Stressors	Description	Basis of establishing ECF_{RC}	Stressor-Effects Node
Arctic vortex	Trapping winter tropospheric ozone precursors and methane emissions	100% contribution	Node 7
Arctic seasonal regional air pollution	Tropospheric ozone, methane and black carbon	100% contribution	Nodes 1-3
Changes in global oceanic currents	Regional changes in climate dynamics, and thinning of the eastern Arctic Perennial Ice Sheet	Contribution to thinning of eastern Arctic Perennial Ice Sheet — % to be determined	Node 6
Stressors originating from outside Arctic	Tropospheric ozone, methane and black carbon	Contribution to Arctic tropospheric ozone loading — % to be determined	Nodes 1-3
Arctic coolants originating from outside Arctic	Tropospheric sulfate aerosols	Contribution to Arctic TSA loading — % to be determined	Nodes 1-3

3.1.2. Annual Time Horizon Required

Temperature thresholds at node 5, and arguably in some instances, at node 7, of the Arctic stressor-effects network have already been exceeded, as evidenced by the retreat of the Arctic Perennial Ice Sheet ("APIS" or "the ice sheet") starting in 1979, and the subsequent ecosystem changes observed, such as polar bear endangerment. For this reason, the Arctic GHG accounting protocols rely on the annual time horizon to establish equivalencies.

3.1.3. Characterization of Key GHGs, Warming Potentials and Cooling Potentials for the Arctic Region

As regional radiative forcing (RF) data have become more available from the Goddard Institute for Space Studies (GISS), it has become possible to link RMT changes to GHG radiative forcing vectors related to specific regional sources. This development allows for the characterization of the key Arctic GHGs in a manner similar to the establishment of their global counterparts. Based upon available data, the key Arctic GHGs resulting in positive RF over +0.1 W/m^2 are methane, tropospheric ozone, and black carbon, while the key Arctic GHGs resulting in negative RF exceeding -0.1 W/m^2 in the region are tropospheric sulfate aerosols (TSA) and selected halocarbons.

- **Global Versus Regional Radiative Forcing Differences**

  In order to establish the key GHG list for the Arctic region, it was first necessary to conduct a regional RF assessment. The relative importance of various regional RF vectors is significantly different than global RF vectors.

  For example, while the global RF value for tropospheric ozone has been established by the IPCC and other researchers at +0.35 W/m^2, regional Arctic RF from

tropospheric ozone plumes can reach +4.0 to +5.0 W/m^2 — an order of magnitude higher. The Arctic tropospheric ozone plumes can last for weeks and cover large portions of the Arctic during the peak regional forcing season (MOZART 4 observations, 2009).[1] Global RF values cannot be used to set up the Arctic RF assessment because tropospheric ozone: 1) is not dispersed evenly across the globe like the long-lived GHG emissions; 2) affects the polar regions disproportionally, with seasonal averages (+2 W/m^2 or greater); and 3) only occurs during the ozone formation seasons. Calculations of Arctic RF must be normalized to the ozone season, since amortization of the RF over the full 12 months dilutes the effects of tropospheric ozone seasonal maximums that occur for only a portion of the year.

At the same time, NASA GISS has recently uncovered the fact that tropospheric sulfate aerosols (TSA) are having a negative RF on the Arctic region of between -2.0 to -3.0 W/m^2. The data suggest that between 1940 and 1970, negative RF levels reached as high as -4 to -5 W/m^2. These negative RF values in the Arctic are significantly higher that global average TSA values of -0.9 W/m^2.

Unlike the short-lived GHG RF values that are significantly higher within the Arctic region, the global RF contributions from long-lived GHGs on the seasonal Arctic RF anomaly are less than their global average value because: 1) global annual averaged RF values during dark months have no effect; and 2) total column concentrations of these long-lived GHGs are lower in the Arctic because of the lower height of the tropopause at the poles. As can be seen in Table B3-2, among the long-lived GHGs, only carbon dioxide still qualifies as a key GHG for the region from a strictly RF perspective; both nitrous oxide and halocarbons are below the minimum current RF threshold of +0.1 W/m^2. None of the long-lived GHGs contribute sufficiently to the overall projected 2030 RF to qualify as key Arctic GHGs.

Table B3-2. Radiative Forcing of Long-Lived GHGs in the Arctic

GHG	Global Annual Averaged RF	Arctic ECF_1 to account for short RF season (4 months)	Arctic ECF_2 to account for lower Arctic tropopause	Current Adjusted Arctic RF	2030 Projected Arctic RF
Carbon Dioxide	1.66	x 0.33	x 0.5	0.27	0.05
Nitrous Oxide	0.16			0.03	Negligible
Halocarbons	0.34			0.06	Negligible

The annual time horizon is used as the basis for establishing the Arctic regional warming potentials (RWPs), pulse warming potentials (PWPs), and regional cooling potentials (RCPs). Additional characterization steps are required to adequately account for seasonal radiative forcing surrounding regional methane sources and concentrations; these steps are described below. The Arctic region category indicators and relevant RWPs are shown in Table B3-3. TSA and halocarbons (specific species yet to be determined) are listed as Arctic coolants with their respective RCPs.

[1] See Footnote 11.

- **Establishing the Arctic LCSEA Category Indicator List**

Identification of the key GHGs for the Arctic completes the classification step within the LCSEA GHG Accounting Framework (Table B3-2). Next, regional categories are characterized by their specific midpoints and timeframes. For example, specific plumes of black carbon and tropospheric ozone should be tracked in real time by contributing countries. The category indicators representing specific plumes are then aggregated into annual averages by category indicator by country.

Table B3-2. Regional Category Indicators, Warming Potentials and Cooling Potentials

Arctic Category Indicator	**Arctic Regional Warming, Regional Cooling and Pulse Warming Potentials**		
	RWP	RCP	PWP
Seasonal Arctic Methane Loadings • Alaskan (US) • Russian • Canadian • European	117		
Annual Biogenic Arctic Methane Loading *(Permafrost melt)*	117		
Annual Biogenic Arctic Methane Hydrate Loading			3,387*
Annual Tropospheric Ozone Loading • Alaskan (US) • Russian • European • Iceland	19,560		
Annual Black Carbon Loading • Alaskan (US) • Russian • Canadian • Finland • Sweden • Norway • Central Asia	41,000 to 82,000		
Annual TSA Arctic Cooling • Lower United States • Russian • Canadian • Finland • Sweden • Norway		-4,826	

Listing category indicators by country is considered the appropriate limit to differentiation of such regional category indicators, consistent with the Kyoto treaty structure requiring reporting of annual GHG inventory by country. As in the case of the global GHG accounting protocols, it is important to establish current baseline GHG levels for each of the listed country category indictors. Because of the time urgency and the acute nature of the Arctic crisis, mitigation goals are scaled towards reducing the Arctic RMT by 2015, a necessary step towards climate and APIS structural stabilization in the region.

3.2. Factors Influencing the Key Arctic GHGs

3.2.1. Accounting for Enhanced Background Methane Concentration Levels in the Arctic Region

Background concentration levels of methane in the Arctic region are higher than corresponding concentration levels at lower latitudes. These higher atmospheric levels reflect a greater "effective" methane potency in the Arctic region, as characterized below.

As shown in Figure B3-2, a study conducted by NOAA showed the distribution of atmospheric methane to be about 14 percent higher in the Arctic region than in lower latitudes from 1992 - 2001. Much of this difference results from the latitude-dependent rate of photochemical destruction of methane. This enhanced background Arctic concentration serves as the basis for computing methane's RWP_{Arctic}, using the 2008 global background concentration of methane as the baseline.

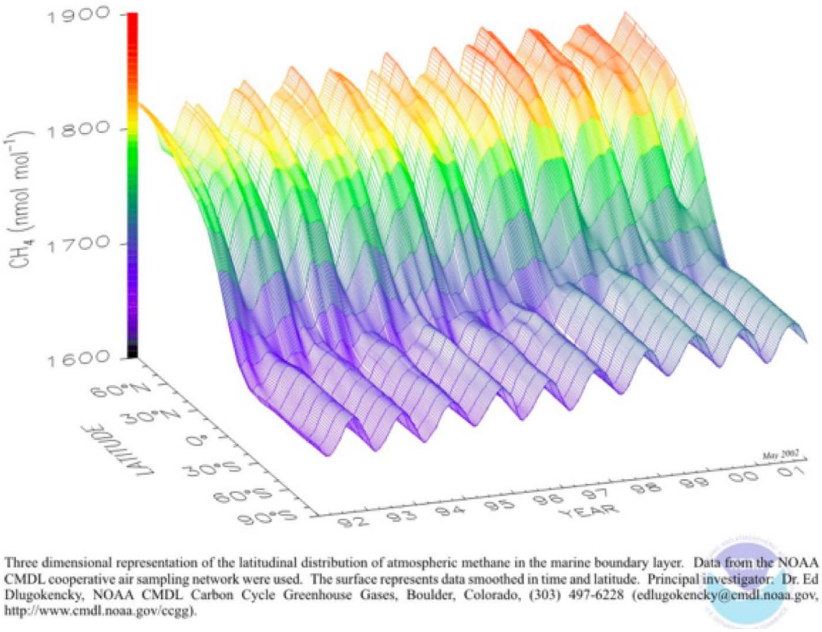

Figure B3-2. Higher Methane Concentration Levels in the Arctic than at Lower Latitudes
(Source: NOAA CMDL Carbon Cycle Greenhouse Gases)

Although relatively stable over the ten years covered by the NOAA study, global methane concentration levels have more recently increased to a historic high of 1,790 parts per billion (Figure B3-3). Applying an Arctic concentration factor of 14%, the adjusted Arctic methane levels are estimated at 2,020 parts per billion volume (ppbv). At this level, methane concentrations are 300 percent higher than the historic 10,000-year Arctic methane concentration baseline. To account for this regional increase above baseline, the Arctic accounting system increases the annual time horizon GWP of methane at 105 by 14 percent. This yields an RWP_{Arctic} of 117.

Figure B3-3. Increases in Global Methane Concentration Levels

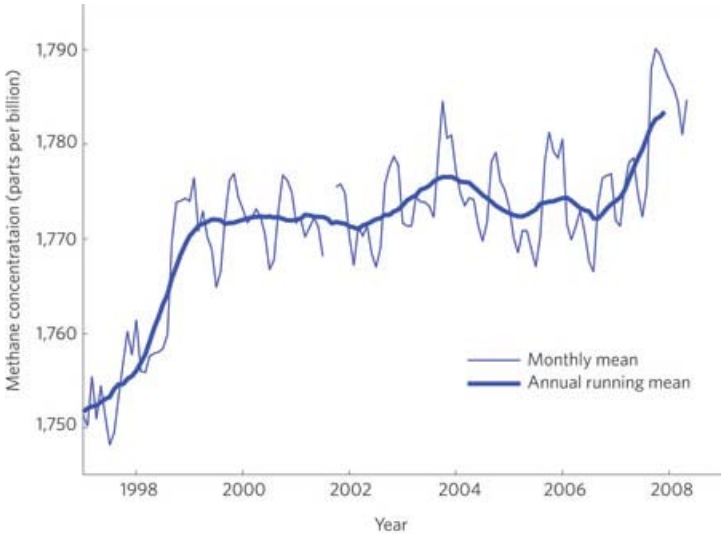

3.2.2. Accounting for the Effects of the Arctic Vortex and Oscillation

The Arctic stressor-effects network takes into account specific Arctic climate dynamics, such as seasonal variations in the Arctic vortex and oscillations that can affect regional concentrations of the key GHGs. The Arctic Vortex refers to the prevailing winds that circle the Arctic. The vortex forms during the winter months and strengthens or weakens by opposing atmospheric pressure patterns in northern middle- and high-latitudes. This strengthening and weakening cycle is known as the Arctic Oscillation.

In some years, the Arctic Oscillation exhibits a "negative phase" with relatively high pressure over the polar region and low pressure at mid-latitudes (about 45 degrees North), and a "positive phase" in which the pattern is reversed. In the positive phase, higher pressure at mid-latitudes drives ocean storms farther north, bringing wetter weather to areas such as Alaska, Scotland, and Scandinavia, as well as drier conditions to the western U.S. and the Mediterranean. In this phase, frigid winter air does not extend as far into the middle of North America as it would during the negative phase of the oscillation. This positive phase keeps the United States east of the Rocky Mountains warmer, but leaves Greenland and Newfoundland colder in the winter (positive phase). Regional weather patterns in the negative and positive phases are illustrated in Figure B3-4.

Over most of the past century, the Arctic Oscillation alternated between positive and negative phases. Starting in the 1970s, however, due to climate changes and further destruction of Arctic stratospheric ozone, the oscillation has tended to stay in the positive phase, causing lower than average pressure in the Arctic and higher than average temperatures in much of the United States and northern Eurasia.

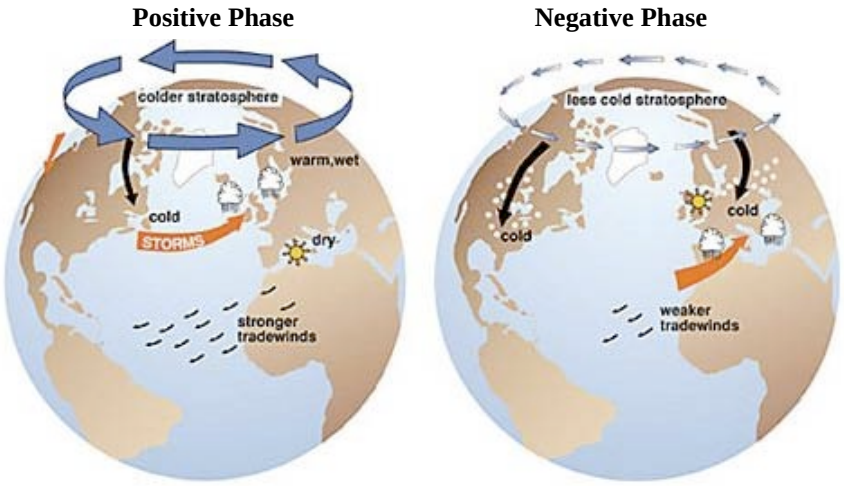

Figure B3-4. Arctic Oscillation
(Source: J. Wallace, University of Washington)

In addition, the positive phase of the oscillation has exhibited changes that can affect the degree of key Arctic GHG loadings. For example, while stronger vortex winds are observed during the positive phase, this phase tends to weaken earlier in the spring, allowing for the formation of static air columns that are favorable to tropospheric ozone formation. These conditions also favor increases in early springtime background methane concentration levels that are significantly higher than the current Arctic methane concentration anomaly (2,020 ppb) discussed above. The RWP_{Arctic} for methane is adjusted to account for these higher concentration levels.

Using NASA monitoring data on these early-spring Arctic methane concentration anomalies, the RWP_{Arctic} for methane is calculated as the percentage increase compared to the current Arctic methane concentration anomaly in accordance with the following Equation B3-1.

Equation B3-1.

Methane RWP_{Arctic} Vortex Adjustment Calculation

RWP_{Arctic} Vortex Adjustment = Methane RWP_{Arctic} x Vortex Concentrations / 2,020 ppb

3.2.3. Arctic TSA Cooling

Tropospheric sulfate aerosols (TSAs) have been shown over the past 100 years to reverse the Node 5 Arctic RMT anomaly through their regional cooling effect. Regional radiative forcing trends provided by NASA GISS (Shindell, March 2009) correlate closely with Arctic RMT changes observed over the past 100-year time period. Figure B3-3 shows that the 1940-1970 reversal of Arctic RMT (-1.09°C) corresponded with

increases in TSA emissions from coal plants largely operating in the US and Europe. As evident in the chart, the initiation of efforts by the US and Europe to reduce SO_2 emissions (starting in 1970) coincided with the removal of TSA-related cooling in the Arctic. The apparent effect of removing this amount of cooling from the Arctic has been to accelerate the Arctic warming trend, with the RMT rising rapidly toward +3°C exceedance of threshold level.[2] This loss of cooling has had the unintended consequence of adding back at least 1.09°C in the Arctic RMT.

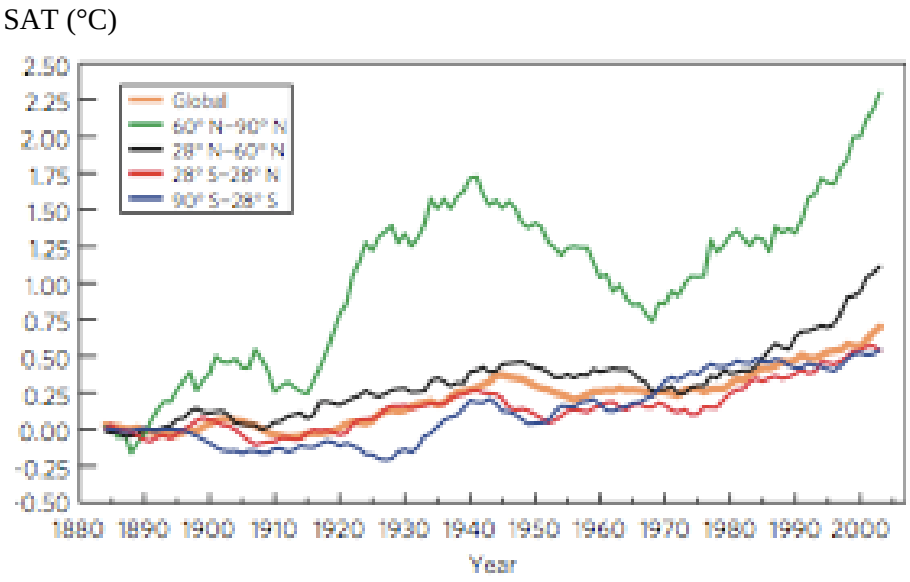

Figure B3-3. Area-weighted mean Observed Surface Temperatures over the Indicated Latitude Bands
The values are nine-year running means relative to the 1880-1890 mean. Correlations (R2) with the global mean over 1931-2007 by region are: 0.94 tropics, 0.61 SHext, 0.86 NHml and 0.53 Arctic.
Source: NASA GISS 2009

3.3. Nodal Characterization of the Arctic Stressor-Effects Network

Table B3-3 provides an overview of the Arctic stressor-effects network by node. Sufficient data were available for the nodes involving thresholds (starting at node 5) to establish the Arctic GHG accounting protocols.

Global and regional stressors have been classified into appropriate nodes. Descriptive information is provided for the each of the nodes in the table and in the subsequent text. Data on specific regional sources and amounts remain to be compiled, but are not critical.

[2] The 2009 temperature of 2.9°C is extrapolated from the data provided in the figure, which shows an area-weighted mean observed surface temperature of 2.3°C in 2003 (Shindell, 2009).

Table B3-3. Arctic Stressor-Effects Network —Nodal Characterization

Node	Nodal Characterization —Anomalies and Exceedances of Thresholds
Node 1: Annual Emissions of Key GHGs for Arctic Region	Major sources of key GHGs — % Contribution • Regional Arctic GHG emissions by major source — 100% • Specific nearby regional GHG emissions by major sources (*to be identified*) — TBD
Node 2: Annual Loadings of Key GHGS for Arctic Region, by type	Annual Arctic Loadings from Key GHGs — % Contribution • Methane — TBD • Tropospheric Ozone — TBD • Black Carbon — TBD Annual Arctic Cooling from Key GHGs • TSA — TBD • Halocarbons — TBD
Node 3: Accumulated Long-Lived and Mid-Lived GHG Loadings	Accumulated Loading Anomalies — Contribution • Long-Lived GHG Excluded (do not meet minimum key GHG thresholds for region) — NA • Methane — TBD
Node 4: Radiative Forcing Anomalies	Arctic Radiative Forcing anomaly = > +1.5 W/m^2 annual avg.; > +3.0 W/m^2 seasonal Positive Radiative Forcing — % Contribution to Regional RF Anomaly • Tropospheric Ozone — 20 to 40% • Black Carbon — 30 to 50% • Methane — 20% • N_2O (at 0.02 W/m^2, below min. threshold) — <1% • Halocarbons (at 0.05 W/m^2, below min. threshold) — <1% • Carbon dioxide — 10% Negative Radiative Forcing • TSA — -50% to -100% • Halocarbons — TBD
Node 5: Exceedance of Arctic RMT Threshold	2009 RMT anomaly = estimated at +2.5 to 2.9°C Positive RMT Contributors — Contribution to RMT • Tropospheric Ozone[3] — 0.43°C • Black Carbon — +0.5 to +1.4°C • Methane — +0.34°C • Carbon dioxide (current/projected) — + 0.3°C / < + 0.1°C Historic Negative RMT Contributors • TSA — -1.09°C
Node 6: Exceedance of Structural and Ecosystem Threshold	Large-scale structural habitat damage observed to date: 1) Arctic Perennial Ice Sheet (APIS): 50% loss compared to 1979 baseline • 2009: 50% contribution to perennial ice sheet loss from global oceanic current vectors, 50% from regional pollution, nearby regions and global pollution • 2013 – 2020: The Arctic is projected to lose its perennial ice sheet. 2) Conversion of Siberian and other tundra structures is taking place as permafrost melts, leading to formation of bogs and lakes that are becoming major methane sources.
Midpoint Node 7: Global Climate Change Tipping Point	Temperatures in Arctic swamps (post-tundra) continue to warm and are projected to increase the annual RMT to more than 3°C, increasing the potential for release of shallow deposits of up to 20,000 billion tonnes of methane hydrates, causing a major methane pulse that would raises the GMT by an additional +2°C or more.
Endpoint Node 8: Catastrophic Structural Changes; Ecosystem Damage	Structural changes leading to new ecosystem.

*TBD means to be determined. NA means not applicable.

[3] Shindell *et. al.*, 2008

3.3.1. Node 1: Key GHG Emission Sources in the Arctic

The 2009 Arctic Monitoring and Assessment Project (AMAP) study has identified tropospheric ozone, black carbon and methane as the major GHG emissions affecting the Arctic.[4]

Major sources of annual tropospheric ozone, black carbon, and methane emissions affecting the Arctic have yet to be fully identified, classified and characterized. For example, a single nickel smelter in Western Russia within the Arctic Circle currently emits 90,000 tonnes of black carbon annually, which disperses into the Arctic region. Two major black carbon sources are Boreal fires burning in Alaska and Russia, and traditional agricultural burning practices (e.g., in Kazakstan).[5] A persistent haze now blankets the region for much of the ozone season (Figure B3-4).

Figure B3-4. Arctic Carbon Black Plumes over Northern Alaska and the Arctic Ocean, April 2008
Source: Science News Photo Credit: J. Cozic/CIRES/NOAA Chemical Sciences Division

Data gathered by the National Oceanic and Atmospheric Administration (NOAA) in April 2008 show springtime plumes of black carbon forming over northern Alaska and the Arctic Ocean. Other significant sources of black carbon are coal-fired power plants and transportation sources.[6]

Tropospheric ozone related emissions impacting the Arctic region are derived from regional urban transportation and power generation sources. Besides being the major source of Arctic black carbon, boreal fires also contribute significantly to the regional tropospheric ozone loading; for instance, in the beginning of July 2009, MOZART 4 recorded a tropospheric ozone column exceeding +4.0 W/m^2 derived from Alaskan boreal fires (Figure B3-5).

[4] Arctic Monitoring and Assessment Programme (AMAP), *Update on Selected Climate Issues of Concern Observations, Short-lived Climate Forcers, Arctic Carbon Cycle, and Predictive Capability,* 2009.
[5] Science News, March 14th, 2009; Vol.175 #6, http://www.sciencenews.org/view/access/id/40871/title/sp_arctic_haze.jpg
[6] As of the date of publication of this Annex, specific plumes of tropospheric ozone and black carbon are being identified by source.

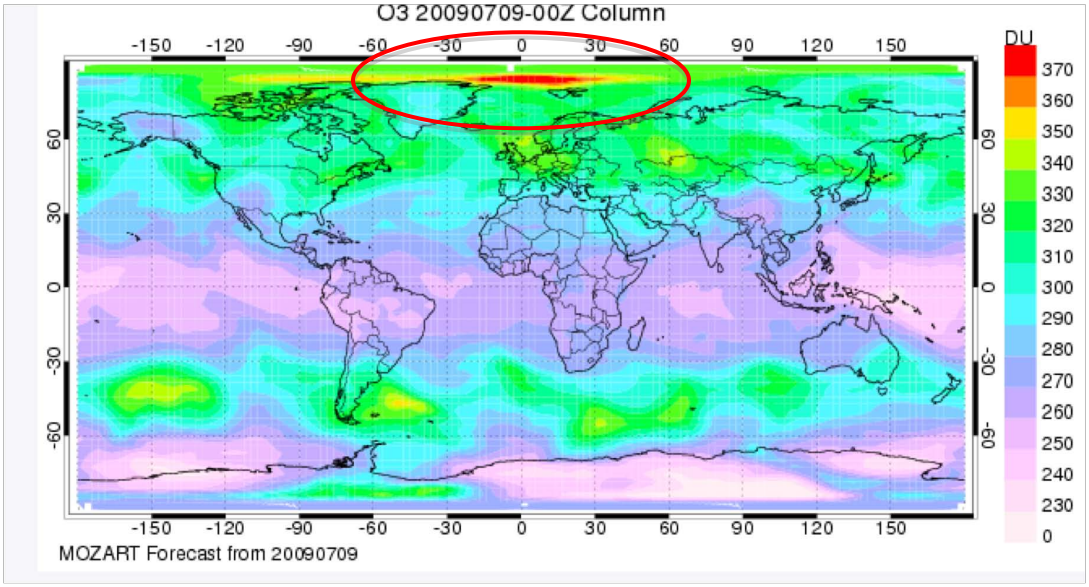

Figure B3-4. Arctic Tropospheric Ozone Plume in Dobson Units
Source: MOZART 4 Simulation based on emissions data from July 9, 2009

TSA emissions have been dispersed into the Arctic region largely from coal-fired power plants in the US and Europe. The rate of TSA emissions transport into the Arctic has been significantly reduced over the past 40 years as a result of government policies aimed at reducing SO_2 emissions.

3.3.2. Node 2: Annual Arctic GHG Loadings

Annual methane, tropospheric ozone, black carbon and TSA loadings have yet to be characterized. However, major sources have been identified. For example, Russian black carbon plumes account for 82 percent of the annual biogenic and 50 percent of the annual anthropogenic Arctic black carbon loading.[7] Based upon this contribution analysis, the current $ECF_{\text{Russian BC fraction}}$ has been set at 0.82.

3.3.3. Node 3: Contributions from Long-Lived and Mid-Lived GHG Accumulated Loadings

The current accumulated global loadings for carbon dioxide, nitrous oxide and halocarbons fail to contribute enough RF to qualify as key GHGs. Only accumulated loadings of methane contribute significantly to the Arctic stressor-effects network.

3.3.4. Node 4: Arctic Radiative Forcing Anomaly

[7] R. Damoah, Around the World in 17 Days – Hemispheric-Scale Transport of Forest Fire Smoke from Russia." *Atmospheric Chemistry and Physics*, Vol. 4, pp. 1311–1321, 2004. Also, Ashley Pettus, Clean Air Task Force, *Agricultural Fires and Arctic Climate Change: A Special CATF Report*, May 2009.

The three key Arctic GHGs contributing to warming — methane, black carbon, and tropospheric ozone —contribute up to 90 percent of the summertime Arctic positive RF.

- **Tropospheric Ozone** — The current annual RF from tropospheric ozone alone is estimated to equal one-third to one-half of the current total Arctic RF anomalies in the region (Shindell *et. al.*, GISS -NASA):[8]

  "In the first global assessment of the impact of ozone on climate warming, scientists at the NASA Goddard Institute for Space Studies (GISS), New York, evaluated how ozone in the lowest part of the atmosphere (the troposphere) changed temperatures over the past 100 years. Using the best available estimates of global emissions of gases that create ozone, the GISS computer model study reveals how much this single air pollutant and greenhouse gas has contributed to warming in specific regions of the world.

  Ozone was responsible for one-third to half of the observed warming trend in the Arctic during winter and spring, according to the new research. Ozone is transported from the industrialized countries in the Northern Hemisphere to the Arctic quite efficiently during these seasons. ... The impact of ozone air pollution on climate warming is difficult to pinpoint because, unlike other greenhouse gases such as carbon dioxide, ozone does not last long enough in the lower atmosphere to spread uniformly around the globe. Its warming impact is much more closely tied to the region it originated from. To capture this complex picture, the GISS scientists used a suite of three-dimensional computer models that starts with data on ozone sources and then tracks how ozone chemically evolved and moved around the world over the past century."

- **Black Carbon** — Between 30 percent (Zender et. al. 2008) to 50 percent (NASA GISS 2009) of total Arctic RF comes from black carbon plumes.

- **Methane** — Regional methane radiative forcing is estimated to be double that of carbon dioxide in the region, based upon of relative global concentrations, corrected for the enhanced background concentration levels of methane in the Arctic, as discussed above.

- **Tropospheric Sulfate Aerosols** — The negative radiative forcing levels of Arctic tropospheric sulfate aerosols have been established by NASA GISS (Shindell 2009), and are estimated globally to range from -0.6 to -2.4 W/m^2, depending on the region. The strongest negative forcing levels occur in the Arctic, due to the enhanced indirect effects of aerosols. At this level of radiative cooling, these aerosols have played a significant role as a coolant in the Arctic region.

[8] NASA Goddard Institute for Space Studies, http://svs.gsfc.nasa.gov/vis/a000000/a003300/a003340/index.html

Projections of Arctic Radiative Forcing — Radiative forcing from short-lived GHG emissions is projected to rise more rapidly in both polar regions, with the greatest increases occurring in the Arctic, according to Geophysical Fluid Dynamics Laboratory (GFDL) modeling (Figure B3-8). Radiative forcing from the short-lived regional GHG emissions could double, adding +2.0 W/m^2 on annual basis by 2050.[9] This projection is based on the GFDL modeling conducted by the NOAA Cooperative Institute for Climate Studies (CICS); other models project more modest increases.

Figure B3-8. 2000-2050 Projected Increases in Radiative Forcing from Key Arctic GHGs (+W/m^2)
Source: CICS[10]

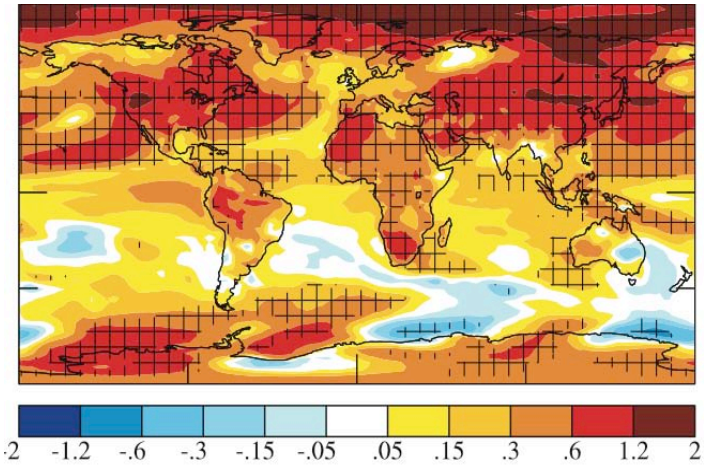

At the same time, as the rate of regional methane releases increases from both biogenic and anthropogenic sources, methane could become the dominant contributor to the regional RF anomaly over the next ten to twenty years.

3.3.5. Nodes 5 and 6: Arctic RMT Anomaly, Arctic RMT Threshold and Retreat of Arctic Perennial Ice Sheet

The Upper-Latitude RMT anomaly is now estimated at +2.5 to +2.9°C above the 10,000-year average. (Figure B1-1 in section 1 above shows a rise of up to 1.1°C by 2001).[11] When the loss of albedo effect on the APIS is included for this node, the effective RMT anomaly over the APIS is equivalent to about +5.0°C.

These thermal anomalies and their albedo anomaly equivalencies now exceed the Arctic RMT anomaly thresholds at Node 5, and arguably at Node 7. As stated earlier, the retreat of the ice sheet is well documented; satellite photographs show that the ice sheet shrank from seven million square kilometers to just under four million square kilometers. The Arctic region could be free of summer ice by as soon as 2013, and likely by 2020, according to the IPCC latest findings. During this same time period, losses of habitat supporting keystone species, such as polar bears, have been well documented. Other

[9] Shindell *et. al.*, 2008.
[10] *Ibid.*
[11] *Ibid.* NASA, http://data.giss.nasa.gov/modelforce/

evidence of threshold exceedances, including the loss of tundra and the inundation of villages, has also been observed and documented.

Mitigation strategies should be scaled to the timeframes and intensity of these latter nodes for which thresholds have been established. For example, according to Quinn et. al. (2008): "Marine shipping emissions in the Arctic have the potential to increase Arctic tropospheric ozone levels by a factor of two to three relative to present day."[12] (For further examples, see break-out box).

Black carbon and tropospheric ozone combine to currently account for +1.5 to 2.0°C out of the total current estimated RMT anomaly of +2.5 to 2.9°C. Over the next twenty years, as the Arctic thaws, these loadings are projected to increase as even more industrial development occurs and as the health of boreal forests degenerates under attack from disease and insect vectors associated with changing climate.

The historic data provided by NASA GISS shows that Arctic cooling from tropospheric sulfate aerosols could reverse RMT levels in time to help stabilize the APIS. Given their demonstrated ability to reverse the Arctic RMT (see discussion of Node 4, above), these aerosols are the only GHG coolant capable of reversing the Arctic RMT within the critical near-term timeframe required to stem the complete loss of the APIS. Using the historic tropospheric sulfate aerosol emission rates and locations from the US and Europe, it is possible to estimate the TSA emission rates that would be required to change the Arctic RMT -1.0°C by 2015, and -1.5°C by 2020.

Reducing RMT Through Targeted Mitigation Efforts

1. Establishing the Node 6 Baseline

In order to establish Arctic GHG load reduction goals, an Arctic stressor-effects network baseline must be established. The Node 6 1979 APIS level baseline, which is close to the 10,000 year APIS baseline, serves as a credible nodal baseline, providing a restoration target for meeting the goal of Arctic stability.

2. Establishing Mitigation Goals and Steps

LCSEA findings suggest that the Arctic region could be stabilized and to some extent restored, if the following goals were adopted and immediate steps were undertaken.

First Goal: 2.0°C Arctic RMT Reduction

- Major reductions in Arctic black carbon plumes (up to -1.0°C)
- Major reductions in annual Arctic tropospheric ozone loading (up to -0.4°C) — for example, through establishment of shipping-related emission limits.
- Sufficient Arctic tropospheric sulfate aerosol releases to provide -1.0°C of near-term added protection

Second Goal: Controlling the Methane Pulse Releases

- Extraction of methane hydrates into the natural gas markets should be initiated as soon as possible —e.g., through construction of floating liquid natural gas (LNG) platforms with mobile extraction units set up for maximum extraction.
- While it is not practical to extract all of the methane releases from such a vast area, some of the remaining methane can be burned off. An infrastructure of volunteers could be established to facilitate the spring burn-off. Attempts to modify the landscape in order to minimize lake formation and other biological sources of methane could be developed and deployed on an Arctic regional scale.

[12] P.K. Quinn *et. al.* "Short-lived pollutants in the Arctic: Their climate impacts and possible mitigation strategies." *Atmospheric Chemistry and Physics.* Vol. 8, pp 1723-1735, 2008.

3.3.6. Nodes 7 and 8: Methane Pulse Indicators, Pulse Warming Potentials and the Global Tipping Point

Methane hydrate pulses from the Russian, Alaskan and Canadian tundra are not classified as loadings but as separate category indicators due to their scale and their strong linkage to the global climate tipping point (Node 7). The Pulse Warming Potential (PWP) represents the possible effects of such pulses. It is based upon the scale of anthropogenic loadings from all major sources and the scale of the projected pulses over the same time period.

IPCC modeling shows that if the ice sheet continues to retreat at current rates, the Arctic RMT will increase by up to +3°C as far as one thousand kilometers south over tundra areas (Figure B3-9) containing shallow major methane hydrate deposits. These tundra areas, combined with the methane hydrates stored in shallow seabeds, contain up to 20,000 billion tonnes of methane that could be released.

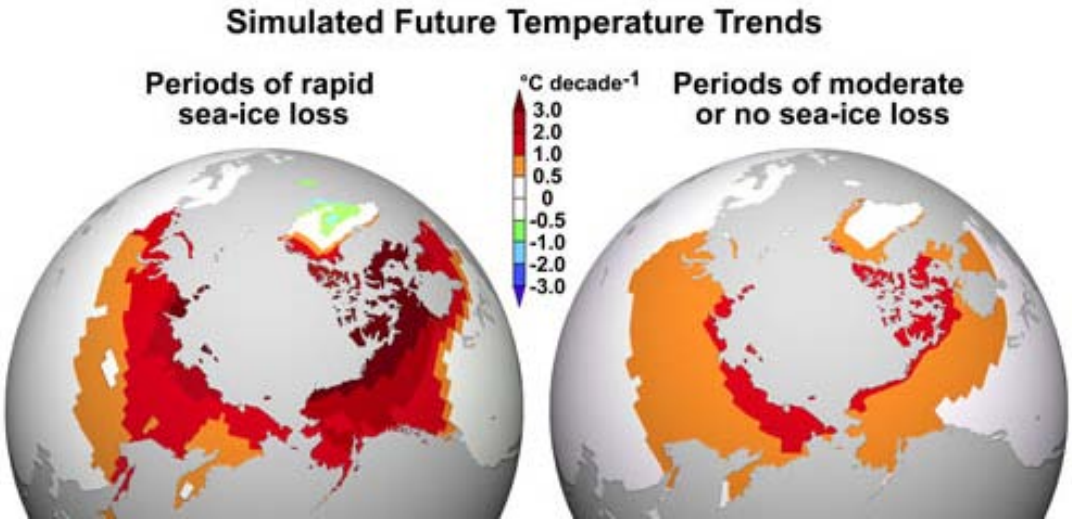

Figure B3-9. Simulated Future Temperature Trends[13]

This amount compares to the 620 billion tonnes from all projected anthropogenic methane accumulated loadings between now and 2030.[14] Accordingly, the PWP for Arctic methane hydrate pulses is calculated as 20,000/620 x 105 (methane GWP_{annual}) = 3,387. Given reports of current regional releases of biogenic methane (between 31 to 100 million tonnes yearly) in the Arctic region, this PWP is listed along with the other category indicators.[15] A release of even 20 percent of the total 20,000 tonnes would be

[13] *AMAP, 2009.*

[14] This value assumes annual anthropogenic methane emission rising from 62 billion tonnes to over 75 billion tonnes in CO_2e over the next 20 years. The data to support this accumulated methane loading can be found in section 2.

[15] AMAP, *2009.*

sufficient to push the global climate over the GMT Anomaly Threshold of +1.5°C.[16]

3.4. Establishing Antarctic GHG Assessment Protocols

As noted in sections 1 and 2 above, significant anomalies, including the unexpected tropospheric ozone loading in the region (node 2), the widely publicized loss of the western Antarctic land and sea-based ice (node 6), and the impending reduction in cooling associated with substitution of HFCs for older halocarbons (node 5), provide evidence of the need for a distinct set of Antarctic GHG accounting protocols. Though not yet fully developed, a few of the considerations that will be addressed within those protocols are described below.

The current list of key Antarctic GHGs includes regional sources of tropospheric ozone from South America and South Africa as warming agents, and selected halocarbons as Antarctic coolants.

3.4.1. Ozone's Role in Warming and Cooling Antarctica

Figure B3-10 shows the 1990 annual tropospheric ozone loading over Western Antarctica, along with the location of tropospheric ozone loadings that correlate to the nearby oceanic warming observed at the node 6 level.

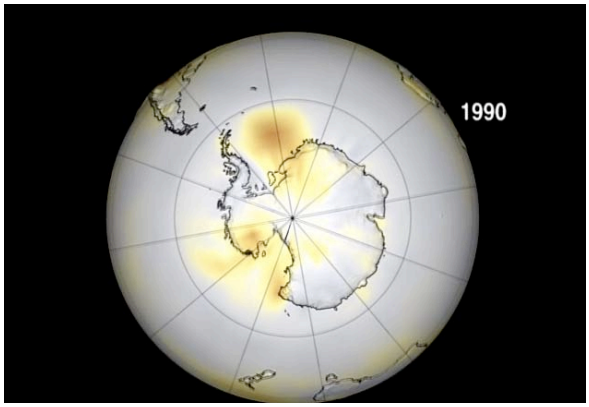

Figure B3-10. NASA Satellite Tropospheric Ozone Loading over Antarctica
Satellite images show annualized anthropogenic tropospheric ozone loading, especially over and near Western Antarctica

NASA's OMI satellite shows the South American tropospheric ozone plume from burning forests and agricultural lands to extend from the Amazon to nearby oceans and southward toward Antarctica. This plume provides significant additional positive radiative forcing, heating nearby oceans and thereby hastening the loss of sea ice in Western Antarctica as well as increasing the observed RMT anomaly over Western Antarctica (GISS, Streig *et. al.*).

[16] Probability modeling for the onset timeframe of the breakup of the ice sheet, projecting the Global GMT anomaly timeframes, and continued monitoring of the stability of the methane hydrates and potential for pulse level releases are the highest priorities for the Arctic and global protocols.

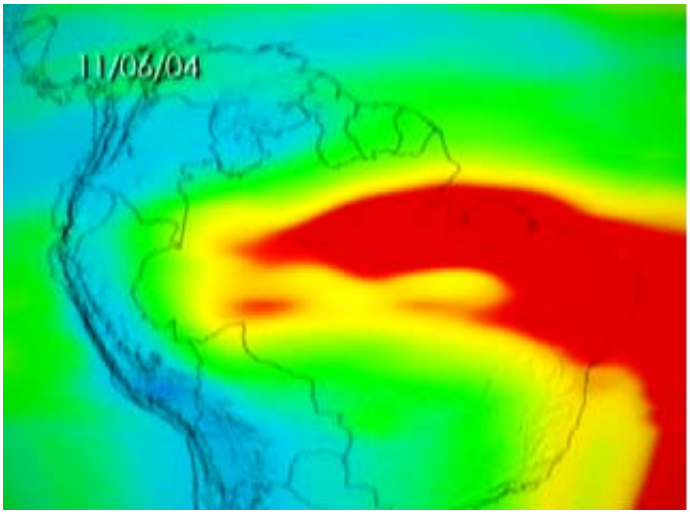

Figure B3-11. Tropospheric Ozone Plume — NASA OMI Satellite[17]
The plume formed over Amazonia, disperses to the southeast.

At the same time, the MOZART-4 model data show a combined loss of stratospheric and tropospheric ozone in the range of 100-120 Dobson Units (DUs) as compared to historic levels within the Antarctic vortex in 2009, based on the IPCC conversion factor of 0.04 W/m^2 per DU. This loss corresponds with an overall change in total radiative forcing of more than -4 W/m^2. This chemically-induced Antarctic Cooling Zone is expected to maintain its current intensity for another 20 years, followed by a gradual warming until the zone disappears altogether by around 2050. As can be seen in Figure B1-3 (section 1 above), the lowest ozone concentrations on record at 85 DU coincided with record cold temperatures for Antarctica, suggesting the importance of the Antarctic cooling zone in mitigating the rise of the RMT anomaly.

3.4.2. Classification of Halocarbons as Antarctic Coolants

In 2009, NASA reported that the upper stratospheric ozone layer is growing cooler in temperature. This cooling is due to the indirect effect of the warming of the troposphere from GHG emissions, which increases the thermal stability of ozone and results in increases to total stratospheric ozone concentrations.[18] At the same time, reductions in the release of CFCs and HCFCs have reduced stratospheric chlorine and bromine further, allowing partial recovery of the lower stratospheric ozone concentration at most latitudes except at the poles. The overall effect of halocarbons on decreasing the stratospheric ozone layer is becoming increasingly insignificant at most latitudes. Therefore the halocarbons are classified as only polar coolants.

Collectively, CFCs, HCFCs and halons have had a dramatic cooling effect on Antarctica (-4.0 to -6.0 W/m^2) and therefore are classified as key Antarctic coolants. However, since the contribution of specific halocarbon coolants to the overall negative radiative

[17] *http://acdb-ext.gsfc.nasa.gov/Data_services/cloud_slice/*
[18] F. Li, R. S. Stolarski and P. A. Newman, "Stratospheric ozone in the post-CFC era," *Atmospheric Chemistry and Physics*, Vol. 9, pp. 2207–2213, 2009.

forcing in the region has not been reported, it is not yet possible to establish the regional cooling potential (RCP) values of the specific chemicals.

3.4.3. Node 5 Consideration — Intensification of Antarctic Regional Mean Temperature

The current rate of intensification of the Antarctic RMT is about +0.25°C on an annualized basis, or +0.5°C on a seasonal basis (Figure B3-12). Major melting of the Western Antarctica ice sheet is already underway, possibly as a result of this RMT anomaly.

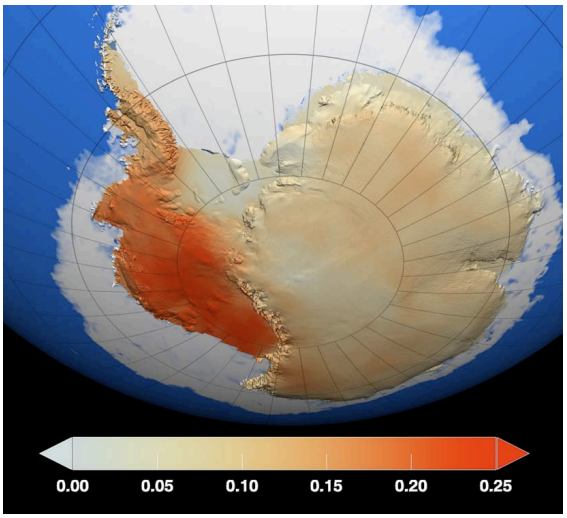

Figure B3-12. NASA RMT Anomaly: 1957-2008 (degrees centigrade)

When stratospheric and tropospheric ozone levels return to their historic levels, the Antarctic radiative forcing will regain +4.0 to +6.0 W/m^2, effectively tripling the radiative forcing of the Antarctica atmosphere. This increase of radiative forcing is projected to start as soon as 2025, and will ultimately raise the Antarctica RMT anomaly by over +1.2°C by 2050, up from the current RMT anomalies observed in Western Antarctica of +0.6°C.[19]

[19] Steig *et. al.*, 2009.

4.0. Calculation of Key GHG Category Indicators

This section describes the methods for calculating the key GHG loadings for the global and Arctic climate GHG accounting systems, including the following sets of category indicators: 1) GHG loadings by source of emission (using the functional unit of GHG loading per units of production); and 2) accumulated GHG loadings over decades from continuous emissions. Likewise, accumulated avoided GHG emissions can also be calculated. Together, these indicators can inform strategic, investment and security decisions — e.g., as related to new infrastructure options for electricity and fuel production systems.

4.1. Establishing GWP Values for All Key GHG Emissions

The general equation for establishing the global warming potential (GWP) of a GHG emission is shown in Equation B4-1.

Equation B4-1

$$GWP_i \equiv \frac{\int_0^{TH} RF_i\,(t)\,dt}{\int_0^{TH} RF_r\,(t)\,dt} = \frac{\int_0^{TH} a_i \cdot [C_i\,(t)]\,dt}{\int_0^{TH} a_r \cdot [C_r\,(t)]\,dt}$$

Where:

- "*TH*" is the time horizon
- "*i*" is the specific GHG
- "*r*" is the reference GHG — i.e., CO_2
- "RF_i" is the global mean RF (radiative forcing) of the GHG *i*, and "RF_r" is the global mean RF (radiative forcing) of the reference gas, *r*.
- "a_i" is the RF per unit mass increase in atmospheric abundance of the GHG *i* (i.e., radiative efficiency)
- "$C_i(t)$" is the time-dependent abundance of the GHG *i*, while "$C_r(t)$" is the corresponding quantity for the reference gas, *r*, in the denominator.

The numerator and denominator are called the absolute global warming potential (AGWP) of *i* and *r* respectively ("a_i" and "a_r"). The GWP of the reference gas, CO_2, is assigned a value of one (IPCC 2007).[1] The radiative efficiencies, a_i and a_r, can be considered constants, and can be removed from the integrations.

4.2. General Atmospheric Decay Equations

As evident from Equation B4-1, both the radiative forcings *RF* and the GWP values are affected by the atmospheric lifetimes of the emissions, and by the time horizon *TH* applied. The following discussion addresses the temporal characteristics of emitted GHGs.

[1] IPCC Fourth Assessment Report, Working Group 1: *The Physical Science Basis,* Chapter 2 "Changes in Atmospheric Constituents and in Radiative Forcing", 2007.

The GHG concentration following a *pulse emission* (i.e., emission per tonne) decays according to the atmospheric lifetime *LT*. Because carbon dioxide is included in the definition for the GWP of all GH gases, its decay function is first described. The decay of carbon dioxide cannot be described using a single lifetime constant, but is given by IPCC as:

Equation B4-2

$$C_r(t) = 0.217 + 0.259\, e^{-t/172.9} + 0.338\, e^{-t/18.51} + 0.186\, e^{-t/1.186}$$

When the carbon dioxide emission is from a *continuous source* (e.g., from a power plant over its lifetime), the concentration increases with time as described by the integral of Equation B4-2[2], as shown in Equation B4-3:

Equation B4-3

$$\int_0^{TH} C_r(t)\, dt = 0.217\, TH + 0.259 \cdot 172.9 \times (1 - e^{-TH/172.9}) + 0.338 \cdot 18.51(1 - e^{-TH/18.51}) + 0.186 \cdot 1.186 \times (1 - e^{-TH/1.186})$$

The concentrations of all other GHGs decay according to the atmospheric lifetime *LT*. The general decay function C_i for a pulse emission of a specific GHG is determined in accordance with Equation B4-4.

Equation B4-4

$$C_i(t) = e^{-t/LT}$$

When the GHG_i emission is from a continuous source, the concentration increases with time as described in Equation B4-5, until a *de minimus* limit is reached as TH >> LT:

Equation B4-5

$$\int_0^{TH} C_i(t)\, dt = \int_0^{TH} (e^{-t/LT})\, dt = LT\,(1 - e^{-TH/LT})$$

This general algorithm represents the retained atmospheric concentration loading caused by a constant emission flow, starting from the onset of the GHG emission at time $t = 0$.

[2] The IPCC decay formula for CO_2 includes a constant value, 0.217, which implies that 21.7 percent of every carbon dioxide emission stays in the atmosphere forever, and that the concentration caused by a continuous emission source in the long term is continuously increasing, instead of attaining a constant limit value, as is the case for all other GHGs. Earlier decay functions for CO_2 assumed two weighted lifetimes: 5 and 150 years. Such a decay function reduces the concentration of a pulse emission to zero in about 300 years.

4.3. General Equation Used to Calculate GHG Loadings

By comparing the concentration equations above (B4-3 and B4-5) to the general GWP definition in equation B4-1, it can be seen that the GWP definition for a pulse emission includes the ratio of two integrated concentration decay functions.

In LCA, however, category indicators are represented as loadings based on the accumulation of continuous emissions over a selected time period, as illustrated by Berntsen (2005).[3] These loading are represented as integrals, as shown for carbon dioxide in Equation B4-6.

Equation B4-6

$$\int_0^{TH}\int_0^{TH} C_{CO2}(t)\,dt = TH^2 / 2 \times 0.217 + 0.259 \times 172.9\,[TH - 172.9\,(1- e^{-TH/172.9})] + 0.338 \times 18.51\,[TH - 18.51\,(1- e^{-t/18.51})] + 0.186 \times 1.186\,[TH - 1.186\,(1- e^{-t/1.186})]$$

The corresponding integral for other GHGs is shown in Equation B4-7.

Equation B4-7

$$\int_0^{TH}\int_0^{TH}(e^{-t/LT})\,dt = LT\,(1 - e^{-TH/LT}) = LT\,[\,TH - LT\,(1 - e^{-TH/LT})] \qquad \text{(B4-F)}$$

The new GWP for continuous emission cases can now be defined, as shown in Equation B4-8, and is referred to as GWP*:

Equation B4-8

$$GWP^* = (a_i/a_r)\,\frac{\int_0^{TH}\int_0^{TH}(e^{-t/LT})\,dt}{\int_0^{TH}\int_0^{TH} C_{CO2}(t)\,dt} = (a_i/a_r)\,\frac{LT\,[\,TH - LT\,(1 - e^{-TH/LT})]}{\int_0^{TH}\int_0^{TH} C_{CO2}(t)\,dt}$$

The GHG *loading* is the *accumulated* GHG emissions *E* relative to CO_2 over the time horizon *TH*:

Equation B4-9

For pulse emissions:	GHG Loading = E x GWP
For continuous emissions:	GHG Loading = E x GWP*

[3] Berntsen *et al.:* "Response of Climate to Regional Emissions of Ozone Precursors: Sensitivities and Warming Potentials." Tellus, 57B, pp. 283-304, 2005.

The loading includes the integrals over the time horizon *TH* for one mass unit emission of the GHG_i and the GHG_r (CO_2):

Equation B4-10

$$GHG_i\ Loading = E_i \times (a_i/a_r) \quad \frac{LT\,[TH - LT\,(1 - e^{-TH/LT})]}{\int_0^{TH} \int_0^{TH} C_{CO2}(t)\,dt}$$

In sum, Equation B4-10 represents the basic GHG loading formula to be used for all time horizons as well as with long-lived and short-lived GHG loadings from pulse or continuous emission sources (on a per tonne basis).

4.4. Establishing GWP and RWP Values Using Annualized Radiative Efficiencies

4.4.1. Establishing Relative Radiative Efficiency and the One-Year GWP

The general equation for establishing a GWP represents the relative *radiative efficiency* of a GHG, comparing its radiative forcing *RF* at a given background concentration above baseline (i.e., the anomaly) to the radiative forcing *RF* of CO_2 at its background concentration above baseline (Equation B4-11). The annualized global emission can also be used as the basis of establishing the amount of GHG_i required to produce a given level of radiative forcing *RF*.

Since the present anomaly background concentration of carbon dioxide corresponds to an amount in the atmosphere of about 1,400 billion tonnes CO_2, this formula can be used to estimate the one-year GWP from known radiative forcing *RF* and global emission values.

Equation B4-11

$$GWP_{GHGi} = \frac{\text{Global RF}_{GHGi} \times \text{1400 billion tonnes CO}_2 \text{ accumulated loading}}{\text{Global RF}_{CO2} \times \text{Annual tonnes global GHG}_i \text{ emissions}}$$

4.4.2. Establishing the RWP

Regional warming potentials (RWP) are also established using Equation B4-11, substituting regional values for each factor.

4.4.3. Determining the 20-year Time Horizon GWP

Based on the one-year GWPs readily calculated from Equation B4-11, it is possible to establish 20-year GWPs. To convert the one-year GWP to a 20-year GWP, it is multiplied by the factor 0.93/13.6, which is the ratio of the atmospheric decay integrals for CO_2 (Equation B4-12).

Equation B4-12

$$[\int_0^1 C_{CO2}(t)\,dt] / [\int_0^{20} C_{CO2}(t)\,dt] = 0.93/13.6 = 0.068$$

These integrals have been calculated and results shown in Table B4-1 and Table B4-2 in the column "Integrated CO_2." This simple conversion is valid for all short-lived substances, where the atmospheric lifetime is significantly less than one year ($LT << 1$ year).

4.5. Selection of Carbon Dioxide as the Reference GWP

Consistent with the IPCC framework, GWP and GWP* values for nitrous oxide, black carbon, tropospheric sulfate aerosols, tropospheric ozone and methane are benchmarked against the weakest of the key GHG emissions, carbon dioxide, with a value of GWP = 1.

4.6. Limits of Aggregation

The individual GHG loadings are first calculated as CO_2-equivalents. These loadings must then be aggregated into an overall GHG loading separately within the Global and Arctic GHG accounting systems.

4.7. Calculating Category Indicator Loadings for the Longer-Lived GHGs: Methane, Nitrous Oxide and Carbon Dioxide

4.7.1. Establishing the GWPs for Methane and Nitrous Oxide

The calculated GWP values for nine time horizons for methane were derived according to standard IPCC protocols by using Equation B4-1, assuming a 12-year atmospheric lifetime (Table B4-1). The annual time horizon value of 105 reflects the intensity of methane during its first year in the atmosphere, and is consistent with current published values (Shindell, 2009).[4] (This intensity is particularly noteworthy within the Arctic region, given the current and projected releases from regional sources.)

[4] Drew T. Shindell, Greg Faluvegi, Dorothy M. Koch, Gavin A. Schmidt, Nadine Unger, Susanne E. Bauer "Improved Attribution of Climate Forcing to Emissions," NASA Goddard Institute for Space Studies and Columbia University, New York, NY 10025, USA), October 30, 2009. www.sciencemag.org

Table B4-1. Temporally Characterized Methane GWP Values

Time horizon (TH) year	Decay CO_2	Decay CH_4	Integrated CO_2 *1)*	Integrated CH_4 *2)*	GWP *3)*	GWP* *4)*
1	0.8748	0.92	0.93	0.96	105	104
2	0.8109	0.8465	1.77	1.84	106	105
3	0.7738	0.7788	2.56	2.65	105	105
5	0.7294	0.6592	4.06	4.09	102	105
10	0.6584	0.4346	7.52	6.78	92	99
20	0.5624	0.1889	13.59	9.73	73	86
50	0.4336	0.0155	28.15	11.81	43	60
100	0.3638	0.0002	47.82	12.00	26	40
500	0.2314	0	157.27	12.00	8	13

1) Eq. B4-6
2) Eq. B4-7, where LT = 12 years
3) Eq. B4-1, where $a_i/a_r = 101.7$
4) Eq. B4-8, where $a_i/a_r = 101.7$

For methane, the a_i/a_r can be determined from IPCC 2007[5] as (3.07 E-4)/(1.4E-5) on a $Wm^{-2}ppbv^{-1}$ basis. This ratio must be multiplied by the inverse molecular weight ratio $Mw_r/Mw_i = 2.75$, and also multiplied by 1.4 to account for indirect effects, resulting in $a_i/a_r = 102$ on a mass basis.

Corresponding data for N_2O has likewise been calculated. In this case, the a_i/a_r can be determined from IPCC 2007 as (3.03 E-3)/(1.4E-5) on $Wm^{-2}ppbv^{-1}$ basis. This ratio is multiplied by the inverse molecular weight ratio $Mw_r/Mw_i = 1.00$, resulting in $a_i/a_r = 216.4$ on a mass basis.

Table B4-2. Temporally Characterized GWP Values for N_2O

Time horizon (TH) year	Decay CO_2	Decay N_2O	Integrated *CO_2 1)*	Integrated N_2O *2)*	GWP *3)*	GWP* *4)*
1	0.8748	0.991	0.93	1.0	232	227
2	0.8109	0.983	1.77	2.0	242	235
5	0.7294	0.957	4.06	4.9	261	251
10	0.6584	0.916	7.52	9.6	276	265
20	0.5624	0.839	13.59	18.3	292	280
50	0.4336	0.645	28.15	40.5	311	301
100	0.3638	0.416	47.82	66.6	301	306
500	0.2314	0.012	157.27	112.6	155	211

1) Eq. B4-6
2) Eq. B4-7, where LT = 114 years
3) Eq. B4-1, where $a_i/a_r = 216.4$
4) Eq. B4-8, where $a_i/a_r = 216.4$

[5] *Ibid.*

4.7.1.1. Establishing RWP Values for Regional Methane Loadings

The atmospheric lifetime of methane varies by latitude from 8.5 years in the tropics to 20 years in areas above 30-degrees latitude north. Due to its reactive nature, methane is converted by hydroxyl radicals into ozone, carbon monoxide and carbon dioxide at lower latitudes. In the latitudes between 30 degrees north and 30 degrees south, the rate of photochemical oxidation is reported to be 77 percent (stratosphere and troposphere combined) resulting in an atmospheric lifetime *LT* of 8.5 years, while above 30 degrees this rate drops to less than 10 percent,[6] resulting in regional atmospheric lifetime of up to 20 years, and a regional background concentration that is 20 percent higher than observed at lower latitudes. These higher northern latitude methane background concentrations are accounted for by adjusting the GWP by a corresponding 14 percent compared to the global average one year GWP value (105) as the benchmark, resulting in an adjusted Arctic RWP of 117.

While it has been assumed that methane is a uniform, well-mixed GHG emission similar to CO_2, these upper latitude enhanced concentrations demonstrate the regional nature of the RF within the northern polar region, providing an important justification for establishment of the Arctic RWP. Additionally, regional sources of methane (e.g., releases from melting of the permafrost; releases of methane hydrates) can also be trapped by the winter Arctic Vortex, adding to the early spring regional methane RF intensity and potentially leading to a seasonal RWP if such pulses are found.

4.7.2. Establishing GWPs, RWPs, GCPs and RCPs for Halocarbons

Discussion to be inserted.

4.7.3. Calculating GHG Loadings

Equation B4-13 is used to calculate the loadings for the long-lived GHG category indicators by emission source. This equation is consistent with standard IPCC calculations, and requires the use of standard UNFCCC protocols for land use conversion in the case of industrial systems that involve biobased materials derived from agricultural production. Such systems must account for nitrous oxide fluxes to determine the net GHG loading or sequestration.

Equation B4-13

GHG Loading/Sequestration from Industrial Sources

$$\text{GHG Loading/Sequestration} = \sum_i [\sum(\text{GHG} \times \text{GWP*})]\ \text{TH} - \sum s_i [\sum(\text{GHG} \times \text{GWP*})]\ \text{TH}$$

[6] T. M. Butler. "Automated Sequence Analysis of Atmospheric Oxidation Pathways: SE QUE NCE Version 1.0," *Geoscience.* Model Dev. Discuss., 2, pp. 1001–1021, 2009.

Where:

- *i represents the total number of unit processes.*
- $\sum s_i$ *represents the unit processes involved in offsets or sequestration (included as negative loadings)*
- *GHG represents the total annual emissions in tonnes of each key GHG*
- *GWP* represents the global warming potential for each key GHG emission*
- *TH = Time horizon*

4.8. Calculating Category Indicator Loadings for the Short-Lived GHGs: Tropospheric Ozone, Black Carbon and Tropospheric Sulfate Aerosols

4.8.1. Tropospheric Ozone Loadings

Tropospheric ozone (TO) is considered a key GHG based upon Brasseur and IPCC RF intensity estimates. IPCC has reported a range of tropospheric ozone RF values from 0.25 to 0.65 W/m^2, with the general consensus around 0.48 W/m^2.[7] As cited by Mastuno and Kido (2001):

> *"The globally averaged radiative forcing produced by the changes compared to per-industrial levels in ozone is estimated to be 0.48 Wm–2 (Brasseur et al., 1998), with regional RF effects reaching almost 1.4 Wm–2."*[8]

Unger *et al.* projected an increase in global tropospheric ozone RF of 0.14 W/m^2 (28 percent) from 2010 to 2030, with regional RF effects reaching up to 2.00 W/m^2.[9]

The calculation of tropospheric ozone loadings from specific sources requires the establishment of specific characterization factors to account for the seasonal nature of this GHG and the fact that tropospheric ozone is formed from the NO_x precursor and not directly emitted from sources (Equation B4-14).

1. The precursor conversion factor (PCF) represents the conversion rate of NO_x into TO on a per-tonne basis.
2. ECF_{OS} represents the fraction of the year in which photooxidation conditions are sufficient to form TO (widely known as the "ozone formation season").[10]

[7] IPCC Climate Change 2007

[8] Guy P. Brasseur, Jean-Francois Müller, Xuexi Tie and Larry Horowitz "Tropospheric Ozone and Climate: Past, Present and Future", published in *Present and Future of Modeling Global Environmental Change: Toward Integrated Modeling*, Eds., T. Matsuno and H. Kida, pp. 63–75. 2001.

[9] Nadine Unger, Drew T. Shindell, Dorothy M. Koch, and David G. Streets; "Air Pollution Radiative Forcing From Specific Emissions Sectors at 2030;" *Journal of Geophysical Research*, Vol. 113, 2008.

[10] The use of PCFs in characterizing indicator results is described in Annex A.

Equation B4-14

Calculating TO Loadings

$$\text{TO Loading} = (\text{Tonnes of } NO_x \text{ Emissions} \times ECF_{os} \times PCF)(GWP)$$

Where:

- *PCF represent the conversion efficiency of NOx into eq. tonnes of TO*
- *GWP represents the global warming potential of TO*
- *ECF_{os} represent the TO formation season (fraction of the year that forms TO from source)*

4.8.1.1 Establishing the GWP

The GWP values for tropospheric ozone were derived by comparing its radiative efficiency to CO_2 in accordance with Equation B4-11.

The method of establishing the GWP for TO involves the use of annual TO and CO_2 emissions, their global loadings and their global RF values.

- TO annual emissions: 340 million tonnes
- Range of IPCC values for RF of TO: +0.25 to 0.65 W/m^2 (2008 consensus on median value of 0.37 W/m^2)[11]
- CO_2 legacy loading: 1,400 – 1,558 billion tonnes
- CO_2 RF: 1.66 W/m^2

$$\text{TO GWP}_{\text{annual}} = \frac{0.37 \text{ W/m}^2 \times (1400 \text{ to } 1558 \text{ billion tonnes } CO_2)}{1.66 \text{ W/m}_2 \times 340 \text{ million tonnes TO}} = 918 \text{ to } 1022 \text{ t } CO_2e \text{ / t TO}$$

$$\text{TO GWP}_{\text{20year}} = (918 \text{ to } 1022) \times 0.068 = 62 \text{ to } 69 \text{ t } CO_2e \text{ / t TO}$$

Based on the ranges shown in the above equation, the average $GWP_{20\text{-year}}$ for TO is therefore 66, , while the GWP_{annual} is 970.[12]

4.8.1.2 Establishing the TO Precursor Conversion Factors

TO is formed indirectly from a series of linked atmospheric reaction between ultraviolet radiation, the NO_x mixture of emissions, available hydroxyl radicals and volatile organic carbon (VOC) background concentrations and regional emissions. The contribution of these precursors to the formation of TO can be highly variable, depending on regional conditions. Atmospheric conditions that

[11] Unger et al., 2008.

[12] The variation in the reported radiative forcing values for tropospheric value are dependent on the regional nature of the data used by different models rather than on the certainty of the models themselves. The reported upper end value of +0.45 W/m^2 therefore has equal certainty to the mean value reported of +0.37 W/m^2. The higher value would yield a 20-year GWP of 1,243, and an annual GWP of 84. (The range of reported radiative forcing values are shown in M. Gauss, et al., 2006.)

result in TO formation can be unique to specific geographic regions and seasons of the year. TO can transport over long distances with atmospheric lifetimes greater than 30 days, with columns as high as 14 km (at the tropopause) and concentrations reaching 50-85 Dobson Units (DU),[13] depending upon prevailing wind patterns and mixing and formation conditions.[14]

While the precursor conversion factor (PCF) for the conversion of NO_x to form ground level ozone (GLO) has been extensively studied, no comparable factors have been published to describe the conversion of NO_x into TO on a per tonne NO_x emission basis. NO_x gases convert through several distinct reaction pathways. Some isomers of NO_x include "hot atom" free radicals, such as $NO^{\bullet}$ that are capable of initiating the oxidation sequence with any molecule they comes into contact with, including oxygen.

NO_x gases undergo several distinct chemical stages over the course of their dispersion. In the immediate area of their release, partially oxidized isomers of NO_x, such as "hot atom" free radical ($NO^{\bullet}$) scavenge ozone out of the atmosphere, leading to a net reduction of ozone concentrations close to the source of the NO_x emissions. However, over their long-range transport (up 2000 km), NO_x emissions lead to the formation of additional ozone sufficient to result in an overall net increase per tonne of ozone produced from a tonne of NO_x —in the range of 0.8 to 1.2 times —depending local and regional conditions.

Ozone formation follows a sequence of specific reactions. The sequence is almost always initiated by the reaction of various VOCs or carbon monoxide (CO) with the hydroxyl (OH) radical. This initial reaction is followed by the conversion of NO to NO_2 (through reaction with HO_2 or RO_2 radicals), which also regenerates OH. NO_2 is photo-oxidized into hot atom atomic fragments, which recombine with oxygen (O_2) to create ozone (O_3) directly. In the troposphere, the formation of ozone involves more complex sets of reactions than ground level ozone formation, which occurs close to the ground, due to the enhanced photo-oxidation potential of NO_2. Some of the highest concentrations of TO occur near the tropopause, further indicating that conversion rates from NO_x into TO at high altitudes exceed the normal conversion rates found for precursors of ground level ozone.[15]

P. Hoor *et al.* provides the basis for establishing PCF values used herein for transportation sector.[16] However, Hoor's estimates do not follow LCIA

[13] One Dobson Unit refers to a layer of ozone that would be 10 µm thick under standard temperature and pressure.

[14] An important background reference on the contribution of Tropospheric Ozone to climate change is Ivar S. A. Isaksen,'s *Tropospheric Ozone: Regional and Global Scale Interactions,* Series C: Mathematical and Physical Sciences Vol. 227. 1988 (Springer) ISBN 9027726760.

[15] Sasha Madronich, "Tropospheric Photochemistry and Its Response to UV Changes," National Center for Atmospheric Research, Boulder, Colorado USA, 1993, as cited in "The role of the stratosphere in global change," Vol. 18. NATO-ASI Series, ed. M-L. Chanin, pp. 437-61. Amsterdam: Springer-Verlag.

[16] *Atmospheric Chemistry and Physics*, Vol. 9, pp. 3113–3136, 2009. www.atmos-chem-phys.net/9/3113/2009/

characterization and partitioning rules, whereby annual NO_x emission rates are partitioned by ozone season adjusted NO_x conversion into TO on an equivalent tonnage basis. It is assumed here that the annual global ozone season is approximately four months. As a result, the conversion factors shown in the table below must be multiplied by three before being used as PCFs.

Table B4-3. Global annual average ozone burden change per annual integrated NOx-emission of each respective transport sector in molecules (ΔO3)/molecules (NOx-emission)
Source: Hoor et al. 2009, Table 6 [17]

	TM4	OSLO	LMDz	UCl	p-TOM	mean	α
Road	0.31	0.44	0.34	0.35	0.26	0.33	0.05
Ship	0.47	0.65	0.46	0.57	0.57	0.54	0.07
Air	1.32	1.22	1.45	1.39	2.78	1.63	0.58

4.8.1.3 Establishing the $ECF_{Ozone\ season}$

The seasonality in the formation of TO is factored into the calculation through an environmental characterization factor ($ECF_{Ozone\ season}$) that represents the fraction of the year that TO forms within a given region. For example, TO production generally returns to background levels during the fall, winter and early spring when ultraviolet radiation is weakest. Therefore, non-seasonal NO_x emissions are not included in the calculation.

[17] P. Hoor *et..al.*, "The Impact of Traffic Emissions on Atmospheric Ozone and OH: Results From QUANTIFY, *Atmospheric Chemistry and Physics*, Vol. 9, pp. 3113–3136, 2009.

Figure B4-1. TO Plume Concentrations for Ozone Production Season (NASA OMI Satellite)
Source: *http://hyperion.gsfc.nasa.gov/Data_services/cloud_slice/*

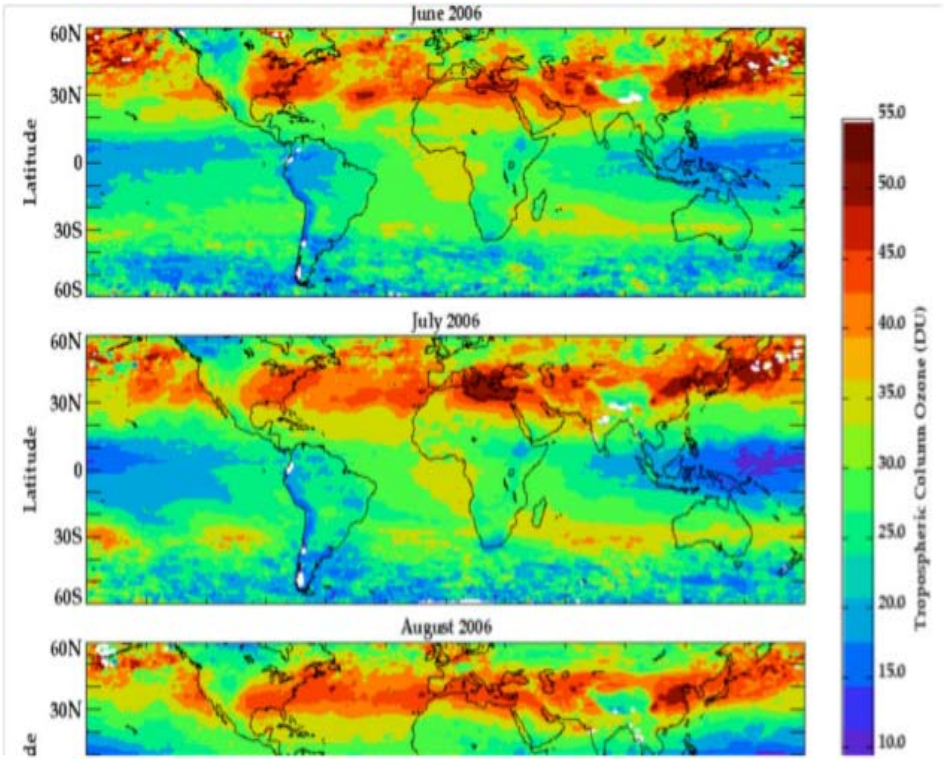

Figure B4-2 below shows the annualized TO loading over the Arctic Climate Assessment Region. Plume data are needed to complete the contribution analysis for these observed TO loadings.

Figure B4-2: Observed TO concentrations in the Arctic Region, aggregated from time-lapsed images over one season.
Source: NASA

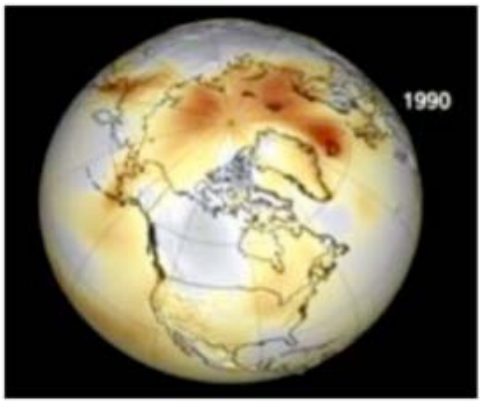

NCAR Mozart-4 atmospheric composition remote sensing and prediction system, now in place, shows the Arctic TO column levels at 370 DU, (July 9th, 2009). This level represents at least a 100 DU anomaly above the baseline for the region. Using the conversion of DU to RF of +0.5 W/m^2 per 10 DUs (Shindell, 2008), this Arctic TO anomaly represents a localized RF anomaly of at least +5.0 W/m^2 — almost three times more intense than the current global RF anomaly of +1.66 W/m^2. Such levels are consistent with Shindell's

regional forcing by latitude,[18] pointing out the need for regional characterization of GHGs to accurately account for regional TO loadings, such as in the Arctic.

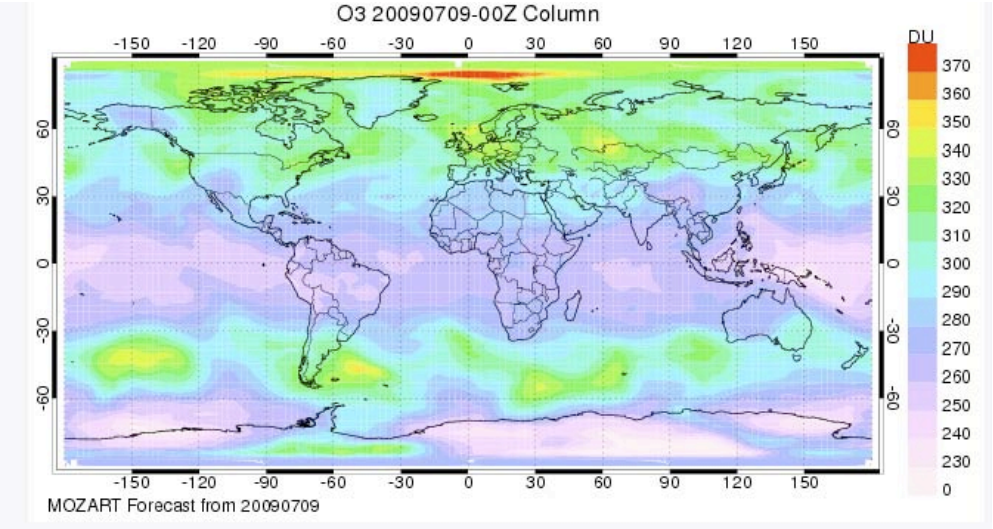

Figure B4-3. Regional variations in ozone distribution
Source: Shindell, 2009

According to Shindell: "Tropical, mid-latitude or polar mean temperatures largely follow the forcing per local unit area when the forcing is applied within that latitude band so that mid-latitude forcing must be ~2.4 times larger than tropical forcing and polar forcing must be 7 times greater than the tropical forcing. Our calculations suggest that black carbon and tropospheric ozone have contributed ~0.5 to 1.4°C and ~0.2 to 0.4°C, respectively, to total RMT of 2.9°C of total Arctic warming since 1890, making them attractive targets for Arctic warming mitigation."

4.8.2 Black Carbon Loadings

The black carbon loading calculations are conducted in accordance with Equation B4-14.

Equation B4-14

Calculating Black Carbon Loadings (by Time Horizon)

$$\text{BC Loading} = (\text{Tonnes of BC Emissions})\,(\text{GWP or } RWP_{eq})$$

Where:

- *GWP represents the global warming potential*
- *RWP values includes the RF equivalent loss of albedo to regional ice sheets.*

[18] Shindell and Faluvegi, April 2009.

4.8.2.1. Establishing the GWP

GWP for black carbon (BC) was calculated based on the reported global BC radiative forcing anomaly of +0.6-0.9 W/m^2 resulting from annual emissions of about 15-22 million of BC emissions (in tonnes) is compared to +1.66 W/m^2 RF from 1,400 billion tonnes of accumulated CO_2 loading (Equation B4-11).

GWP_{Annual} Value for Black Carbon

Lower value

$$\text{BC GWP} = \frac{0.6\ W/m^2}{1.66\ W/m^2} \times \frac{1{,}400{,}000{,}000{,}000\ \text{tonnes}}{15{,}000{,}000\ \text{tonnes}} = 33{,}700$$

Upper value

$$\text{BC GWP} = \frac{0.9\ W/m^2}{1.66\ W/m^2} \times \frac{1{,}400{,}000{,}000{,}000\ \text{tonnes}}{22{,}000{,}000\ \text{tonnes}} = 34{,}500$$

As shown in Figure B4-4, these values line up closely with GWP values established by Venkataraman (2004) over the annual time horizon.

Figure B4-4. Published BC GWP Values

The middle line on the chart represents the medium BC/Medium CO_2 case.

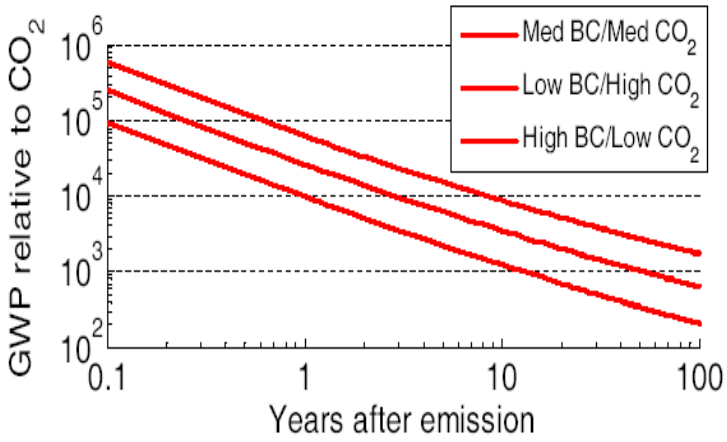

The 20-year time horizon GWP for BC can be calculated using the same method shown for TO above, and is in close agreement with the value depicted in Figure B4-4:

$$GWP_{20\ \text{years}} = 34{,}000 * 0.068 = 2{,}312$$

4.8.2.2 Establishing the RWP_{eq}: Accounting for Loss of Ice Albedo

Aside from its GWP ~ 34,000, BC reduces the albedo (i.e., reflectivity) of surfaces upon which it is deposited, and contributes to the melting of glaciers and the break-up of the Arctic Perennial Ice Sheet. Scientists have established radiative forcing equivalencies by correlating BC contamination levels in Greenland and the Arctic to loss of ice. These radiative forcing equivalencies have been integrated with the established global radiative forcing data to yield an equivalent regional warming potential (RWP_{eq}).

Measurements of BC, vanillic acid and non-sea-salt sulfur in ice cores indicate that both the sources and concentrations of BC precipitating over Greenland have varied greatly since 1788 as a result of boreal forest fires and industrial activities. Beginning about 1850, industrial emissions produced a seven-fold increase in ice-core BC concentrations, with most of the change occurring in winter. Black carbon concentrations after about 1951 were lower, but began to increase sharply over the past decade. At its maximum from 1906 to 1910, estimated climate forcing in early summer from surface BC in Arctic snow was about +3 W/m^2 atmospheric equivalent, or eight times the typical pre-industrial value.[19] Recent radiative forcing equivalency values (Figure B4-5) range from +0.1 to +1.5 W/m^2, with an average of +0.3 W/m^2 over the past decade. These values are in good agreement with NASA data. They serve as the basis for establishing the albedo contribution to total radiative forcing from BC at +1.2 W/m^2, compared to carbon dioxide at +1.85 W/m^2. This additional radiative forcing from the loss of albedo is then used to establish the Arctic warming potential for BC, which is described in Section 3 of this annex.

Figure B4-5. Surface Radiative Forcing by Year in the Greenland and Arctic Ice Cores from black carbon (1800 to 2001).
Source: NASA, 2007

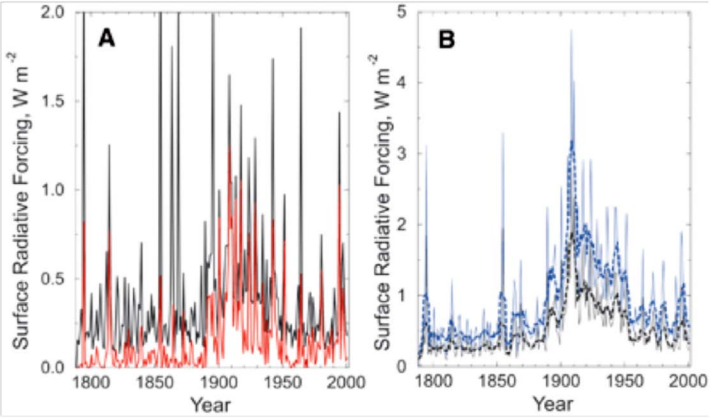

[19] Joseph R. McConnell, Ross Edwards, Gregory L. Kok, Mark G. Flanner, Charles S. Zender, Eric S. Saltzman, J. Ryan Banta, Daniel R. Pasteris, Megan M. Carter, Jonathan D. W. Kahl.. "20th-Century Industrial Black Carbon Emissions Altered Arctic Climate Forcing," *Science* 7, Vol. 317. no. 5843, pp. 1381 – 1384, September 2007.

The Arctic RWP is calculated using the following: 1) total global radiative forcing = +0.9 W/m^2; and 2) radiative forcing from the effects of black carbon contamination of Arctic ice sheets at +0.1 to +1.5 W/m^2 atmospheric equivalent, with an average of +0.3 W/m^2 over the past decade. Table B4-4 presents the GWP and range of Arctic RWPs, depending upon assumptions of annual loading and known annual variations in albedo RF for the Arctic region. This RWP is unique in that the specific value can only be established after the yearly deposition has been estimated. Hence, the BC loadings into the Arctic region can only be retroactively assigned RWP value.

Table B4-4. Establishing the Arctic RWPs for BC

Annual Global BC Loading (tonnes CO_2e)	**A-CO_2 Loading Baseline**	**RF Anomaly CO_2**	**RF Global Anomaly — BC**	**RF Anomaly Equivalency— BC, from Loss of Albedo**	**GWP**
15-22 million	1,400 billion	1.66	0.9	NA	34,000
Regional BC Loadings					**RWP**
Unknown	1,400 billion	1.66	0.9	0.3 (Average)	45,000 (1995-2005)
Unknown	1,400 billion	1.66	0.9	1.5	90,000 (2001)

4.8.3. Accounting for the Cooling Effects of Tropospheric Sulfate Aerosols (TSAs)

4.8.3.1. Direct and Indirect Cooling

Tropospheric sulfate aerosols (TSAs), formed from emissions of sulfur dioxide that are converted into sulfates by photo-oxidation, have an inherent cooling effect (i.e., negative radiative forcing) from their reflectivity of incident solar radiative forcing, as well as an indirect positive increase in the albedo effect of clouds. The cooling effects of TSA (IPCC, 2007; SRES 2000; Jones *et al.* 2000) are shown in radiative forcing equivalents, with significant regional variations (e.g., maximums in industrial areas of Europe, the east coast of the U.S. and southeast Asia). The inherent cooling can result in a net radiative force reduction of up to -2.25 W/m^2. According to the IPCC, this indirect cooling is dependent upon the spatial distribution of the aerosol column concentrations.

The IPCC SRES 2000 estimates of future TSA loadings are highly uncertain, but on average, show a steady decline over the next 50 years that would reduce the net cooling effects of TSA (Figure B4-6). Consistent with the upper end SRES forecasts, Unger *et al.* projected a significant increase in TSA emissions by 2030, with an overall increase in negative forcing of -0.22 W/m^2.[20] In either case, TSA will play a significant role in overall RF changes over the next 20 years.

[20] Unger *et al.*, 2008.

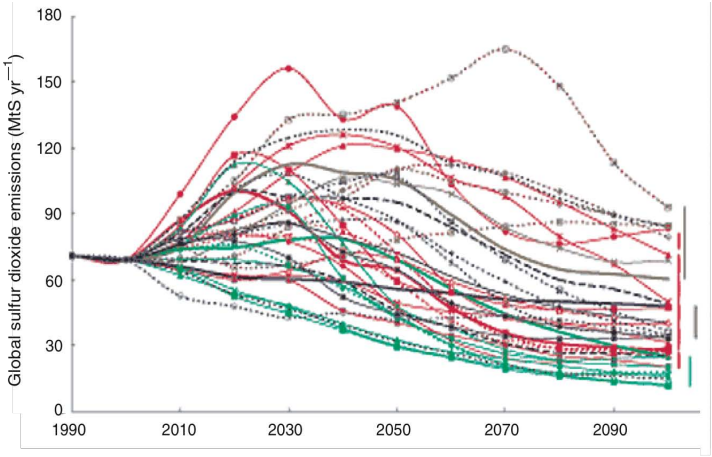

FIGURE 5-2 Global SO_2 emissions (million tons of sulfur per year) for the four SRES scenarios families and from each of the emissions models. Red lines correspond to the A1 family of scenarios, brown lines to A2, green lines to B1, and blue lines to B2. These emissions, along with the ozone precursor emissions of methane, carbon monoxide, nitrogen oxides, and volatile organic compounds, were also gridded onto $1^o \times 1^o$ latitude-longitude maps for use in global climate, atmospheric chemistry, and air quality models. The grids were developed using simple scaling applied to a base-year 1990 map and using the projected four to six regional changes from the SRES emissions models. SOURCE: Nakićenović et al. (2000).

Figure B4-6. SRES SO_2 Emission Modeling[21]

4.8.3.2. Establishing the GCP for TSA

The global cooling potential (GCP) of TSA is reported by the IMAGE 2 model (Brakkee 2008) as -94 for the 100-year time horizon. This value is used here as the basis of establishing GCP values for the annual and 20-year time horizons. [22]

Figure B4-7. Annual-Averaged Global Anthropogenic TSA Force Cooling by Isopleth (W/m^2)
Source: IPCC (2001)

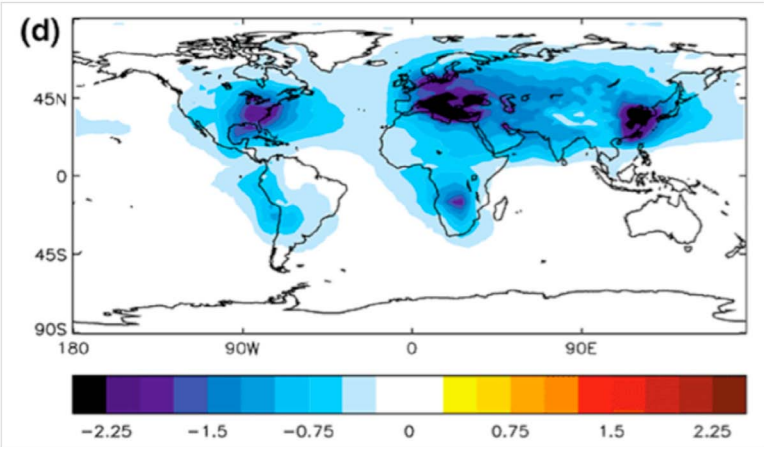

[21] IPCC *Climate Change 2007: Synthesis Report. Fourth Assessment Report.* Chapter 2, P. Forester

[22] Brakkee KW, Huijbregts MAJ, Eickhout B, Hendriks AJ, van de Meent D. 2008. Characterisation Factors for Greenhouse Gases at a Midpoint Level Including Indirect Effects Based on Calculations with the IMAGE Model. *The International Journal of Life Cycle Assessment 13* (3): 191-201. dx.doi.org/10.1065/lca2007.10.365.

The 100-year time horizon GCP is converted to annual and 20-year time horizon values using extrapolation factors from Table B4-1 as used for TO:

$$GCP_{Annual} = - 94 \times 47.8/0.93 = - 4{,}826$$
$$GCP_{20\text{-}Year} = - 94 \times 47.8/13.6 = - 330$$

Establishing the Ocean Albedo Cooling Potentials (OACP)

Coal-fired plants located on the coast may be specifically designed to emit sulfur dioxide emissions for dispersion over the open ocean, resulting in significant direct and indirect TSA cooling effects, based on the inherent cooling effects of TSA and increased reflectivity of clouds. The GCP values may significantly understate the cooling potential from such planned designed releases, thereby justifying the establishment of an additional point source "ocean albedo cooling potential" (OACP). In such cases, the OACP would be established per tonne of SO_2 emitted that exceeds the global average established by the IMAGE 2 model.

4.8.3.2 Allocation of TSA Emissions into Unwanted and Beneficial Cooling

While TSA emissions provide significant global cooling that to some degree counteract the heating effects of the other key GHG emissions, aerosol releases during cold seasons can result in unwanted cooling during Heating Degree Days (HDD). If HDD-TSA is dispersed over populated areas, these emissions have the potential to further cool a region already using fossil energy to heat buildings, thereby indirectly adding to CO_2 emission trade-offs from the extra heating requirements. This "extra" heating is referred to here as "unwanted cooling."

On the other hand, TSAs emitted during Cooling Degree Days (CDD) can result in a reduction in the use of HVAC and other temperature cooling equipment and related energy consumption. These TSAs are therefore referred to as "beneficial cooling" releases. TSA emissions are partitioned into unwanted cooling and beneficial cooling, with ECF_{HDD} representing the fraction of HDD to total days per year, and ECF_{CDD} representing the fraction of CDD to total days per year.

4.8.3.3. Establishing Precursor Conversion Factor (PCF) from SO_2 to TSA

The rate of conversion of sulfur dioxide into TSA is both regionally and seasonally dependent, and is based upon the angle of the incident sunlight. The regional rates of conversion of sulfur dioxide have been established by various studies. For example, Figure B4-8 shows the summer high conversion in the range of 90 percent and the winter low conversion rates in the 30 percent range; correspondingly, the PCF for summer would be up to 0.9, and around 0.3 for winter. The PCF is highly dependent upon season and therefore should be established only completing the full time integral for a full 12-month period.

$$PCF = [SO_4/ SO_2]_t$$

Beneficial cooling per tonne of sulfur dioxide releases may be reported, provided that known human health and/or environmental impact indicator results are negligible and as long as other indirect GHG emissions are included in the overall reported results.

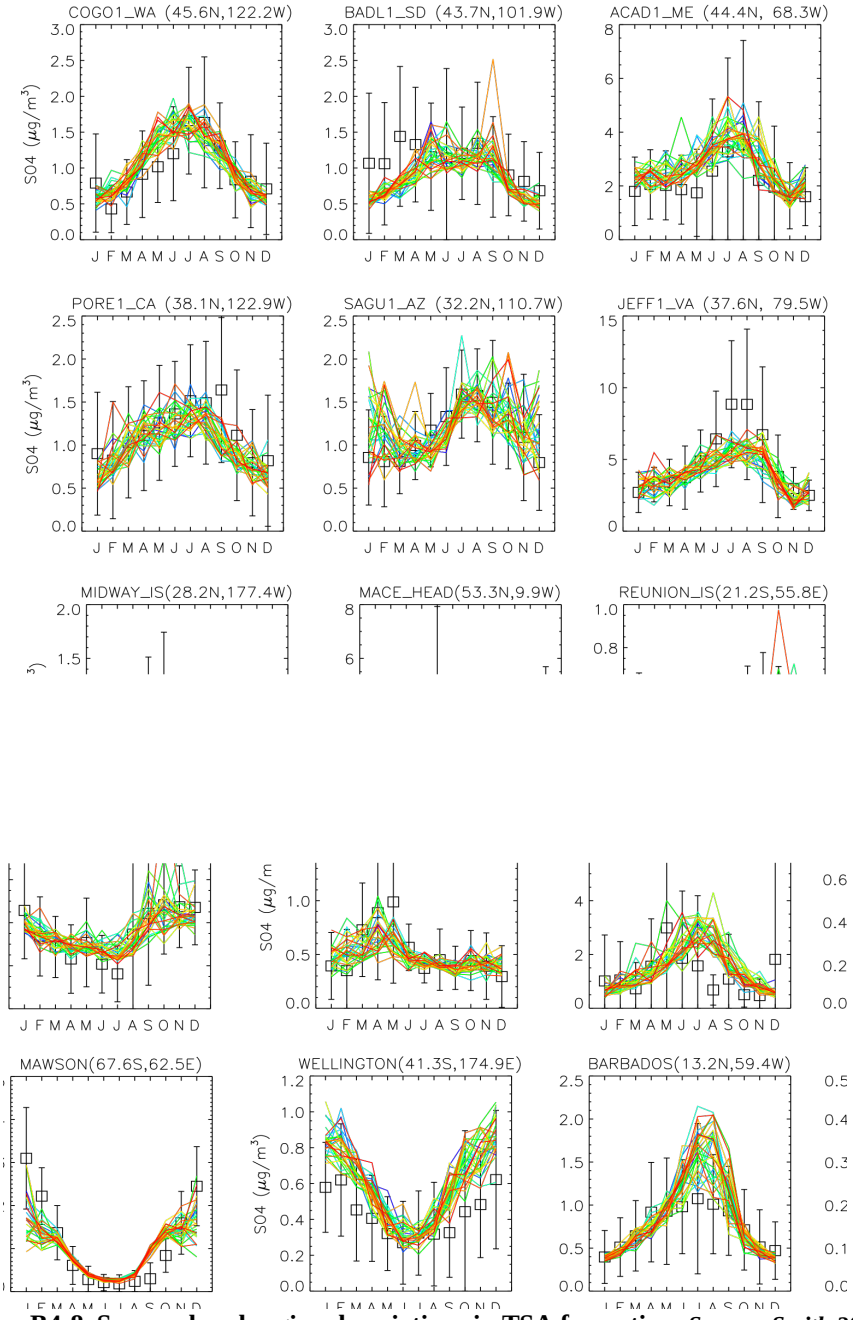

Figure B4-8. Seasonal and regional variations in TSA formation. ***Source: Smith 2006***[23]

[23] Cameron Smith, *et al.*, "Towards an Earth System Model: Atmospheric Chemistry, Coupling, Petascale Computing," *Journal of Physics*, Conference series 46, pp 343-350, 2006.

4.8.3.4. Calculation of Aerosol Beneficial Cooling

Equation B4-15 is used to calculate the beneficial TSA cooling, expressed in minus CO_2 equivalents ($-CO_2e$) to represent negative radiative forcing. If GHG emission trade-offs are predicted to be involved in annual TSA releases from specific sources, the equation must be expanded to include an accounting of such trade-offs.

Equation B4-15

Calculating the Beneficial Cooling for TSA

Beneficial TSA Cooling *(in tonnes $-CO_2e$)* $= (\text{Tonnes } SO_2 \text{ Emissions})(PCF)(-GCP)(ECF_{CDD}) + (\text{Tonnes } SO_2 \text{ Emissions}) - OACP - \text{Tonnes GHG emissions}_{\text{Indirect from CDD}}$

Where:

- *SCF represent the conversion factor of SO_2 to aerosol sulfates*
- *ECF_{CDD} is the fraction of the year with CDD*
- *GCP = Inherent Global Cooling Potential*
- *OACP=Ocean Albedo Cooling Potential*

In this equation, substituting HDD for CDD will yield the unwanted cooling from TSA.

4.9. GWP Values for Short-Lived GHG Emissions over Seven Time Horizons

The radiative efficiencies a_i, or radiative ratios a_i / a_r, for short-lived GHG emissions can be calculated from known GWP values described above and from the lifetime *LT*, as shown in Table B4-5 (below). Using these radiative efficiency ratios, GWP and GWP* values can be calculated for any time horizon.

By transformation of Equation B4-8 (and the corresponding GWP equation), the following equation is the result:

Equation B4-16

$$(a_i/a_r) = GWP^* \frac{\int_0^{TH}\int_0^{TH} C_{CO2}(t)\,dt}{\int_0^{TH}\int_0^{TH}(e^{-t/LT})\,dt} = GWP \frac{\int_0^{TH} C_{CO2}(t)\,dt}{\int_0^{TH}(e^{-t/LT})\,dt}$$

Using the GWP values in sections 4.8.1 to 4.8.3, the a_i/a_r (mass) ratio is calculated with B4-16 and shown in Table B4-5, together with the resulting GWP/GCP and GWP*/GCP* values for seven time horizons.

Table B4-5. GWP/GCP, a_i/a_r, and LT values for short-lived GHG emissions over seven time horizons

		CO_2	Tropospheric Ozone			Black Carbon			Tropospheric Sulphate Aerosols		
ai/ar (mass)		1	15,000			673,000			-273,000		
LT		Eq. (6)	0.060			0.047			0.016		
TH			Eq. (3)	GWP	GWP*	Eq. (3)	GWP	GWP*	Eq. (3)	GCP	GCP*
1	yr	0.93	0.06	970	1785	0.047	33,706	62,876	0.016	-4,826	-9,286
2	yr	1.77	0.06	510	956	0.047	17,714	33,453	0.016	-2,536	-4,863
5	yr	4.06	0.06	222	419	0.047	7,721	14,602	0.016	-1,105	-2,103
10	yr	7.52	0.06	120	226	0.047	4,169	7,854	0.016	-597	-1,128
20	yr	13.59	0.06	66	123	0.047	2,307	4,283	0.016	-330	-614
50	yr	28.15	0.06	32	58	0.047	1,113	2,004	0.016	-159	-287
100	yr	47.82	0.06	19	33	0.047	656	1,163	0.016	-94	-167

4.10. Accounting for Changes to Global GHG Background Concentration Balances

The ECF_{GBC} is an environmental characterization factor related to potential changes in the percentage contribution of each key GHG on a global basis (where "GBC" stands for global background concentration). For example, if the methane pulse (described in section 3) occurs during the twenty years from 2010 to 2030, then the percentage of carbon dioxide to total atmospheric GHG loading could fall from its current 33 percent (see section 2) to less than 10 percent. Since GWP values are intended to reflect the relative importance of the various GHG emissions, the value of the carbon dioxide GWP should be adjusted to reflect its contribution to the total global loading for the time period selected.

Equation B4-17

$$\mathbf{GWP_{GBC} = GWP \times ECF_{GBC}}$$

Where:
ECF means Environmental Characterization Factor
GBC means Global Background Concentration

4.11. Calculating Accumulated GHG Loadings and Accumulated Avoided GHGs for Strategic, Investment and Security Purposes

IPCC-based metrics have typically focused on pulse emission rates on a per tonne basis. However, when applied to assessments of major infrastructure systems and associated investments, such as energy sector changes, climate metrics must take into account the useful lifetime of the assets being evaluated, utilize specific industrial sector baselines, and evaluate implications within the near-term 20-year time horizon. The following equations provide methods for: 1) calculating the accumulated GHG ("A-GHG") loading baseline and the accumulated avoided GHG ("AA-GHG") benefits from new energy source options and upgrades; 2) establishing the GHG efficiency (i.e., GHG/unit produced) compared to its baseline; and 3) establishing the AA-GHG benefits relative to the scale of its baseline. These GHG

accounting methods can be used to link AA-GHG values to their respective investment timeframes.

The following discussion describes the methodology as it applies to one industrial sector — the energy sector.

4.11.1. Establishing the A-GHG Loading Baseline

The A-GHG loading associated with the energy industry-specific reference system serves as the baseline against which all GHG benefits are measured. This baseline is the basis for determining the total AA-GHG emissions of new energy source options compared to the GHG efficiencies of the baseline (current versus projected GHG emission rate per unit of production). In addition, the baseline establishes the relevant scale of production against which new source benefits should be compared. For example, both solar and nuclear options might provide equal GHG efficiencies on per 1000 GWh basis, but in terms of the scale of production, the total AA-GHG from the nuclear option could be 10 to 100-times higher than the AA-GHG from the solar option, and thus have a far greater effect in terms of reducing the total GHG loadings of the NERC during the 2010-2030 time horizon.

4.11.2. Calculation of Accumulated GHG Loadings

This section outlines the parameters necessary to establish the correct GWP for all key A-GHG loadings.

4.11.2.1. Averaged Background Concentrations of Continuous Carbon Dioxide Emissions within a Defined Operating Timeframe

The CO_2 case contains the following assumptions: a continuous emission of one mass unit of CO_2 per year that stops after 40 years. The concentration is shown as relative units.[24] Its development at varying time horizons *TH* is shown in Figure B4-9.

[24] Instead of concentration the value can also be interpreted as number of mass units still present in the atmosphere at each point in time.

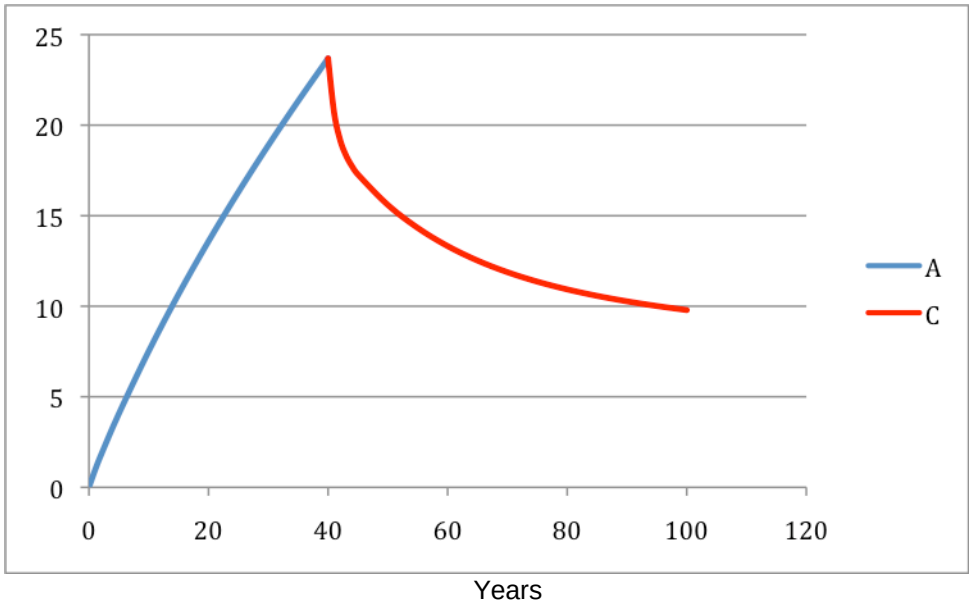

Figure B4-9. Carbon dioxide concentrations resulting from a continuous emission, starting at t = 0 and ending at t = 40 years. The A-line represents the emission phase, while the C-line represents the decay phase.

The calculations are shown below, as derived from Equation B4-3.

Concentration during the emission phase (blue line A)[25]

$C_A = 0.217\ TH + 0.259 \times 172.9 \times (1- e^{-TH/172.9}) + 0.338 \times 18.51(1- e^{-TH/18.51}) + 0.186 \times 1.186 \times (1- e^{-TH/1.186})$

Where TH means time horizon in years (variable)

Concentration during the decay phase (blue line C)[26]

$C_C = 23.7 \times [0.217 + 0.259\ e^{-t/172.9} + 0.338\ e^{-t/18.51} + 0.186\ e^{-t/1.186}]$

Where 23.7 is the concentration at emission stop.

As can be seen, the concentration (and therefore also climate effect) in this CO_2 example is not negligible, even after 100 years.

In Figure B4-10, the concentration has been averaged, first separately for the emission phase, then for the decay phase, and thirdly for these two combined.

[25] Source: Integrated IPCC 2007 decay function
[26] Source: Modified IPCC 2007 decay function

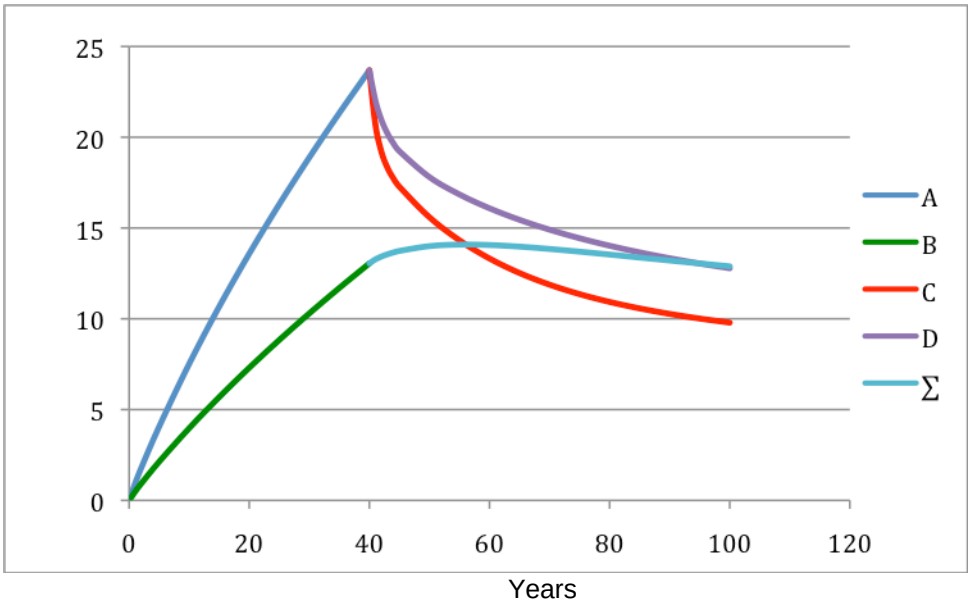

Figure B4-10. Carbon dioxide average concentrations resulting from a continuous emission starting at t = 0 and ending at t = 40 years.

The three calculations are shown as follows:

The average concentration varying with TH from t = 0 during the emission phase is the integral of the concentration during the emissions phase, divided by elapsed time (green line B):

Average concentration during the emissions phase

$$C_B = \{ TH^2 / 2 \times 0.217 + 0.259 \times 172.9 [TH - 172.9 (1- e^{-TH/172.9})] + 0.338 \times 18.51 [TH - 18.51 (1- e^{-t/18.51})] + 0.186 \times 1.186 [TH - 1.186 (1- e^{-t/1.186})]\}/TH$$

The average concentration varying with TH from t = 40 years onwards during the decay phase is the integral of the concentration during the decay phase, divided by elapsed time (purple line D):

Average concentration during the decay phase

$$C_D = 23.7 \times \{0.217 (TH-40) + 0.259 \cdot 172.9 \times (1- e^{-(TH-40)/172.9}) + 0.338 \cdot 18.51(1- e^{-(TH-40)/18.51}) + 0.186 \times 1.186 \times (1- e^{-(TH-40)/1.186})\}/(TH-40)$$

Finally, average concentration varying with TH from t = 0 years onwards is the combination of the average concentrations during the emissions and decay phases (green line B continuing in turquoise line ∑):

Average Concentration Overall
$\sum = [C_B \times 40 + C_D \times (TH-40)]/TH$

Over this 40-year period, the average concentration is thus 13.1. The average concentration (proportionate to RF) after 100 years is 12.9, and after 200 years, 10.7.

The products of the average concentration and time (i.e., the A-GHG loading, are 522, 1,289, and 2,138 mass unit years of CO_2 for the 40-, 100-, and 200-year time horizons, respectively.

4.11.2.2. Averaged Background Methane Concentrations in CO_2e from Continuous Emissions with a Defined Operating Timeframe

As in the carbon dioxide case presented above, the concentration is shown as relative units, and its development at varying time horizons *TH* is shown in Figure B4-11.

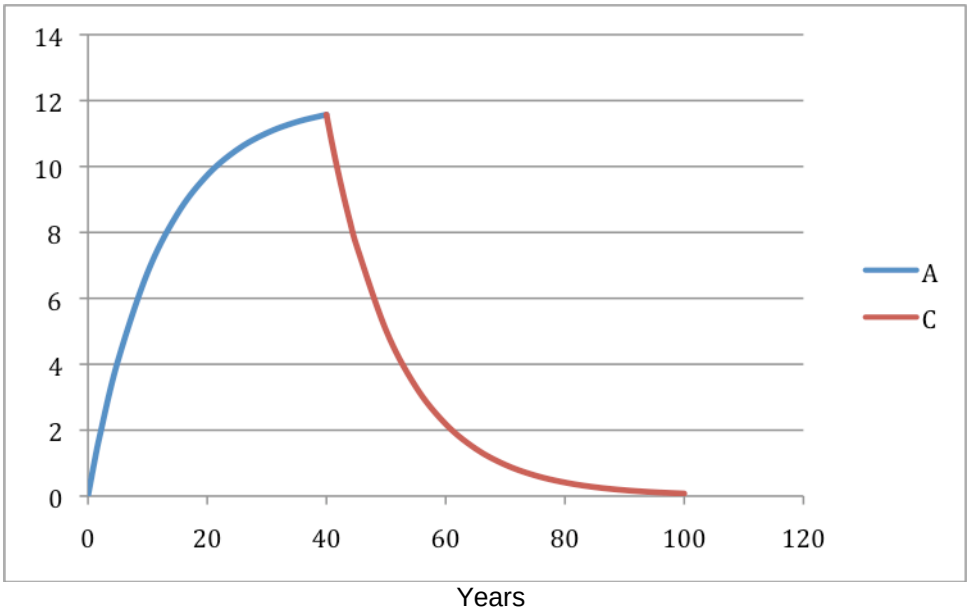

Figure B4-11. Methane concentrations resulting from a continuous emission starting at t = 0 and ending at t = 40 years.

The two calculations are shown below.

Concentration during the emission phase (blue line A)

$C_A = LT\ (1 - e^{-TH/LT})$
LT = methane lifetime = 12 years

Where TH = time horizon in years, variable.

Concentration during the decay phase (red line C)

$C_C = 11.6 \times e^{-((TH-40)/LT)}$

Where 11.6 is the concentration at emission stop.

In this case, the concentration (and therefore also climate effect) is reduced to almost zero (0.9 percent) within 100 years.

In Figure B4-12, the concentration has been averaged, first separately for the emission phase, then for the decay phase, and thirdly for these two combined.

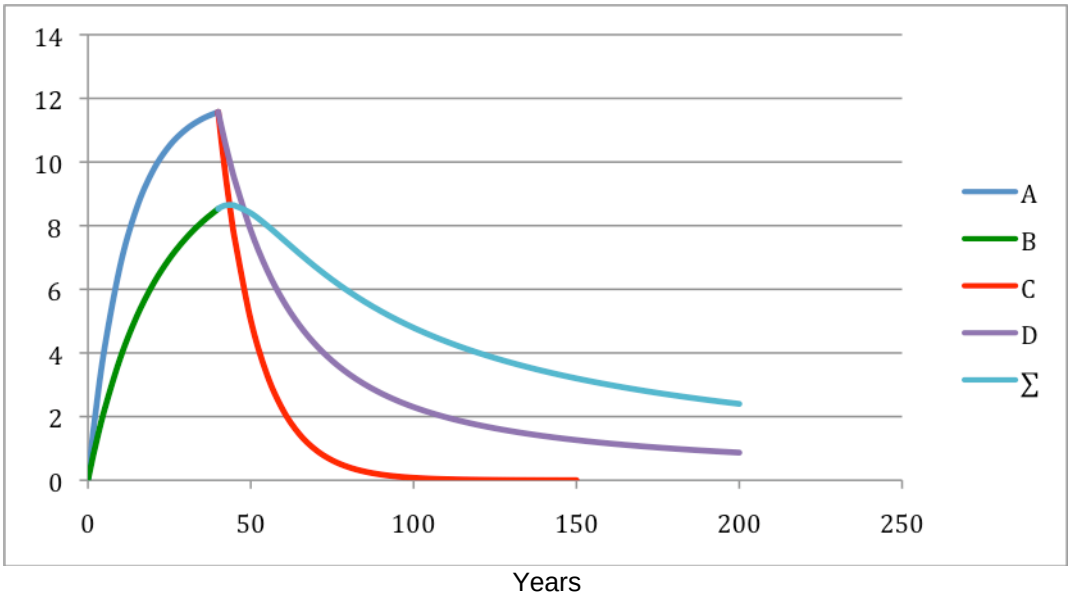

Figure B4-12. Methane average concentrations resulting from a continuous emission starting at t = 0 and ending at t = 40 years.

The calculations are shown below.

The average concentration varying with TH from t = 0 during the emission phase is the integral of the concentration during the emissions phase, divided by elapsed time (green line B):

Average concentration during the emissions phase

$$C_B = LT\,[\,TH - LT\,(1 - e^{-TH/LT})]/TH = 12\,[\,TH - 12\,(1 - e^{-TH/12})]/TH$$

Average concentration varying with TH from t = 40 years onwards during the decay phase is the integral of concentration during the decay phase, divided by elapsed time (purple line D):

Average concentration during the decay phase

$$C_D = \{\int_{40}^{TH-40} 11.6 \times (e^{-((t-40)/LT)})\, d(t)\}/(TH-40) = 11.6 \times 12\,(1 - e^{-(TH-40)/12})/(TH-40)$$

Finally, the average concentration varying with TH from t = 0 years onwards is the combination of the average concentration during the emission and decay phases (green line B continuing in turquoise line ∑):

Average concentration overall

$$\sum = [C_B \times 40 + C_D \times (TH-40)]/TH$$

As indicated by line B-∑, the average concentration is strongly dependent upon the time horizon applied. At 40 years, the average concentration is 8.5. The average concentration (proportionate to RF) after 100 years is 4.8, and after 200 years, 2.4. But the product of average concentration and time, which is the basis for the A-GHG loading quantity, are for these three time horizons is 341, 479, and 480 mass unit years of CH_4, respectively.

Multiplying the A-GHG loading amounts for CH_4 by the radiative efficiency ratio (a_i / a_r = 101 units CO_2e / unit CH_4) results in the A-GHG loading values of 34,440, 48,380, and 48,480 unit years of CO_2e. That the limit value for the A-GHG loading is nearly reached after 100 years is explained by the above mentioned observation that by then, methane decay will have resulted in a near zero concentration level.

4.11.2.3. Establishing Averaged Background Concentrations in CO_2e from Continuous Short-lived GHG Emissions with a Defined Operating Timeframe

This case shows how simple the temporal characterization is for short-lived GHG emissions. The assumptions are as follows: an emission of one mass unit of tropospheric ozone (TO) per year, that stops after 40 years. The concentration development is shown in Figure B4-13.

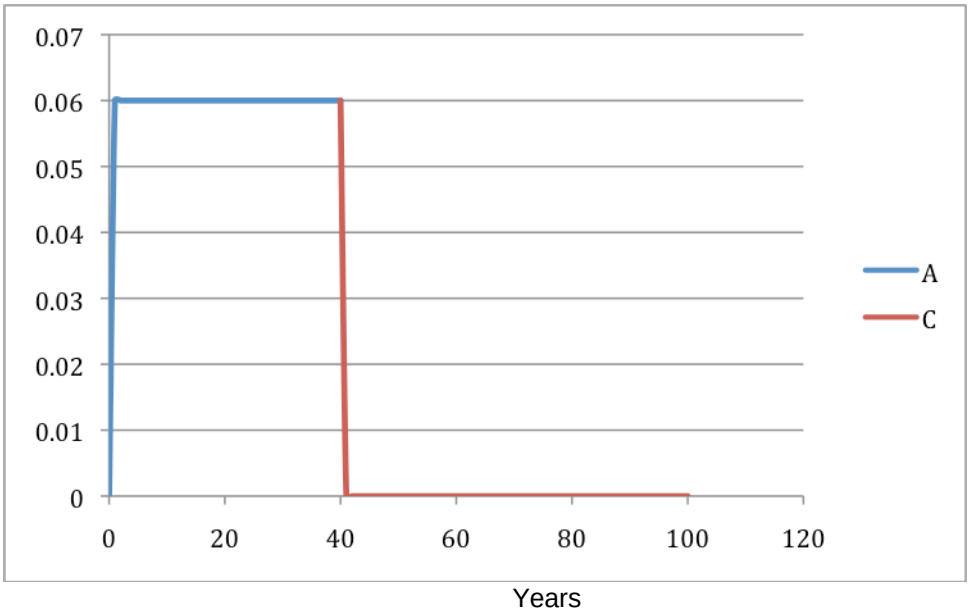

Figure B4-13. TO concentrations resulting from a continuous emission starting at t = 0 and ending at t = 40 years.

The calculations are shown below.

Concentration during the emission phase (blue line A)

$C_A = LT\ (1 - e^{-TH/LT})$

Where
LT means atmospheric lifetime of 0.06 years,
TH means time horizon in years, variable.

Concentration during the decay phase (red line C)

$C_C = 0.06\ e^{-(TH-40)/LT}$

Where 0.06 is the concentration at emission stop.

It can be seen that the concentration (and therefore also the climate effect) in this example is reduced to zero immediately after the end of emission (40 years).

In Figure B4-14, the concentration has been averaged, first separately for the emission phase, then for the decay phase, and thirdly for these two combined.

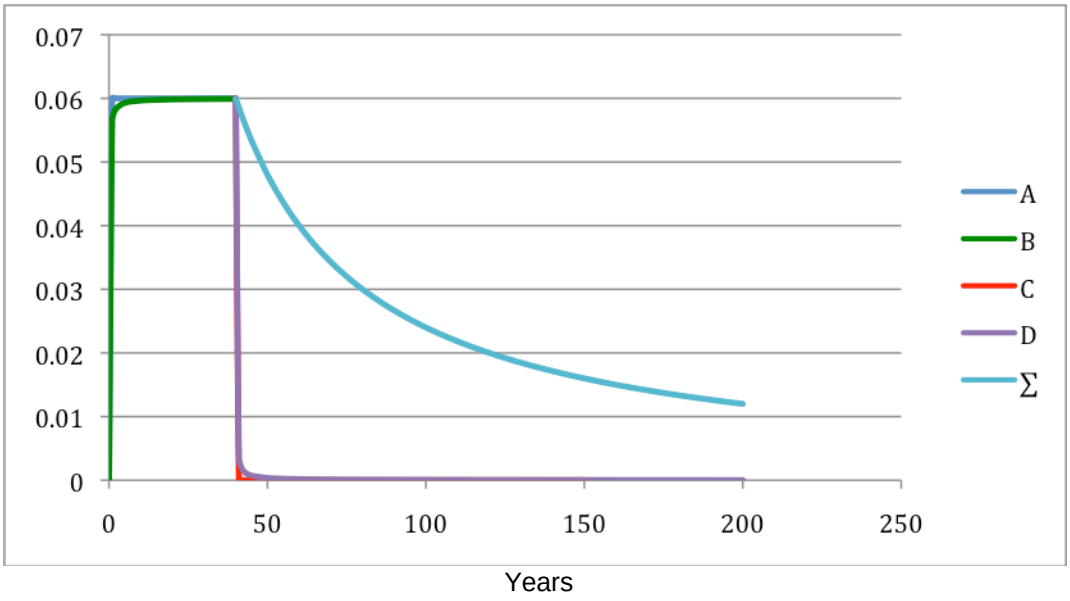

Figure B4-14. TO average concentrations resulting from a continuous emission starting at t = 0 and ending at t = 40 years.

The calculation are shown below:

Average concentration varying with TH from t = 0 during the emission phase is the integral of the concentration during the emissions phase, divided by elapsed time (green line B):

Average concentration during the emissions phase

$$C_B = \{\int_0^{TH} LT\,(1 - e^{-t/LT})\,d(t)\}/TH = LT\,[\,1 - (1 - e^{-TH/LT})\,/\,(TH/LT)\,]$$

Average concentration varying with TH from t = 40 years onwards during the decay phase is the integral of the concentration during the decay phase, divided by elapsed time (purple line D):

Average concentration during the decay phase

$$C_D = \{\int_{40}^{TH-40} 0.06 \times e^{-((t-40)/LT)}\,d(t)\}\,/(TH-40) = 0.06\,LT\,(1 - e^{-(TH-40)/LT})\,/(TH-40)$$

Finally, the average concentration varying with TH from t = 0 years onwards is the combination of the average concentrations during the emissions and decay phases (green line B continuing in turquoise line ∑):

Average concentration overall
$\sum = [C_B \times 40 + C_D \times (TH-40)]/TH$

The calculation of short-lived GHG emissions simplifies greatly when the atmospheric lifetime *LT* is short in comparison to the time horizon *TH*. The time variable $e^{-TH/LT}$ approaches zero at TH/LT=10 — i.e., in the TO case after TH=0.6 years. For those TH values > 0.6 years, the above equations for TO simplify to the following:

$C_A = LT$

$C_C = 0$

$C_B = LT$

$C_D = 0$

The average concentration in this case is not necessary to calculate. The A-GHG loading is simply the constant concentration during the emission period multiplied by 40 years (0.06 * 40 = 2.4 mass unit years).

Multiplying the A-GHG loading amounts as TO by the radiative efficiency ratio results in an A-GHG loading value of 55,200 unit years CO_2e.

a_i / a_r = 23,000 units CO_2e/unit TO

This limit value for the A-GHG loading is reached when the emission stops.

4.12. GWP Values Based Upon Accumulated Radiative Efficiencies

The previous derivations show results for a process emitting one mass unit per year of each substance during 40 years at three time horizons — 40, 100, and 200 years. It is essential to keep separate the two timeframes: process emission time (now called T), and temporal characterization time horizon (TH). The process emission time T will be kept constant at 40 years, as shown below, but results for other project lifetimes can easily be derived using the formulas developed above.

To see the general pattern caused by the variation of TH, consider first the results from short-lived TO in section 4.12.2.3. The accumulated loading shows a final value of 2.4 mass unit years of TO (55,200 mass unit years CO_2e), achieved after about 0.6 years after the end of TO emissions. The loading does not increase by extending the TH further.

In the case of methane (Chapter 4.12.2.2), the final loading, the constant limit 480 mass unit years of CH_4 (48,400 mass unit years CO_2e) is achieved practically in 100 years.

Correspondingly, the constant limit 2.4 mass unit years for TO is realized within one year.

A corresponding limit for carbon dioxide is never reached because of the constant term 0.217 in the decay function.

By examining further the equations derived and the calculation results, it becomes clear that for substances with simple lifetime decay functions:

$$C = C_0 \, e^{-t/LT}$$

This A-GHG loading limit is equal to *T x LT*, the product of process emission time and substance atmospheric lifetime:

CH_4: 40 x 12 = 480
TO: 40 x 0.06 = 2.4

As a general conclusion, it can stated that, for any process emission time *T*, the A-GHG loading as mass unit years is equal to:

A-GHG Loading = LT x T

in all cases where a simple exponential decay factor *LT* applies, provided that the time horizon *TH* is clearly longer (>10 times) than the atmospheric lifetime *LT*. The A-GHG loading divided by emission time is hereafter called the Accumulated Loading Factor ("ALF").

These results have been summarized in Table B4-6.

Table B4-6. Accumulated Radiative Forcing, TH = 100 years

	Emission, t/year	GHG atmospheric lifetimes, years	Accumulated loading factor (ALF), tonne GHG per average emission year	Radiative Efficiency Ratio (mass) a_i/a_r	Accumulated lifetime radiative forcing factor per average emission year
CO_2	1	NA	32.2	1	32.2
N_2O	1	114	66.4	216	14,342
CH_4	1	12	12	101	1,212
TO	1	0.06	0.06	23,000	1,380
BC	1	0.047	0.047	673,000	31,631
TSA	1	0.016	0.016	-273,000	-4,368

In Table B4-7, the effect of restricting the time horizon *TH* upon the accumulated loading factor *ALF* (fourth column in Table B4-6) has been illustrated.

Table B4-7. Accumulated GHG Loading Factors

	Emission, t/year	GHG lifetime, years	Accumulated GHG Loading Factors ALF, per tonne GHG per emission year				
			TH > 1000 years	TH = 100 years	TH = 50 years	TH = 20 years	TH = 1 year
CO_2	1	NA	NA	32.2	17.5	7.3	0.48
N_2O	1	114	114.0	57.2	25.9	9.4	0.50
CH_4	1	12	12.0	12.0	10.5	6.2	0.49
TO	1	0.06	0.06	0.06	0.06	0.06	0.06
TSA	1	0.016	0.016	0.016	0.016	0.016	0.016
BC	1	0.047	0.047	0.047	0.047	0.047	0.047

The shorter the atmospheric lifetime, the closer the ALF gets to a constant value equal to the atmospheric lifetime, independent of time horizon. For such substances, the radiative forcing and the climate effect per emitted unit are directly proportional to the atmospheric lifetime after multiplying by the radiative efficiency ratio a_i / a_r, and independent of time horizon value. Even methane, with a 12-year lifetime, shows a constant value of 12 down to a 50-year TH.

When combining the ALF results with radiative efficiency ratios as used in Table B4-6, the resulting climate loading effect and GWP* results are as shown in Tables B4-8 and B4-9.

Table B4-8. Accumulated Radiative Forcing Factor as a Function of Time Horizon (TH)

	emission, t/year	GHG life-time, years	Accumulated Lifetime Radiative Forcing factor as tonnes CO_2e per emission year				
			TH > 1000 years	TH = 100 years	TH = 50 years	TH = 20 years	TH = 1 year
CO_2	1	NA	NA	32.2	17.5	7.3	0.48
N_2O	1	114	24,624	12,355	5,594	2,030	1,050
CH_4	1	12	1,212	1,210	1,061	622	390
TO	1	0.06	1,380	1,380	1,380	1,380	1,380
TSA	1	0.016	-4,368	-4,368	-4,368	-4,368	-4,368
BC	1	0.015	31,631	31,631	31,631	31,631	31,631

Observe that the specific radiative forcing effect for short-lived substances is a substance constant over all practical time horizons, for methane down to TH = 50 years. For long-

lived substances this value is steadily increasing with the time horizon, because the emitted substance decays slowly after the end of emission.

The opposite situation is seen when GWP* is calculated (Table B4-9), since the radiative forcing has to be related to the substantial variation in CO_2-specific radiative forcing as *TH* is varied.

Table B4-9. GWP* Values By Time Horizons

	emission, t/year	GHG life-time, years	GWP*			
			TH = 100 years	TH = 50 years	TH = 20 years	TH = 1 year
CO_2	1	NA	1	1	1	1
N_2O	1	114	383	320	278	225
CH_4	1	12	38	61	85	103
TO	1	0.06	43	79	189	2,875
TSA	1	0.016	-136	-250	-598	-9,100
BC	1	0.015	982	1,807	4,333	65,898